3-23-2017

Evaluating the Autonomous Flying Qualities of a Simulated Variable Stability Aircraft

Ali M. Hamidani

Evaluating the Autonomous Flying Qualities of a Simulated Variable Stability Aircraft

THESIS

Ali M. Hamidani, Captain, USAF

AFIT-ENY-MS-17-M-261

DEPARTMENT OF THE AIR FORCE
AIR UNIVERSITY

AIR FORCE INSTITUTE OF TECHNOLOGY

Wright-Patterson Air Force Base, Ohio

AFIT-ENY-MS-17-M-261

EVALUATING THE AUTONOMOUS FLYING QUALITIES OF A SIMULATED VARIABLE STABILITY AIRCRAFT

THESIS

Presented to the Faculty

Department of Astronautical Engineering

Graduate School of Engineering and Management

Air Force Institute of Technology

Air University

Air Education and Training Command

in Partial Fulfillment of the Requirements for the

Degree of Master of Science in Astronautical Engineering

Ali M. Hamidani, B.S.A.E.

Captain, USAF

March 23, 2017

AFIT-ENY-MS-17-M-261

EVALUATING THE AUTONOMOUS FLYING QUALITIES OF A SIMULATED VARIABLE STABILITY AIRCRAFT

THESIS

Ali M. Hamidani, B.S.A.E.
Captain, USAF

Committee Membership:

Dr. D. L. Kunz, PhD
Chair

Lt. Col C. S. Hale, PhD
Member

Capt. A. L. Comer, PhD
Member

Abstract

Whether delivering internet connectivity from high altitudes, at airspeeds of just 30 knots, gathering data from active volcanoes and forming hurricanes, or collecting Intelligence, Surveillance, and Reconnaissance (ISR) over hostile territories, UAVs are at the ready to perform those missions that are too 'dull, dirty, or dangerous' for manned aircraft. However, the proliferation of this new technology has its fair share of challenges. Over 460 military UAV mishaps have occurred since 2001, with almost half resulting in damages of $2 million or more. One mishap almost ended in fatalities, when a UAV, suffering from loss of control, collided with a C-130. That loss of control is what this undertaking aims to address—toward establishing design criteria for UAV stability and control characteristics, or flying qualities. Open-source flight simulation software, known as JSBSim, was used to investigate the correlation between F-16 flying qualities, and aircraft workload and performance, while executing a set of precision-aggressive tasks under autopilot command. The results suggest techniques by which workload and performance metrics can be used to specify design requirements for UAVs. This research effort is intended to serve as a precursor for real-world flight testing using the NF-16D Variable stability In-flight Simulator Test Aircraft (VISTA).

Acknowledgements

In the Name of God, Most Gracious, Most Merciful

This research undertaking is the final seal of eighteen months of arduous graduate education—a journey intended as a humble act of devotion to my Lord, and dedicated to the benefit of the human family. As engineers, we are charged with harnessing the cutting edge of science to break through to the next technological advancement. As military officers, it is our duty to accomplish our mission at all cost, but without ever losing perspective of our impact on the bigger picture. Thus, it is the overarching hope that the results of this work may one day contribute to creating autonomous aircraft, that not only offer advanced capability, but that do so safely, and that can be readily employed in bringing prosperity to our global society.

Indeed, this effort could not have been accomplished alone. I owe a great debt of gratitude to my mother and my father. Thank you for your tireless encouragement and unending sincere prayers. To my loving wife, thank you for your enduring moral support throughout my studies, and for your patience in spite of the long hours I had to spend on campus, away from home.

I would like to also thank my advisor, Dr. Kunz, for all of his time and guidance in surmounting the sometimes overwhelming challenges associated with uncharted research. I look forward to continuing to work with you, as we venture toward future endeavors. I am also grateful to the members of my committee. Lt Col 'Shadow' Hale, thank you for providing valuable insights from your flight test engineering background; and Capt Comer, thank you for your flexibility and helpful feedback. It was a privilege to be able to work with all of you.

Ali M. Hamidani

Table of Contents

Page

Page

List of Figures

List of Tables

Table Page

List of Symbols

$A_{1,2,3}$	command input amplitude variations
b	wing span
CAP	control anticipation parameter
C_{m_α}	non-dimensional pitch stiffness coefficient
C_{m_q}	non-dimensional pitch damping coefficient
$\vec{F}$	force vector
G_{HOS}	gain of higher-order system at a given frequency
G_{LOES}	gain of lower-order equivalent system at a given frequency
g	gravitational acceleration of earth
h	altitude
h_{CMD}	command altitude input
[I]	moment of inertia tensor
J	cost value of minimization functions
K_d	derivative gain value
K_i	integral gain value
K_p	proportional gain value
K_θ	LOES pitch transfer function gain

$\mathcal{L}_2$	Normalized relationship between actuator positions and trimmed actuator position during simulation
$\vec{M}$	moment vector
n	Number of values/instances
p	roll rate
p_{lat}	latitude of aircraft
p_{long}	longitude of aircraft
q	pitch rate
$\bar{q}$	dynamic pressure
r	yaw rate
s	Laplace operator
S	wing surface area
TIC	Theil's Inequality Coefficient
T_{θ_1}	long-term (low-frequency) numerator time constant in the transfer function for pitch response to longitudinal control input
T_{θ_2}	short-term (high-frequency) numerator time constant in the transfer function for pitch response to longitudinal control input
u	longitudinal body component of aircraft velocity
V_T	aircraft total velocity
v	lateral body component of aircraft velocity

w	vertical body component of aircraft velocity
$\vec{x}$	state vector
$\dot{\vec{x}}$	derivative state vector
$x_1(i)$	actuator position at a given instant
$x_2(i)$	actuator position in trimmed flight configuration
x_i	command input to aircraft at a given instant
$\tilde{x}_i$	actual aircraft state at a given instant
$\vec{y}$	output vector
α	angle of attack
β	sideslip angle
γ	flight path angle
δ_a	aileron deflection
δ_e	elevator deflection
δ_r	rudder deflection
δ_t	throttle position
ζ_p	phugoid damping ratio
ζ_{sp}	short period damping ratio
θ	pitch angle
θ_{CMD}	command pitch-attitude input

τ_θ	equivalent time delay of pitch response to longitudinal control input
τ_{θ_p}	pitch attitude phase delay
ϕ	roll angle
$\phi_{1,2,3}$	command input phase angles
ϕ_{HOS}	phase of higher-order system at a given frequency
ϕ_{LOES}	phase of lower-order equivalent system at a given frequency
ψ	yaw angle
ω_{BW}	bandwidth
$\omega_{1,2,3}$	command input frequency variations
ω_p	phugoid natural frequency
ω_{sp}	short period natural frequency

List of Acronyms

ACTD Advanced Concept Technology Demonstration

AFFDL-TR Air Force Flight Dynamics Laboratory Technical Report

CAP Control Anticipation Parameter

CAS Control Augmentation System

DoD Department of Defense

FAA Federal Aviation Administration

FDM Flight Dynamics Model

ISR Intelligence Surveillance Reconnaissance

HALE High-Altitude Long-Endurance

HOS High-Order System

JSBSim Jon S. Berndt [Flight] Simulator

LOES Lower-Order Equivalent System

MATLAB Matrix Laboratory

MIL-HDBK Military Handbook

MIL-STD Military Standard

MTE Mission Task Element

NACA National Advisory Committee on Aeronautics

NASA National Aeronautics and Space Administration

PID	Proportional, Integral, Derivative
PIO	Pilot Induced Oscillation
RPV	Remotely Piloted Vehicle
SAS	Stability Augmentation System
TMP	Test Management Project
UAS	Unmanned Aerial System
UAV	Unmanned Aerial Vehicle
US	United States
USAF	United States Air Force
VISTA	Variable stability In-flight Simulator Test Aircraft
XML	eXtensible Markup Language

EVALUATING THE AUTONOMOUS FLYING QUALITIES OF A SIMULATED VARIABLE STABILITY AIRCRAFT

I Introduction

At the time of this writing, a weary U-2 pilot is disengaging autopilot while lining up for final approach at an undisclosed airfield. The eleventh and final hour of the spy plane's mission marks the twelfth consecutive flight hour for a seemingly indefatigable RQ-4 Global Hawk, as it turns on course for its hundredth spiral pattern search. The RQ-4 will continue aloft over hostile territory for yet another twenty-six hours [8]. As the gray aircraft collects valuable intelligence, another RQ-4, this one painted white and bearing the National Aeronautics and Space Administration (NASA) emblem, is on hour twenty of its mission over the Atlantic, gathering time-critical meteorological data from the latest tropical depression [50].

Just beneath these Global Hawks, a myriad of MQ-1 Predator and MQ-9 Reaper aircraft are soaring at 20,000 feet. Some are operated by the Department of Homeland Security and serve as vital assets in the War on Drugs. Others are indispensable by the Department of Defense (DoD) in the Global War on Terror. Even NASA has its own version of the MQ-9 set to task, in pushing the envelope of earth science research [71]. While the RQ-4, MQ-1, and MQ-9 aircraft may be the most well-known of their kind, they are part of a wide family of tens of aircraft, including, the RQ-7 Shadow, used by US and foreign militaries, or the RQ-14 Dragon Eye, used by the US Marine Corps, and recently flown by NASA to collect geological data in the treacherous atmosphere of volcanic plumes [51].

Not to be limited to government use alone, the private sector is also rushing to

exploit and improve the utility of these aerial machines. Corporations like Google are actively testing high-flying aircraft, which are intended to remain airborne for days, while providing internet access from over 60,000 feet [65]. Amazon recently demonstrated a proof of concept for a fixed-wing vehicle that will provide deliveries, around the clock, through the company's Prime Air program [15]. Speaking of deliveries, a humanitarian focused start-up, called Zipline, has already partnered with Rwanda to provide air-dropped packages of life-saving medical supplies, thereby improving healthcare for millions of people, otherwise isolated by rough terrain [63]. These are just a few examples of over 400 commercial organizations that are producing and testing, both, fixed and rotary-wing aircraft in the fight for their share in this emerging market [69].

Colloquially known as "drones", Unmanned Aerial Vehicles (UAVs), are becoming ever more pervasive across the wide blue skies. These machines are at the ready to perform those missions that are deemed too dull, dirty, or dangerous for human pilots. However, there is indeed a grave side to the proliferation of this technology.

1.1 Background

Almost every aircraft mentioned above, has suffered some sort of accident, due to design issues. In May 2015, Google's Solara 50 experienced an anomaly after hitting a thermal updraft, an upset which exceeded the vehicle control system's disturbance rejection capability. The aircraft was jolted into an unsafe airspeed, causing structural failure of the left wing and ultimately leading to a crash just four minutes after takeoff [9]. About a year later, Facebook's Aquila aircraft suffered a similar fate. During landing, after almost 90 minutes of otherwise uneventful flight, a wind gust caused the autopilot to pitch the aircraft downward, thereby driving the aircraft to exceed its nominal airspeed. The control system susequently attempted to arrest the descent by

commanding an upward elevon deflection. Combined with the already fast airspeed, the rapid actuation of the elevon created excessive torsional stress on the outer wing panels. The aircraft crashed at a groundspeed of 25 knots and sustained substantial damages [10].

Since 2001, with military UAVs alone, there were 237 crashes classified as Class A mishaps—those which resulted in damages of $2 million or more. An additional 224 incidents were recorded as Class B mishaps, resulting in damages between $500,000 and $2 million each [27]. In 2009, the United States Central Command (USCENTCOM) Combined Forces Air Component Commander (CFACC) voiced his concerns when he stated:

> So far we have been fortunate. What I worry about is the day I have a C-130 with a cargo load of soldiers, and a UAV comes right through the cockpit windshield [30].

Just two years later, the hypothetical instance almost became a fatal reality. In August 2011, while an MC-130 was descending toward a forward operating base, it was suddenly struck by a 375 pound RQ-7B Shadow. The impact was so severe, that it ruptured a fuel tank, causing large amounts of jet propellant to spew over the left wing. Fortuitously, the UAV missed the cockpit by about 20 feet, and the MC-130, already configured for landing, touched-down safely within two minutes of the collision. It was later determined that the the RQ-7B was suffering from loss of control that could not be immediately addressed by the remote operator [27].

With about a quarter of accidents occurring domestically, these mishaps are not exclusive to Areas of Responsibility abroad. In June 2012, a US Navy RQ-4 crashed on Maryland's Eastern Shore, sparking a brush fire [61]. A few months later, a US Air Force MQ-9 spun out of control and plummeted toward Lake Ontario at a sink rate of 5,000 feet per minute [62]. In April 2014, an RQ-7, operated by the US Army National Guard, crashed just in front of a Pennsylvania elementary school. Safety

is, in fact, such a concern, that UAV flights are restricted to only a small number of designated airspace areas around the Continental United States [57], as can be seen in Figure 1.

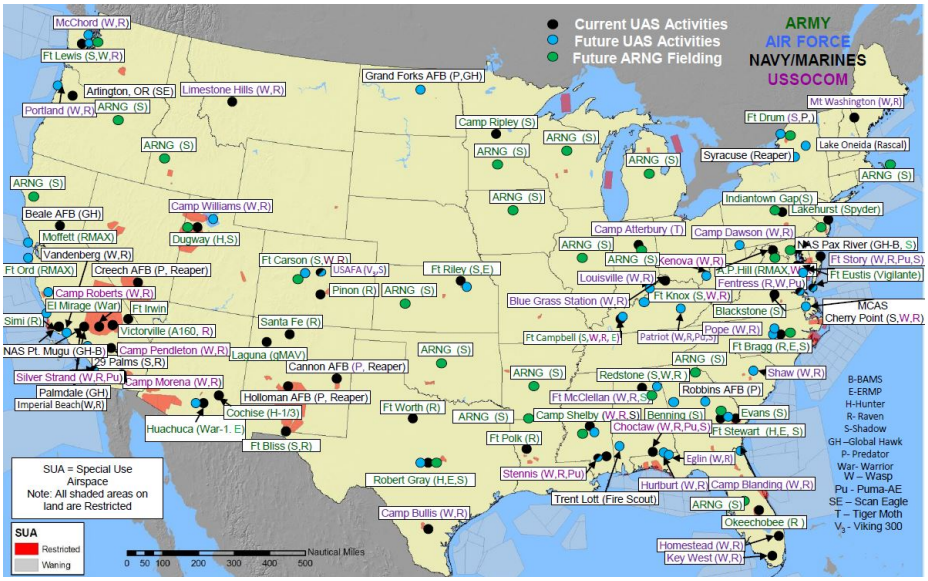

Figure 1. Airspace Areas Designated for UAV Operation [57]

In spite of these challenges, the DoD is actively working toward cooperative missions between manned and unmanned aircraft, as was demonstrated with the deployment of 104 Perdix micro-drones from three F/A-18 aircraft in an October 2016 flight test [11]. At the same time, commercial industry is continuing the push for new legislation, allowing UAVs to depart the bounds of special use airpsace and take part in routine operations across the wider national airspace system. Before this is possible, operators must take part in an airspace integration process which is built on a foundation of three key elements, namely, regulatory compliance, pilot or operator qualification, and vehicle airworthiness [57].

The overarching military handbook for airworthiness certification, MIL-HDBK-516C, defines an aircraft as airworthy if it is able to "safely attain, sustain, and terminate flight in accordance with the approved usage and limits" [7]. In order to achieve certification of airworthiness, the document specifies criteria that must be

met, as they relate to key aircraft elements including avionics, software, structures, propulsion, and the systems engineering techniques by which these components should be integrated and tested.

UAV mishaps can be attributed to a number of problems with the design of any of these subsystems. However, the analysis, presented herein, draws its impetus from the significant number of UAV accidents which resulted from aircraft stability and control issues. Thus, the focus area of this effort lies in the field of aircraft flying qualities research. Standards for aircraft flying qualities, or the stability and control characteristics that ensure an aircraft's safety of flight, are detailed in Section 6 of MIL-HDBK-516C [7]. Being a qualitative document, the handbook points to other references for quantitative specifications. For fixed-wing aircraft, the current authoritative document is MIL-STD-1797B "Flying Qualities of Piloted Aircraft" [6].

1.2 Research Problem Motivation and Description

MIL-STD-1797B [6] draws its origins from almost a century of aviation experiments, citing results and lessons from source documents dating as far back as 1919. The requirements that it lays out stem from flying qualities data that was collected from countless hours of flight testing and catalyzed by the advent of the variable stability aircraft. However, as the document's title implies, almost all of this research was focused on manned aircraft. Applying MIL-STD-1797B requirements to UAVs, creates a number of problems for which solutions must be discovered.

To date, there has been no concerted effort to establish a flying qualities database that would reveal just which aircraft stability and control characteristics have the most important bearing on unmanned flight. The design of safe and effective UAVs, that can be safely integrated into the nation's airspace system, thereby minimizing risk to life, limb, and property, necessitates such an undertaking. After all, the sustained

flight of an aircraft is not possible unless it was built to with the necessary stability and control characteristics. As such, flying qualities research is the very bulwark of aircraft design, and continued investigations in this discipline are key to realizing the future of aviation.

1.3 Research Objectives

To that end, the goal of this effort is to further the knowledge-base of UAV flying qualities. The results discovered from this endeavor, combined with findings from similar investigations, are intended to serve as the basis for more precise and applicable airworthiness standards for unmanned aircraft. While this particular research effort deals exclusively with flight simulation, it is designed to be a precursor for real-world flight testing.

The software tool of choice is the open-source, platform-independent, six-degree-of-freedom, flight dynamics model, known as JSBSim. It will be used to simulate the flight dynamics of an F-16 as it flies through two precision-aggressive mission tasks under autopilot control.

The US Air Force Test Pilot School currently operates a modified version of this aircraft, designated as the NF-16D, and known as the Variable stability In-flight Simulator Test Aircraft (VISTA), pictured in Figure 2. The results of this research should, therefore, be readily comparable to future data collected from full-scale flight tests.

Figure 2. The US Air Force Test Pilot School NF-16D Variable stability In-flight Simulator Test Aircraft (VISTA) [47]

There are five specific objectives for this research:

1. Model the F-16 aircraft in JSBSim and evaluate its flying qualities using current standards outlined in MIL-STD-1797.

2. Design two autonomous flight controllers that enable the aircraft to perform two types of precision-aggressive longitudinal tracking tasks.

3. Simulate the aircraft executing the designated maneuvers and establish a baseline for metrics that capture aircraft workload and performance.

4. Increase the complexity of maneuvers and evaluate the workload and performance of the aircraft in a nominal flight configuration. Then, vary the aircraft stability and re-evaluate its workload and performance throughout the same set of maneuvers.

5. Compare simulation results and provide a path forward for establishing metrics that can eventually guide the development of design requirements for autonomous aircraft.

1.4 Thesis Overview

Chapter I provided the background and motivation for further researching the flying qualities of unmanned aircraft. Chapter II begins with a brief history of the evolution of manned aircraft, and highlights flying qualities research as the keystone of aircraft design. It also discusses previous research efforts, and presents current techniques for determining aircraft flying qualities, as described in MIL-STD-1797. Chapter III details the specific methodology for implementing computer-based flight simulation, building the aircraft in JSBSim, evaluating its flying qualities, designing autonomous controllers for longitudinal tracking, and calculating metrics for assessing aircraft workload and performance. The results of the flight simulations are then analyzed in Chapter IV. Finally, Chapter V summarizes the research conclusions, touches on lessons learned, and provides recommendations for future research.

II Literature Review

The term *flying qualities* was perhaps best defined in National Advisory Committee for Aeronautics (NACA) Report 927 by William H. Phillips, in 1949. The report stated that an aircraft's flying qualities are "the stability and control characteristics that have an important bearing on the safety of flight and on the pilots' impressions of the ease of flying an airplane in steady flight and in maneuvers" [59]. The results presented in the NACA report are owed to over a decade of flight testing using about 60 different aircraft types. However, the field of flying qualities research traces its roots far deeper in the course of history.

2.1 A Brief History of Flying Qualities Research

One cannot gain a true appreciation for how exciting and pertinent flying qualities research is to the miracle of flight, without first taking time to explore just how early aerial machines evolved into skyfaring aircraft. This journey begins well before the Wright Brothers' famed flight, for indeed their flying machine did not take to the sky just with altitude borrowed from a hilltop, but also from that borrowed from their perch on the shoulders of giants—those brilliant minds from their past who strove to "slip the surly bonds of Earth" [45] through endless trial and error.

2.1.1 The Evolution of the Aircraft

Abbas ibn Firnas, a ninth century inventor and engineer, is first cited [74] with attempting to take flight by assembling wings of feathers and diving from an elevation. Although reported to have glided a notable distance, he was said to have crashed upon attempting to return to the ground, because he did not consider that birds rely on their tail to land, and therefore omitted it from his design. There are many accounts

thereafter of dauntless individuals such as these who aimed for the skies, but were unsuccessful. No doubt, their mettle inspired some of the more well-known figures in history.

It was eventually realized that raw human muscle power would simply not suffice to provide the thrust to weight ratios that birds enjoyed. In order to address the challenge of creating both lift and propulsion, Leonardo da Vinci, some seven centuries later, brainstormed a vehicle that featured mechanical flap wings [56]. This machine, known as an "ornithopter", would operate on the premise that mechanical levers could sufficiently augment human arm strength, and impart it into flapping wings. Unfortunately, this proved unsuccessful yet again.

Almost two centuries after da Vinci's death, humankind finally ascended to the skies in the first sustained aerial flight. While the people of France perhaps assumed the idea was full of hot-air, the irony was palpable, in that they did not know how wrong, yet so right they were. It was late 1783, when the Montgolfier brothers successfully designed and flew their balloon, which carried two men across the roofs of Paris for a total of 25 minutes, an astounding feat for the era [36]. While doing little to address the problem of heavier-than-air flight, the Montgolfiers' balloon enamored civilization with proof that it was, in fact, possible to ascend to the heavens.

Along this wave of creativity, and in the light of future possibilities, a new leader arose in the field. Sir George Cayley of England is credited with being the first to formulate the science of aeronautics [41]. His first design was not much of a departure from ornithopter concepts, in that it called for a pilot to "row" oars for propulsion. Cayley's greater contribution, however, was in his use of a piece of test equipment, known as a whirling-arm. Uniquely shapped lifting surfaces, called airfoils, would be placed on the arm, which would be spun by to a falling weight attached to a pulley and spindle. The apparatus was used to measure the lift and drag associated with

differently shaped airfoils. It was thus realized that lift could be generated by fixed wings, rather than flapping wings. Cayley's experiments led him to design a glider that consisted of such wings, and both horizontal, and vertical tail-surfaces that were adjustable. One of his final designs was published in *Mechanics' Magazine* [60] in 1852 and is illustrated in Figure 3.

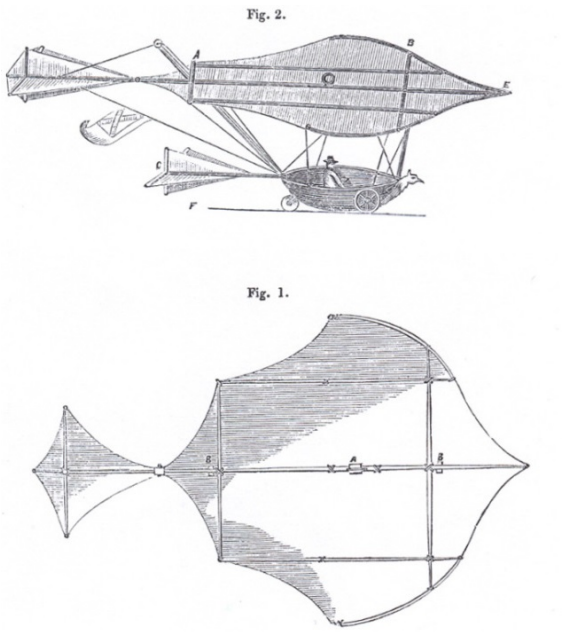

Figure 3. Sir George Cayley's Aircraft Design Featured in *Mechanics' Magazine* [60]

Cayley never got to build this concept, though it was based on a previous design of his, which was able to carry a ten-year-old boy several feet above the ground while gliding down a hill. For his work, he became known as the "grandfather of the modern airplane". The design was further solidified by William Samuel Henson who incorporated the fixed wing, fuselage, and tail. Henson also augmented Cayley's design by adding propellers instead of oars [16]. This new design, known as the aerial steam carriage, pictured in Figure 4, was also never actually built, but it gave the world a new imagination of what a functioning airplane may look like.

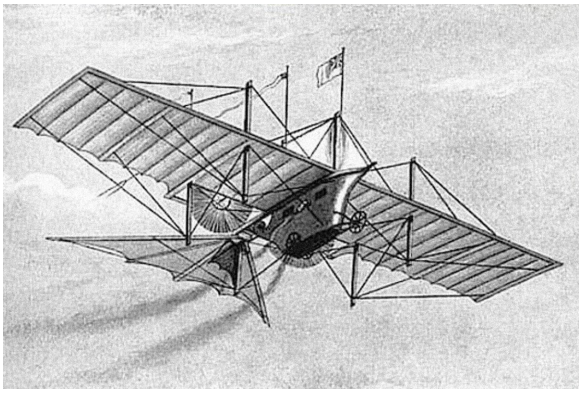

Figure 4. William Samuel Henson's proposed 1842 Aerial Steam Carriage [16]

In 1874, a French designer by the name of Felix Du Temple tested a machine with forward-swept wings. After being launched from an inclined plane, the machine was able to leave the ground for a brief instant. A decade later, a Russian designer, Alexander F. Mozhaiski, tested a machine of his own. Because of the short distance covered, both of these experiments were referred to as "powered hops", and were a far cry from the sustained, and *controlled* flight required for an viable airplane. On that subject, Alphonse Pénaud began experimenting with model aircraft. His studies shed light on the relationship between aircraft stability and control with tail incidence angle and dihedral in wing design [16].

During this time, an English inventor, Francis H. Wenham, designed and used the first wind tunnel in history. He discovered that lift was produced from the area of the wing toward its leading edge, and was the first to write about the benefit of high aspect ratio wings. Concurrently, another individual, Richard Harte, theorized a control surface that could counteract propeller torque and differential drag by deflecting about a hinge at the outboard trailing edge of a wing. This airplane steering device is known today as an aileron [2].

According to aviation historian Charles H. Gibbs-Smith [35], this is the same era in which two philosophies emerged in the hunt for the flying machine. The first is termed the "chauffeur" philosophy, and it professed that aircraft should take to the

sky by brute force, or by powerful engines, alone. Once airborne, it was intended that vehicles be driven in the same manner as carriages were steered on the ground. On the other hand, the "airman's" philosophy, which proved vastly more successful, suggested that a "feel" for flight must be obtained by means of test flying gliders. Once this skill was refined, and once an airframe was proven to be flyable, an engine could be added.

The engineer to first advance this philosophy was none other than Otto Lilienthal, a German who is credited with designing and flying the first successful gliders in history. In 1889, he published a book titled *Der Vogelflug als Grundlage der Fliergkunst*, which translates to *Bird Flight as the Basis of Aviation*. The work is known to have been the creed of the Wright Brothers in their early years [41].

The final steps that the Wright Brothers climbed were laid by Smithsonian Institution Secretary, Samuel Pierpont Langley. After hearing about the possibility of manned flight, at an American Association for the Advancement of Science meeting, Langley requested permission to assemble an aeronautical research center. Just as Cayley had done eight decades prior, Langley experimented with whirling arm apparatuses and almost a score of model airplanes. The year 1896 witnessed the pinnacle of Langley's creations. He constructed an unmanned, heavier-than-air flying machine which he called the "aerodrome". The 16 foot vehicle was designed to be launched from a catapult. During one flight test, the vehicle soared for more than 2,500 feet across the Potomac River, clocking a flight time of around 90 seconds. A few months later, the aerodrome, pictured in Figure 5, would double that distance, and fly for a total of two minutes [17].

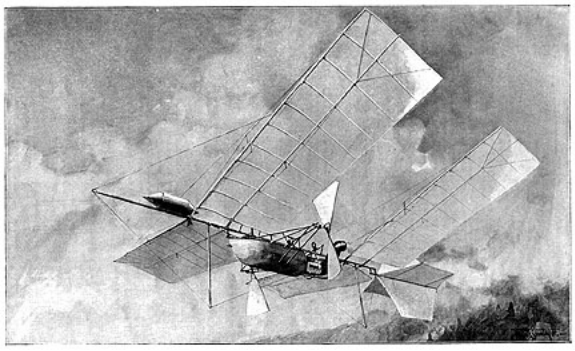

Figure 5. Samuel P. Langley's 1896 Aerodrome [16]

Orville and Wilbur Wright, now 29 and 25 years old, respectively, took a keen interest in the challenge of powered flight. They devoured all the literature they could get their hands on, including a book written by Octave Chanute titled *Progress in Flying Machines* and, as mentioned, Lilienthal's aeronautical research. In 1900 they built a glider with a 17 foot wingspan and flew it at Kitty Hawk, North Carolina. When they found that it did not produce as much lift as they calculated, and did not handle as well as anticipated, they went back to redesign it [68]. A year later, they returned to the proving grounds after modifying the glider to have a 22 foot wingspan. Unfortunately, the augmented glider also failed to perform to their expectations.

At their start, they relied heavily on Lilienthal and Langley's research. However, after two years of air trials, and still unable to grasp success, they decided to gather and rely on data of their own. In 1902, the Wright Brothers carried out over a thousand glider flights [68]. In all of this effort, they achieved only a fraction of Langley's success in terms of distance and airtime. However, the Wrights' accomplishments, to date, were still remarkable. Their aircraft had a stark contrast to those of Langley. While Langley's machines adhered to the chauffeur philosophy, the Wrights' aircraft were actually controllable about all three axes.

Staying true to the "airman" philosophy, they eventually came up with a glider that they were satisfied with, and surmised that the next step was to build a propul-

sion system. With the help of Charlie Taylor, a bicycle mechanic, Orville took on the challenge, and an engine was soon incorporated in the Wrights' design [68]. Their efforts had now come to fruition in the form of their 1903 Flying Machine. Popularly known as the Wright Flyer, and pictured in Figure 6, the aircraft had a wingspan just slightly over 40 feet, featured a double elevator forward of the wings, and was trailed by an aft mounted double rudder system.

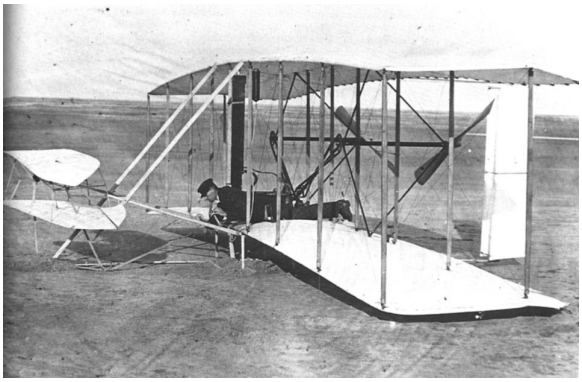

Figure 6. The 1903 Wright Flyer [16]

Upon flipping a coin to see who would be the first to take the controls, Wilbur boarded the aircraft. As soon as the aircraft launched, Wilbur found himself over-controlling and leading the flyer into an excessively high angle of attack which caused a stall, and subsequent hard landing. Within a few days, the damage was repaired, and now it was up to Orville to guide humanity skyward. The successful trial resulted in a 12 second air time, during which the Flyer covered 120 feet over the ground [68]. Their accomplishment was nothing short of remarkable, and cannot be overstated enough. Thankfully, this moment was recorded on film, as depicted in Figure 7. Indeed, a picture is worth a thousand words.

Figure 7. Orville Wright at the Controls as Wilbur Runs Alongside [16]

It should be reiterated here, that the flying qualities of an aircraft are the stability and control characteristics that make it safely flyable. Many historical figures worked to find the aircraft design that would make sustained flight possible. It was the Wright Brothers who finally unlocked the correct configuration by varying airframe geometry, and experimenting with the optimum placement of lifting and control surfaces that would lead to sustained flight. They were, in essence, empirically determining the flying qualities that would make it possible for their aircraft to actually take to the sky.

Thus, the preceding journey, examining how early flying machines morphed into stable, sky-faring aircraft, serves as evidence for the claim that flying qualities research was not just a subset of aircraft design, but rather it was the most paramount. Alas, ultimately even the 1903 Flyer was an intermediate success. More work would have to be done in order to allow for aircraft to remain aloft and in equilibrium for longer.

2.1.2 Toward a More Practical Aircraft

In that vein, the Wright Brothers continued to improve their design. Ascribing to the "airman" philosophy, they firmly believed that the human was inherent to the control of the air vehicle in maintaining flight equilibrium. It is widely accepted that their experience with bicycles helped solidify this mindset. After all, the bicycle is also a machine that is unstable without input from its rider. In fact, much to the

point being asserted, it was Wilbur Wright, who stated:

> When this one feature [balance and steering] has been worked out, the age of flying machines will have arrived, for all other difficulties are of minor importance [46].

The Wrights returned to the workshop and continued making modifications. Having noted pitch stability issues [17], they shifted the aircraft center of gravity forward, by adding weight to the front. They also increased the distance between the forward canards and the wings. In effect, this dampened the elevator input response, and made it easier to control the aircraft. Finally, in late September 1904, they were able to fly in a complete circle, during a sortie lasting about 96 seconds. Exponentially increasing in piloting skills, the Wrights were able to carry out these sustained flights on a routine basis. In October 1905, Wilbur took to the skies in a record setting flight, during which he circled 30 times, flew a distance of over 24 miles, and clocked an impressive 39 minute air time. They were now ready to seek a patent, and showcase their invention to the world.

Shortly thereafter, the first military request for proposal for a flying machine was issued. Signal Corps Specification Number 486 [70] is a monumental document in the field of flying qualities. Not only was it the first-ever contract for the design of an aircraft, but it was the first publication to specify requirements for flying qualities, albeit in just a few sentences. The terms asserted that the aircraft be subject to a trial flight during which it had to "be steered in all directions, without difficulty and at all times under perfect control and equilibrium", and simple enough in operation "to permit an intelligent man to become proficient in its use within a reasonable length of time". The Wrights signed the contract and fervently went to work.

In September 1908, they returned to the skies for the Army observation team [18]. Initially, Orville started again with short flights, but was reported to have been breaking records daily. He achieved flights of over an hour long, and began taking

passengers. However, on September 17th, while taking Lt Thomas Selfridge on a test flight, one of the propellers split and caught onto the aircraft rigging. The two men crashed, nose first. Orville suffered extensive injury, but sadly Lt. Selfridge died shortly after the rescue. Indeed, winning the military bid proved to be a turbulent journey, but thankfully, the Army extended the contract, and the Wrights worked even more tirelessly toward success.

On July 30th of 1909, Lt Benjamin Foulois joined Orville aboard the flying machine [18], and they took to the air with the roar of a 25 horsepower engine. After a successful flight, it was determined that the machine achieved an average speed just above 42 miles per hour, and that all requirements of the contract were either met or exceeded. The Wrights were awarded $30,000 and *Aeroplane No. 1* was officially accepted into the United States Army Inventory.

This "final copy" sported a vertical lever on the left to control the incidence angle of the forward elevator, and a vertical lever on the right to control the warp of the wing and the rudder. In order to perform a coordinated turn to the right, for example, the pilot was required to move the right-handed lever to the right, to cause the right wing to drop, and also aftward to cause nose-right yaw. Inputs would have to be phased. In other words, pilots were required to lead with the yaw input, before the roll input. Aviation historians and engineers alike marvel at the airmanship skills of the Wrights, for their aircraft would be difficult to fly for even the most skilled pilots of today [16].

The airplane was now not only possible, but also becoming more practical than ever. The Wrights' success quickly gave way for a vast number of new inventors to further push the envelope in the United States and abroad. One such example was Louis Blériot, who crossed the English Channel in 1909. He is credited with devising the standard control configuration, illustrated in Figure 8, with which modern day

fixed-wing pilots are most familiar [14]. Blériot's aircraft were the first to feature a central stick that could be moved forward and aft for nose up and nose down, respectively, as well as left and right for left wing down and right wing down, respectively. In addition, these aircraft had a rudder bar on which the pilot's feet would rest.

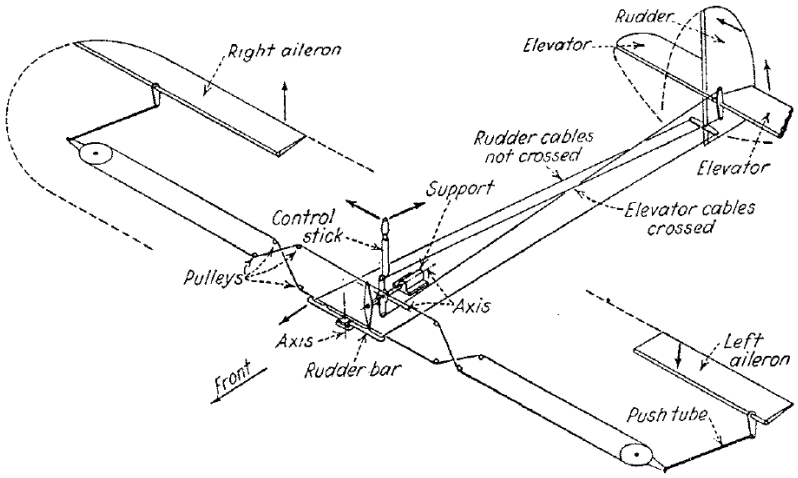

Figure 8. Diagram of Simple Airplane Control System Depicting Control Surface Deflections Corresponding to Control Stick Inputs [26]

.

The years leading up to, and the start of World War I would serve as even greater impetus to further enhance the design of aircraft. During this era, flying continued to be regarded as inherently dangerous, and the risk associated with it was thought of as just another fact of life. Furthermore, material was relatively inexpensive, and aircraft were easily repaired after rough landings, or easily modified if unfavorable flight test results dictated. For example, when Anthony H. G. Fokker flew his model D VII, he quickly realized how unstable and unsafe his design was [14]. He rushed back to the hangar to rebuild in secret before German Air Ministry officials had the chance to perform any inspections.

It was no secret, however, just how much work was still needed when it came to the theoretical aspects of stability and control. There would come a point when people would no longer accept fatalities in the name of empirical advances in flight,

and when aircraft would become too complicated or too expensive to easily return to the drawing board, and re-cut material. For safer and more cost-effective aircraft design, much would need to be done in developing calculable techniques that could be used to predict how well an actual aircraft would fly, before it was fully built.

2.1.3 Devising Analytical Design Techniques

The modern theoretical understanding of aircraft stability and control began with Frederick Lanchester [14]. He was a mechanical engineer who also experimented with gliders. His designs were inherently stable, but were analyzed to have a waving motion in flight. To describe this phenomenon, Lanchester coined the term *phugoid*. This type of longitudinal aircraft motion is a lightly damped oscillation, during which altitude and airspeed are exchanged and angle of attack remains constant. The oscillation occurs during a period of 30 seconds or more [53]. Lanchester published his research in two books in 1907 and 1908, titled *Aerodynamics* and *Aerodonetics*, respectively. He discussed his research with Wilbur Wright, although it did not have an effect, because the Wrights, like many other aircraft builders of the time were empirical experimenters, and did not share the same theoretical understanding of flight stability.

In 1911, George H. Bryan used fundamentals proposed by Isaac Newton and Leonhard Euler, to devise the mathematical theory for aircraft flight dynamics. Bryan was of the first to propose that aircraft dynamics could be split into two distinct categories: longitudinal and lateral [14]. The equations in Bryan's work, titled *Stability in Aviation*, are identical to those used in modern day flight analysis and simulation. At the time, however, little progress was made in incorporating these equations in aircraft design, because of how difficult the calculations were, and because of the lack of instrumentation that could measure the parameters that an aircraft experienced

in flight.

The year 1915 saw the formation of NACA, and by the summer of 1919, the first qualitative stability and control flight testing was being carried out. Professor Edward P. Warner, along with two other NACA employees used the Curtiss JN-4H and de Havilland DH-4 aircraft to measure elevator angle and stick force required for equilibrium in flight [14]. They discovered that the correlation between airspeed and the gradient of elevator equilibrium angle was an index of static longitudinal stability. At the same time, new specialized flight data recording instrumentation, like the photorecorder, were being introduced to the field. Devices like these could save information from individual aircraft instruments on film, thus eliminating the distracting task of pilots having to write down values while maneuvering their aircraft.

In 1935, Warner, now acting as a consultant to the Douglas Aircraft Company, published aircraft requirements based on interviews with both pilots and engineers. He was the first to suggest the need for devising flying qualities requirements by correlating instrumented flight tests with pilot opinion. These ideas were developed further with Harley A. Soulé, a member of NACA, who eventually negated the previous paradigm, when he found that the phugoid oscillatory flight dynamics mode had little to do with pilot opinion of how well an airplane handled [14].

Robert Gilruth, an engineer who joined NACA from the University of Minnesota, published this research in his 1943 paper entitled "Requirements for Satisfactory Flying Qualities of Airplanes" [37]. In this work, requirements were stated first, then a rationale based on flight test was provided. The document concluded with suggested methods for engineers to be able to design requirements-compliant aircraft while they were still in the drawing board phase.

Engineers and test pilots continued to work in concert, to carry out test flights on a routine basis. Initially, a preliminary aircraft design would be flown and evaluated by

a pilot. Then modifications would be made to these aircraft based on pilot inputs. In 1946, an engineer by the name of William M. Kauffman was looking out of a window at the present-day NASA Ames Research Center. He stared at the three Ryan FR-1 Fireball fighters lining the aircraft ramp. Each aircraft was seperately modified to have unique wing dihedral in order to determine the minimum angle that pilots would find satisfactory for control. Looking at the amount of resources required, Kauffman is noted to have remarked, "There has to be a better way." This began the quest for a machine that could modified more easily and more rapidly [14]. The effort would soon generate an augmented Grumman F6F-3 Hellcat. The aircraft had ailerons that could move based on sideslip angle variation. An electronic motor, adapted from a B-29 gun turret, would move the aileron push-pull rods in synchronization with pilot inputs. This novel concept would give way to over twenty new research aircraft.

2.2 The Variable Stability Aircraft

Just as established previously, early aircraft designers would iteratively modify the geometry of their flying machines until their airworthiness could be proven in actual flight. The relationship discovered between aircraft shape and aircraft stability derivatives would bridge the gap between the empirical nature of real-world flight testing, and the theoretical nature of drawing board design. It was eventually found that rather than solely altering aircraft shape to modify its stability characteristics, and an aircraft could also be artificially changed by means of feedback control systems.

Norman Weingarten, of Calspan, offers the example of modifying the yaw damping stability derivative [73]. The natural tendency of the aircraft to oscillate about its vertical axis, or yaw axis, can be damped by sensing yaw rate, multiplying it by a gain, and then feeding it back to the rudder. This system, as its function implies, became known as the yaw damper. Because of how it increases passenger comfort,

the yaw damper is now a standard feature in almost all modern day corporate and commercial aircraft.

Existing aircraft were modified with systems like this, and were then designated as variable stability aircraft. These flying laboratories offered a practical means for correlating pilot opinion with aircraft design. Their use gave insight as to how to improve the design of existing aircraft, as well as future machines still on the drawing board. A significant number of these aircraft were built by NACA and, later, NASA. Under USAF funding, another company, called Cornell Aeronautical Laboratory (now Calspan), would become an industry leader in developing these state-of-the-art machines [73].

Many military aircraft were purposely designed with bare airframes that sacrificed stability in favor of maneuverability [55]. Eventually, by 1953 the USAF realized that much research would need to be done using three-axis variable stability aircraft [73]. In 1957, Calspan delivered a modified Shooting Star jet designated as the NT-33.

The dawn of the space age served to further propel the use of such a machine, in an evermore innovative manner. In order to reach the edge of the atmosphere, NASA and the USAF would experiment with the hypersonic, rocket powered X-15 aircraft built by North American [40]. Naturally, test flights of the X-15 were very short and expensive. Thus, the NT-33 was selected to train pilots to fly the rapidly changing flight profile of the X-15 during re-entry.

The standard procedure required the safety pilot to push the control stick forward, causing the aircraft to pitch downward. Once the aircraft attained zero-G, the evaluation pilot would take the controls and guide the aircraft to a safe landing, by referencing modified flight instruments alone. The modified instruments gave the pilot a sensation of wings-level flight, when in reality, the aircraft would be in an almost 75 degree bank while pulling up to four G's. The NT-33 was so successful in

flying qualities research, that it was used for the next 40 years.

However, the need to replace this aging NT-33 was recognized as early as 1965, after just eight years of service. Calspan was hard at work conducting research and development studies for an eventual replacement [25]. In 1982, the company was awarded a contract for the future Variable stability In-flight Simulator Test Aircraft (VISTA). A two-seat (D-model) F-16 was selected as the final candidate, after being narrowed down from a selection of six different aircraft.

In 1988, development of the six degree-of-freedom variable stability aircraft was underway [73]. Once delivered, it was permanently designated as the NF-16D. It offered a digital flight control computer, a large fairing for adding additional electronics, and high capacity hydraulic and power supply systems. The most notable feature of the VISTA design was its integration of simulation computers with the native F-16 fly-by-wire computers. Even the cockpit was modified to include both a center and specialized side-stick controller that was later used for F-22 simulations. The project was completed in 1992, and flown five times as part of an acceptance program. In the year 2000, the VISTA was transferred to the USAF Test Pilot School. It is currently used for flying qualities instruction, as well as student Test Management Projects (TMPs).

2.3 Flying Qualities Standards

Following the path paved by NACA, the US Air Force and US Navy would continue conducting flight tests, and subsequently issuing formal flying qualities requirements for new aircraft procurement. In 1948, the services enacted a joint specification, MIL-F-8785 "Military Standard, Flying Qualities of Piloted Airplanes" [1]. It was around this time, through successive military specifications, that the emphasis on aircraft phugoid oscillations officially shifted to short period oscillations instead. The short

period flight dynamics mode is characterized by a rapid change in angle of attack and pitch attitude, while airspeed stays constant [53]. Engineers began to iteratively modify stability and control values based on NACA research and flight testing. At first, the stick-fixed damping ratio was decreased, which proved to be agreeable for most pilots. As more experience was gained with higher altitude aircraft, the damping ratios were increased again. Such fluctuation in design trends fueled curiosity, and served to provide additional funding for the use of variable stability aircraft.

Further research was conducted using the NT-33 to hone in a "sweet-spot" combination of short period damping ratios and short period natural frequencies, as they related to pilot opinion. The results were incorporated in following revisions of MIL-F-8785, until version "C" [1], the last update, was published in 1980. The guidance provided in this document was so valuable that eventually all military aircraft would be procured on contracts that ensured that they could meet these specifications [14].

MIL-F-8785C [1] represented aircraft by classical transfer functions. These transfer functions mathematically represented the relationship between control inputs and aircraft dynamics. In the pitch axis, for example, a transfer function would relate forward or aft control stick input with pitch-rate. These bare airframe transfer functions were easily modifiable using control theory concepts, if it was deemed that artificial stability would be required for safe flight, and control effectiveness during military maneuvers.

The document also included a formalized numerical rating scale that pilots could use to describe how adequately an aircraft would handle during set tasks. This rating scale, shown in Figure 9, was proposed by George E. Cooper of NASA, and Robert P. Harper of Calspan [28]. A pilot rating of "1" would be used to describe an aircraft that was excellent in performance, while a rating of "10" described an aircraft that exhibited control loss, which was highly undesirable at the least, or just plain

dangerous at worst. A Cooper-Harper rating between 1 and 3, falls under Flying Qualities Level 1. A rating from 4 to 6 falls under Flying Qualities Level 2. Finally, Level 3 encompasses ratings from 7 to 9.

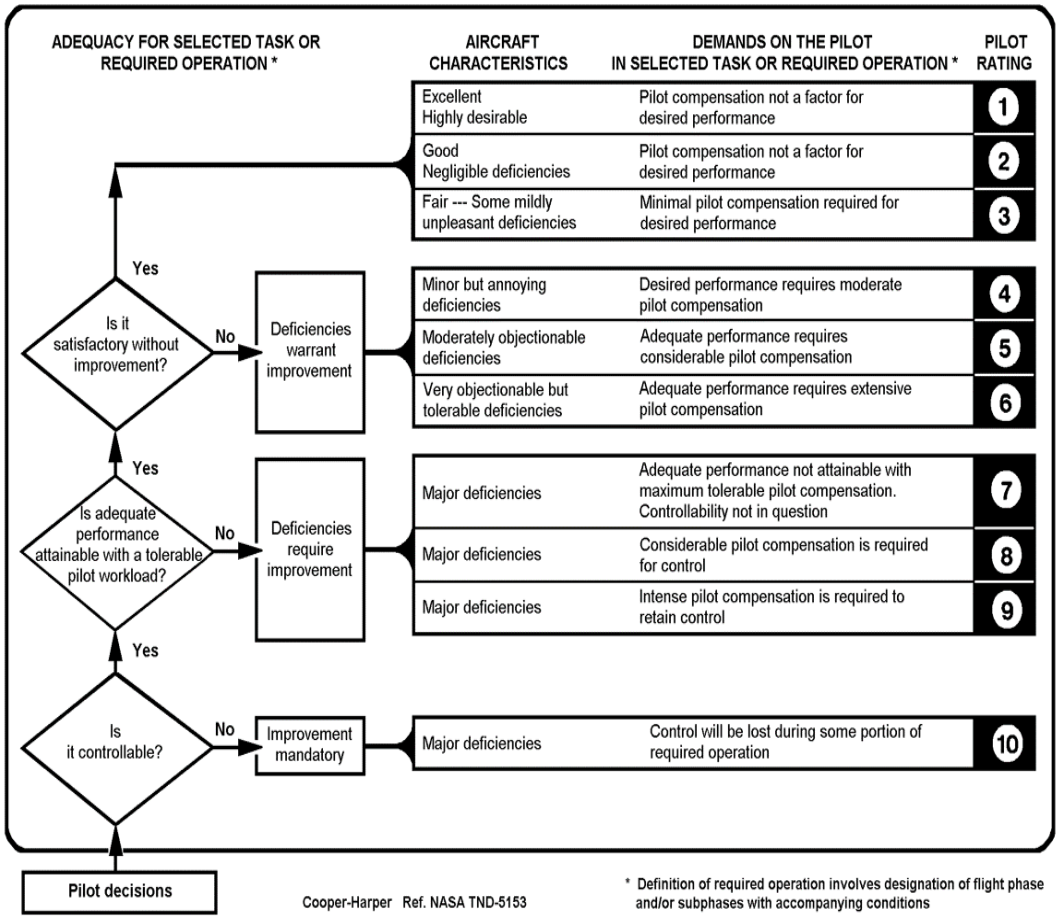

Figure 9. The Cooper-Harper Numerical Pilot Rating Scale [28]

The rigid requirements set forth by MIL-F-8785 were overtaken by a 1987 document known as MIL-STD-1797 "Military Standard, Flying Qualities of Piloted Vehicles" [4]. The document was first created to provide government procurement agencies and military contractors with latitude to negotiate actual numbers for flying qualities requirements, because of how complex aircraft had become with the advent of digital computer systems. It was now possible for aircraft to have a wide variety of flying

qualities by use of any control scheme that a contractor could come up with [14].

After several revisions, the document in use today is designated as MIL-STD-1797B [6], and was published in 2006. It serves as comprehensive guidance which was formed from the earliest aeronautical research. The document cites MIL-F-8785, along with other documents, drawings, and publications dating as far back as 1919. The work is so extensive, that it requires 26 pages just to cite all of these references.

One of the many features inherited from MIL-F-8785, is the manner in which varying airframes are organized. Aircraft are grouped into four separate classes based on the maximum gross weight that they are designed to carry, and their level of maneuvering capability. In this case, designated load factor, or G-loading, is considered a direct indicator of maneuverability. After all, aerobatic, or fighter aircraft, are designed to withstand the highest G-loading, thus allowing them to be highly maneuverable. For manned aircraft, the ratio of load factor to maximum design gross weight directly correlates to aircraft mission. Aircraft that are designed to be light, but not built to endure high load factors, are mostly training aircraft, and fall under Class I. Aircraft that can haul slightly more weight, but not able to withstand high load factors, mostly fulfill a corporate transport type mission, and fall under Class II. Cargo aircraft must carry the highest gross weight, but do not require evasive maneuverability, and therefore they fall under Class III. Fighters do not weigh as much as cargo aircraft, but because of their maximal designed load factor, they fall under Class IV. Examples of these four classes of aircraft can be seen in Figure 10.

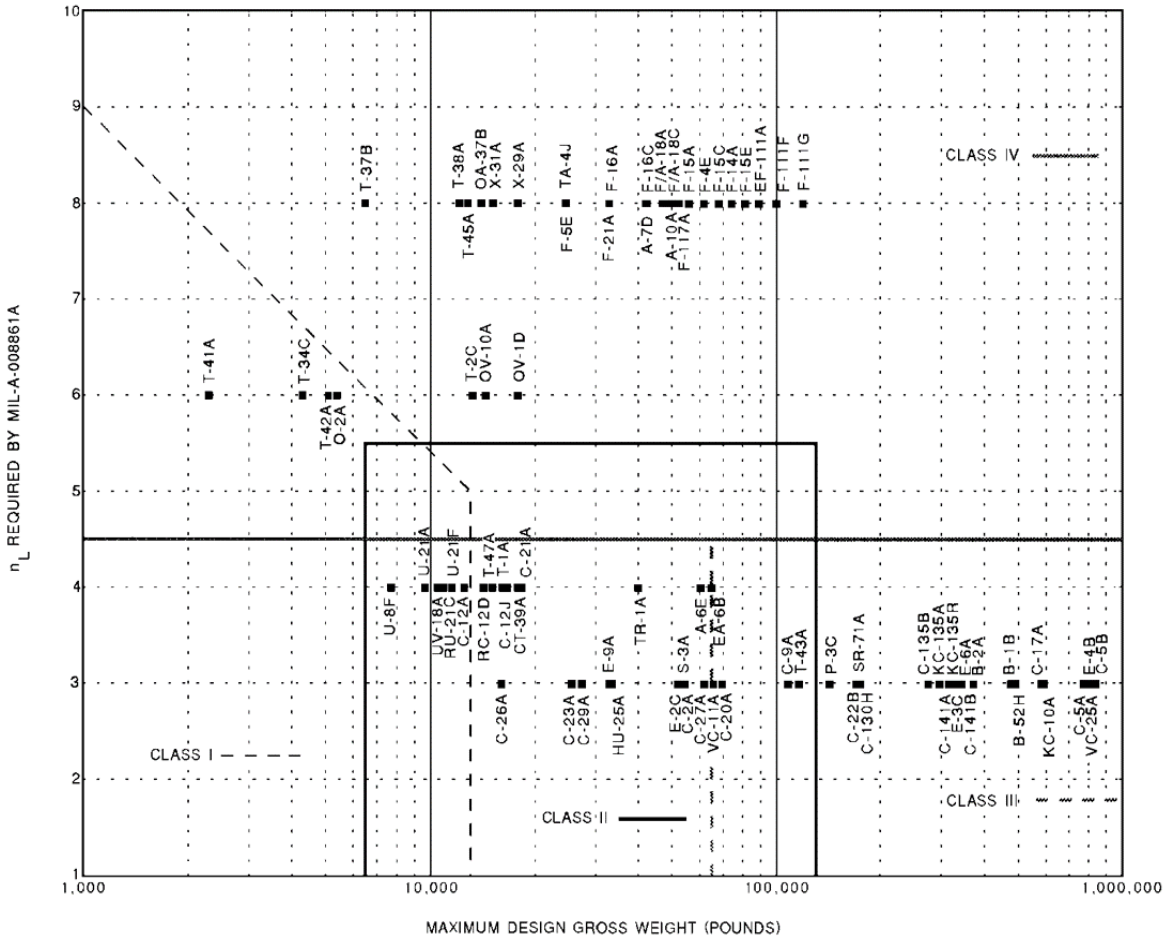

Figure 10. MIL-STD-1797 Classification of Aircraft [4]

Next, an aircraft's intended mission is broken up into three separate categories of flight. Category A flight consists of those phases that would require high maneuverability, or precise target tracking. Category B flight covers those flight phases that are outside the terminal areas, where the aircraft engages in mostly gradual maneuvers. Finally, Category C flight encompasses those phases of flight in the immediate terminal area, such as takeoff and landing. More examples, excerpted from MIL-STD-1797B [6], can be seen in Table 1.

MIL-STD-1797 [6] continues further on to describe requirements for internal and external stores, aircraft loadings, and moments and products of inertia. It also specifies requirements for aircraft configurations and aircraft states. Examples include the

Table 1. Flight Phase Categories [6]

Nonterminal Flight Phases	
Category A	Air-to-air Combat Ground Attack Reconnaissance In-flight refueling (receiver) Terrain following Close formation flying
Category B	Climb Cruise Loiter In-flight refueling (tanker) Descent
Terminal Flight Phases	
Category C	Takeoff Landing Power Approach Go-around

normal state, extreme state, failure state, or special failure state. An aircraft could enter a failure state, for example, if unusual loading is encountered. A special failure state could include a broken control stick, or surface structural failure. Acceptable flying qualities are defined even in the case of an aircraft experiencing these failure states.

Once these states are determined, MIL-STD-1797B [6] establishes the three Regions of Handling. First is the Region of Satisfactory Handling (ROSH) which has its boundaries determined by speeds, altitudes, and load factors required to accomplish aircraft missions with Level 1 flying qualities. Next is the Region of Tolerable Handling (ROTH), within which an aircraft must be able to accomplish its mission with Level 2 flying qualities. Finally, the Region of Recoverable Handling (RORH) is defined to include the regions of the aircraft flight envelope within which safe aircraft operation is allowable and possible. Figure 11 is a notional chart that represents the boundaries of a Region of Handling using airspeed and load factor.

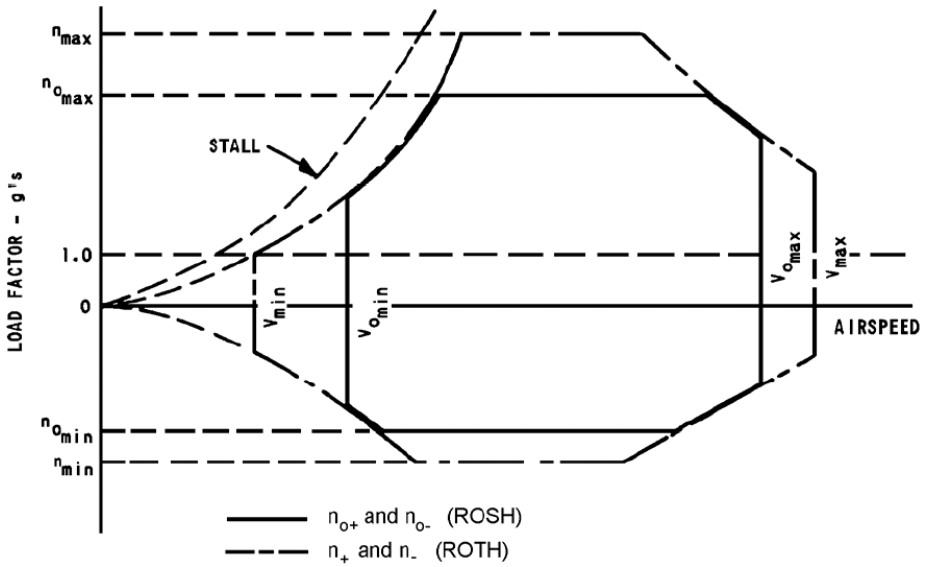

Figure 11. Two Dimensional Boundaries of a Notional Region of Handling using Airspeed and Load Factor [4]

Perhaps the most important part of MIL-STD-1797B [6], especially for the research herein, is contained in its fifth chapter. Up to this point, it is established that an aircraft can be modeled as a mathematical system which can be represented by a collection of transfer functions (e.g. an equation relating elevator deflection command to elevator deflection angle). It is also established, through research with the NT-33, that certain aircraft states, like forces, rates, and accelerations, can be measured and correlated with Cooper-Harper pilot ratings.

The aircraft of today may have well over 20 states that can be measured, and thus would be mathematically represented by means of what is known as a higher order system (HOS). Chapter 5 of the Military Standard [6] shows how a modern aircraft system with a multitude of states can be reduced to a lower order equivalent system (LOES), which exhibits classical aircraft dynamics. This LOES approximation represents longitudinal or lateral aircraft dynamics by means of a second order transfer function. Classical stability values like time delays, and short period natural frequencies and damping ratios, along the longitudinal axis, or Dutch roll natural

frequencies and damping ratios along the lateral axis, can easily be determined from this LOES model. Specific techniques for this calculation will be outlined in Chapter III, the Methodology section of this work.

William Bihrle presented research in AFFDL-TR-65-198 [22] that proposed another literal factor which pertains to flying qualities. The Control Anticipation Parameter (CAP) is the ratio of pitching acceleration to steady-state normal acceleration. CAP directly relates the proprioceptive cues that a pilot would feel in the inner ear and seat of the pants as a result of a pitch command (i.e. stick movement forward or aft). Several techniques for calculating this value are presented in MIL-STD-1797B [6]. The flying qualities of an aircraft can be determined when correlating this parameter to the aircraft's short period damping ratio. This concept is best understood by examining the thumbprint plots, actually included in the previous MIL-STD-1797A [4], and shown here in Figure 12.

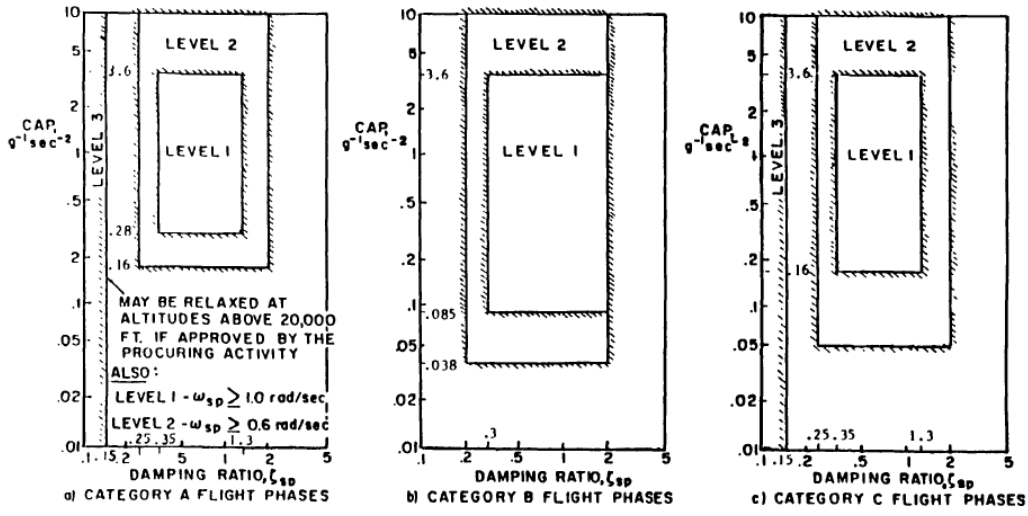

Figure 12. Thumbprint Plots Relating Literal Factors to Flying Qualities Envelopes [4]

According to these plots, if an aircraft has a measured CAP value of 1.0 $g^{-1}sec^{-2}$, and a short period damping coefficient (or ratio) of 1.0 rad/sec, it would exhibit Level 1 flying qualities, in the Category A flight phase.

Another indicator of aircraft flying qualities is presented as the bandwidth and time delay criteria. In control theory, there are certain frequencies of system operation that can result in instability. This instability occurs at frequencies where system gain tends to zero decibels, or where system phase tends to 180 degrees. In order to avoid this, a margin of safety, called the stability margin, is set above these unstable gain and phase bounds. The maximum frequency of operation that can occur without threatening system stability is known as the bandwidth. The flying qualities of an aircraft can be determined by calculating this bandwidth, and then correlating it to system delay. Figure 13 is an example of these values and how they correspond to boundaries of flying qualities during flight phase Category A.

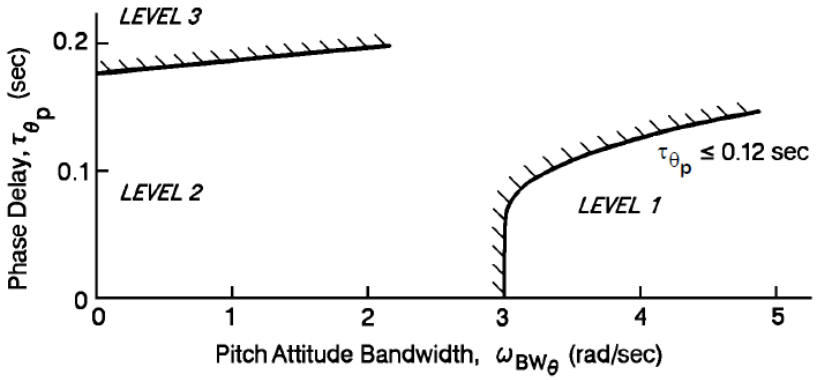

Figure 13. Relationship Between Flying Qualities, Bandwidth and Phase Delay for all Classes of Aircraft in the Category A Flight Phase [4]

Finally, of important note, are the closed-loop control system analysis and criteria that MIL-STD-1797B [6] presents. This method of determining aircraft flying qualities involves mathematically cascading a transfer function representative of a notional pilot, with the transfer function of the aircraft, and then closing the control loop with unity feedback. The mathematical model, representing the pilot, is built using the modified Neal-Smith criteria [6]. Using controls design techniques in the frequency-domain, like the Nichols chart, closed-loop values and their relation to the aircraft's level of flying qualities are determined. The military standard specifies

system bandwidth requirements that must be satisfied with a closed-loop droop of no less than negative three decibels. The Nichols chart in Figure 14 shows a typical plot of an aircraft system in the frequency-domain, where the closed-loop droop of of negative three decibels falls, and how levels of flying qualities relate to closed-loop resonances.

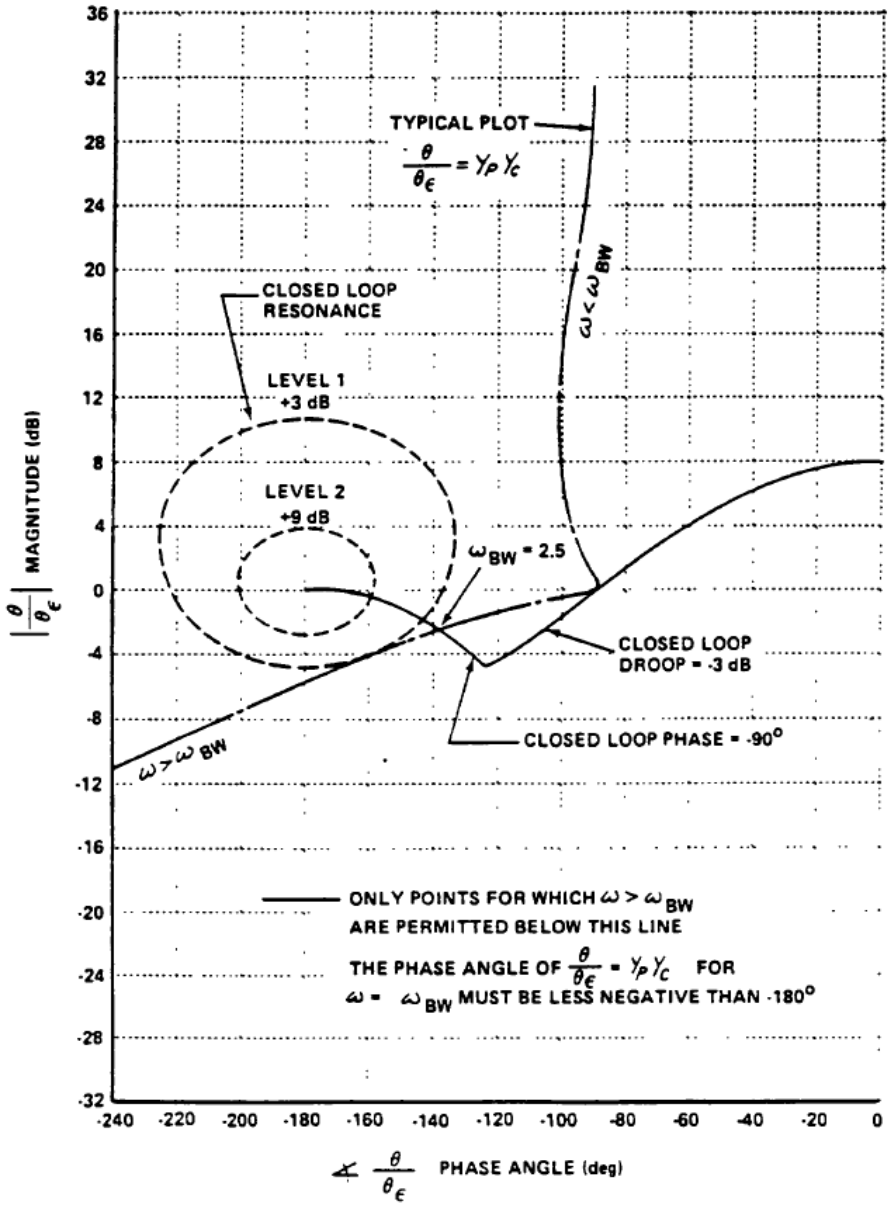

Figure 14. Nichols Chart Depicting Pilot in the Loop Pitch Response Design Criteria [4]

The preceding discussion highlighted the extensive amount of research conducted to determine mathematical techniques for estimating flying qualities of manned aircraft. These accepted concepts constitute the present day standards for the procurement of new piloted aircraft. However, the rays of a new dawn are beginning to illuminate the skies with the advent of the UAV. The manned aircraft flying qualities knowledge-base certainly grants a head start for future research, however, these new machines pose an entirely new set of challenges in the field of aviation.

2.4 The Evolution of the UAV

While UAVs represent the cutting-edge of flight technology, they are not truly a new concept. Unmanned aircraft actually share a history as old as their manned counterpart. Recalling previous discussion, Langley found much success with his invention of his unmanned aerodrome as early as 1896 [16]. However, there would be a sharp schism in the successes of the two different technologies. Manned aircraft went from being few in number, and used solely to dazzle spectators with aerobatics, to suddenly being produced in the thousands, and serving a focused military purpose. At this junction, however, unmanned aircraft, were just barely making it out of the hangar.

Just as it was impossible for a bicycle to ride from point to point without human guidance, so too was autonomous flight. One of the first figures to emerge in solving this problem was Elmer A. Sperry. From his experience working with maritime gyroscopes, Sperry ventured to build a gyrostabilization device for airplanes in 1909 [58]. His initial motivation was to improve manned flight safety, as this device would cause an aircraft to level its wings in case a pilot flew into vision-impairing weather and experienced spatial disorientation. At 30 pounds, the initial design was unfortunately far too heavy. When it was finally integrated onto an aircraft, it was found to perform

poorly in the three flight axes.

In 1911, Sperry re-attacked the problem by using smaller gyros, one for each of the roll, pitch, and yaw axes. Another aviation pioneer, Glenn H. Curtiss, partnered with Sperry and worked to gain support from the US Army and Navy. After witnessing a hand-full of gyrostabilizer induced crashes, the Army ceased its support. Around the same time, the Navy would also defer any purchases, citing that the stabilization machine was simply not a substitute for a well trained pilot [58].

Undeterred, Sperry continued his work which would shock the world just three years later. In 1914, Sperry consolidated the three-gyro system and mounted it on a Curtiss seaplane. Sperry then traveled to France with his son, Lawrence, and entered the nation's Airplane Safety Competition [54]. During the first aerial pass over the Seine River, Lawrence stood up with raised hands, not touching any controls, much to the excitement of a crowd of eager spectators. During the second pass, pictured in Figure 15, mechanic Emile Cachin, climbed out on a wing, while Lawrence's hands were still off the controls. The seaplane automatically maintained stable flight with wings level, further amazing the crowd, and winning Sperry both the competition, and the Collier Trophy for most noteworthy aviation achievement of 1914.

Figure 15. The 1914 Curtiss seaplane augmented by the Sperry gyrostabilizer over Bezons, France [58]

With World War I just over the horizon, further development of this manned flight

augmentation system would soon evolve into a fully unmanned "aerial torpedo" [34]. A new problem arose in the early stages of this effort. The stabilization equipment would simply not function due to the initial upset associated with the violent nature of aircraft launch. The aircraft, ordered from the Curtis Aeroplane and Motor Company, were outfitted and flown for just 12 test flights before all six were completely destroyed. While some crashes were attributed to failures during launch, or gyrostabilizer issues, the chief problem was in the lack of understanding of the aircraft flying qualities. Testing of this sort was of an empirical nature, and sufficient work was not done in relating aircraft geometry to stability derivatives, and incorporating the gyrostabilizer as a system with the required amount of feedback control.

While working on the first aerial torpedo project, Sperry was also pursuing the development of a radio control system. He actually obtained the first patent for such a device in December 1917. This would prove to be a game changer in the coming years. By 1920, military interest peaked again with a renewed realization of the utility of an unmanned aircraft. Sperry was awarded another contract to produce 20 aircraft with unmanned and autonomous capability. While stabilization systems were becoming more and more accurate, they were still insufficient in response to unpredictable winds or gusts. In 1922, the Army initially agreed that adding radio controls would still allow Sperry to meet the terms of his contract. The radio control system that he would install quickly became an invaluable asset, as it was used dozens of times to correct aircraft heading and attitude in subsequent test flights [54]. However, the terms of the contract quickly sparked controversy. After all, the aircraft were intended to be fully autonomous, but were now only as effective as their remote operator and the link between them. Eventually, the Army deemed the experiment to be a success and awarded Sperry $20,000.

Parallel to the Army's effort, the Naval Research Laboratory was also tackling the

problem of radio control. A Curtis N-9 was outfitted with improved technology, and flown perfectly under the supervision of a safety pilot. Once systems were checked out, the N-9 was sent on its first unmanned flight, clocking 40 minutes and successfully executing 49 out of 50 commands [54]. The equipment was then transferred to a new Vought seaplane and flown with a safety pilot for the remainder of 1924. After 30 more test flights, the Vought airplane was finally deemed ready to go unmanned. Unfortunately, upon takeoff, the airplane began to porpoise. On the last bounce, a pontoon tore loose, resulting in a propeller strike as the aircraft sunk to a crash.

Upon investigation, it was found that this oscillation was induced by the operator, because the control technology at the time required that human commands be input through push buttons, rather than a joystick which would have been much smoother [54]. Recalling the closed-loop control criteria mentioned in the previous section, the pilot is mathematically represented as a transfer function with a gain and time delay. In the case of UAVs, if the time delay is too long, the system is driven to instability. Said in plainer terms, a human operator is simply unable to adequately control the aircraft from the ground, because the time delay between sending the commands and seeing the effect of the commands is too long. This is exactly what occurred during flight test with the Vought airplane. The ground-based operator lost control of the aircraft due to the excessive time delay between pushing buttons on the controller and the actuation of the aircraft control surfaces. For manned aircraft, this phenomenon is referred to as a Pilot Induced Oscillation (PIO), and occurs when a pilot begins to move the controls to input a series of opposing commands, and inadvertently executes a series of over-corrections.

In the 1930's, the British began experimenting with using remote controlled aircraft as targets for pilots to be able to refine their airmanship skills [19]. Some say that it was actually there, across the pond, where UAVs earned their most enduring

name as the "drone". It started when the British Fairey aircraft company converted their manned IIIF scout aircraft into an unmanned version, and ended up calling it the Queen Bee. Male bees, of course, are called drones, and thus the term was coined. Although the origins of the naming are somewhat foggy, it is a fact that the lead US Navy radio-controlled unmanned aircraft project officer first referred to the effort as the "drone project" in 1936.

The fledgling field of unmanned aviation would yield many entrepreneurs, just as it did for piloted aircraft. The British Reginald L. Denny is considered the father of the modern Radio Control (RC) aircraft hobby complex [54]. He is credited with leading the way in small scale aircraft, which evolved to become some of the most widely used machines of their type in the 1930s. In 1946, a model based on Denny's OQ-19 was refined and almost 50,000 were built. Soon the aircraft was modified to serve as a reconnaissance machine rather than just an aerial target. Indeed this is what modern UAVs are most known for. Arming them with film-cameras, the Army would introduce these aircraft as the AN/USD-1 Observer and ordered almost 1,500.

The beginnings of the Cold War would serve to reinvigorate efforts to bring unmanned reconnaissance aircraft into service. Data collected from World War II showed just how staggeringly dangerous reconnaissance missions were. One out of four pilots would be killed while flying intelligence missions over North Africa, versus just over one out of 20 pilots being lost in bombing missions over Germany [54]. The tense political climate between opposing nations made things even worse, with the Americans and Soviets blatantly refusing to acknowledge the shoot-down or capture of their airmen. Around the same time, methods for the delivery of nuclear weapons were also being developed. The advent of the intercontinental ballistic missile brought about highly accurate positioning systems, like the inertial navigation system. It also brought about the need for more responsive surveillance.

These new technological and political developments provided momentum for the design of more accurate UAVs, which would be ready just in time for the Vietnam War. The most notable unmanned vehicle of the conflict was the Ryan AQM-34 Lightning Bug. Its concept of operations dictated that the UAV be jettisoned from pylons on a C-130 during mission start, and then recovered by another C-130 while floating under parachute at mission conclusion. Over 20 variants of the AQM-34 were produced [54]. The vehicle was not only used to collect imaging reconnaissance, but also electronic and communications intelligence. Other variants were outfitted with countermeasures like chaff and sent over enemy territory in advance of manned aircraft to carry out suppression of enemy air defense objectives.

Between 1964 and 1975, over 1,000 AQM-34s flew almost 3,500 missions [54]. In contrast to their success rate, over 500 vehicles were lost with one out of six crashes attributed to mechanical or stability issues. Three of these losses were found to be the result of unintentional radio frequency jamming by friendly assets. This underscores the fact that the 'A' in UAV stands for *Aerial*, and not *Autonomous*. A ground-based pilot was still required to fly UAV missions, and thus the term Remotely Piloted Vehicle (RPV) was coined.

As the Cold War carried on, Intelligence, Surveillance, and Reconnaissance (ISR) missions became more prevalent than ever. While satellite technology was getting spun up, and spaceborne assets began providing persistent overhead surveillance, they fell short in the arena of on-demand and real-time data collection. Thus, the workhorse of choice was the manned U-2 Dragon Lady. Operating well above other airborne threats, and capable of exceedingly long dwell times, the U-2 still had its own set of problems. The pilot would be forced to operate his aircraft in what was known as the "coffin corner" of the flight envelope. This region existed just one knot below overspeed, and just one knot above stall speed [54]. Making matters even more

troublesome, the U-2 was still susceptible to high altitude surface-to-air missiles, and was just one shoot down away from international incident.

These factors motivated the hunt for a High-Altitude Long-Endurance (HALE) UAV. These aircraft were designed to fly at altitudes at or above 50,000 feet and for 24 hours or more in a single mission. The year 1974 would see a new record for aircraft endurance, with the success of Teledyne Ryan YQM-98 Tern, which, clock a flight time of 28 hours and 11 minutes in a single sortie [66]. These successes in industry were used as proof that UAV technology was maturing, and positively secured funding for further research in the following decades.

The early 1990s saw the creation of new programs known as Advanced Concept Technology Demonstration (ACTD) projects [67]. UAVs produced under this process would be fielded in three to four years rather than the one or two decades required for typical government acquisition programs. Under the ACTD program, a UAV would be delivered to a combatant commander in the field, without necessarily being a final product that came with a well specified sustainment process, inventory of spares, or even an operator training program. It was left to the commanders to deem if the vehicle would even add value to the fight. This acquisition process considered all products to be experiments, and UAVs were considered successful regardless of operational failures or rejection by commanders in the field [54].

The MQ-1 Predator UAV is one example of the aircraft produced under an ACTD program. Based on the Gnat-750, General Atomics ASI already had a larger vehicle on the drawing board. The Predator's first flight lasted for just 20 seconds. However, in early 1995, it demonstrated a 40 hour endurance, and was flown for 25 out of 26 days during a military exercise in New Mexico. It successfully imaged over 200 ground targets, and delivered 85% of collected imagery during the exercise. After proving itself in the arena, it was quickly delivered to commanders for use in the

Bosnia conflict. To add to its capability, a gimbaling video camera was mounted to the front. Although prone to its own set of problems, the system is so successful, that it has been continuously deployed since 1998 [67].

Another ACTD program led to the creation of the Global Hawk [54]. Officially rolled out in 1997, its first flight was at Edwards AFB, California a year later. During the following years, five test vehicles would break new flight records in altitude (66,400 feet) and flight time (31.5 hours). Not only were these flights record-setting, but they also created a precedent for DoD operations in civilian airspace, requiring approvals from the Federal Aviation Administration (FAA) during domestic flight testing, and even European aeronautical authorities.

As the saying goes in the field of unmanned systems, UAVs have found a niche in performing those tasks which are too "dull, dirty, or dangerous" for their manned counterparts. These aircraft have obvious wartime utility, but their capabilities far outreach the battlspace environment. In 2007, two RQ-4 Global Hawks were transitioned from the USAF for use by NASA in earth science missions [49]. While manned research aircraft, carrying weather sensors, have been safely sent to collect data on atmospheric phenomena, like hurricanes, they simply cannot fly for as long as UAVs. This means that manned aircraft would have to wait for storms to get closer to land, before taking-off and being able to collect any useful data. The NASA operated Global Hawk has already proven itself over the ocean skies of the Atlantic and Pacific. In fact, it was most recently used in November 2016 to collect atmospheric information over Hurricane Matthew [49], filling in the gaps between traditional ground-based and satellite data collection, and considerably improving forecast accuracy.

NASA has also successfully transitioned the RQ-14 Draqon Eye UAV from the US Marine Corps [51]. The UAV was used to conduct earth science research over active volcanoes. Weighing just six pounds, and propelled by two electric engines,

the aircraft were flown directly into a volcanic plume to collect data for up to one hour at a time. Missions like this are undoubtedly hazardous for manned aircraft, as their airframes and engines can be destroyed instantly by strong updraft winds and heavy concentrations of volcanic ash.

Unmanned aircraft technology is seeing unprecedented proliferation today. Figure 16 sheds light on the large number and wide variety of UAVs that the DoD operates. This is just the tip of the iceberg, however, as the Teal Group predicts that the UAV industry will rise annually to $14 billion by 2025 [32]. The "Unmanned Systems Integrated Roadmap" for years 2013 through 2038 [75], asserts that the DoD intends to be the most innovative user of unmanned systems.

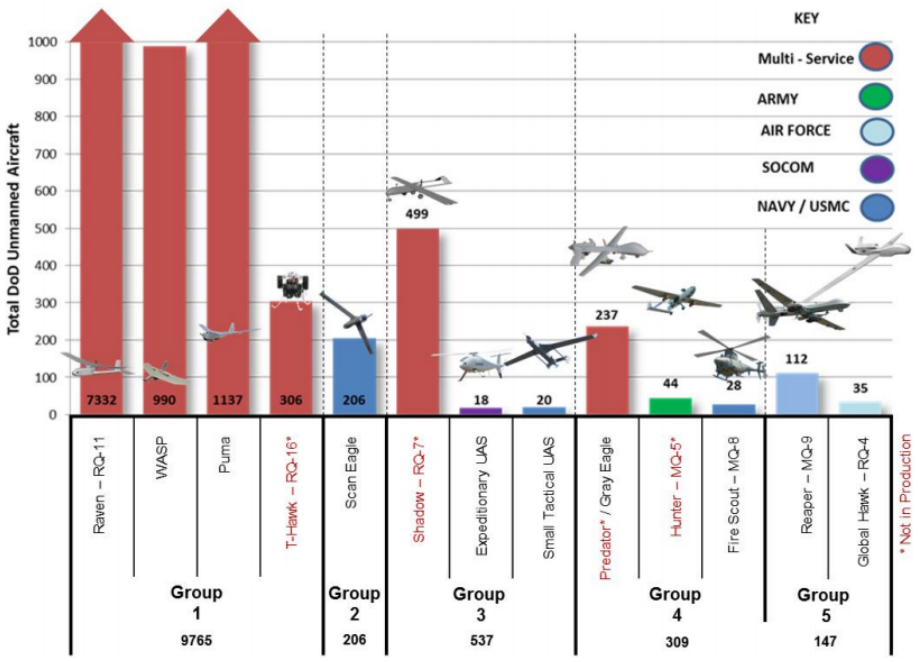

Figure 16. The Diverse Fleet of DoD UAVs as of 2013 [75]

In accomplishing this goal, the Roadmap addresses a new set of safety challenges yet to be surmounted [75]. After all, there is a dark side to the success of these aircraft. They have risen in popularity because they take the human out of harm's way in the traditional sense. However, they introduce a whole new set of risk factors

when considering potential crashes over populated areas, or collisions with manned aircraft. The gravity of this issue was detailed in Chapter I, with flying qualities research being identified as a key area of focus. It is the aim now, to understand how requirements for these aircraft have come to be, and in doing so, provide insight that could guide further research.

2.5 Flying Qualities Standards for UAVs

The first official document for unmanned aircraft flying qualities was published as AFFDL-TR-76-125 "RPV Flying Qualites Design Critera" [3] in 1976. The document was very similar to the manned criteria at the time, MIL-F-8785 [1], in content and organization. However it was not a standard in the true sense, but rather an incremental work as part of a larger four-phase flying qualities research program. It was intended to suggest flying qualities criteria which could then be verified in a following flight test phase. Unfortunately, future work did not occur as planned, and the document has not been updated since its original publication. Nonetheless, it offers some noteworthy points for consideration.

Much like the current MIL-STD-1797B, AFFDL-TR-76-125 shares the aircraft class and flight phase category methods of organizing aircraft. However, in contrast to manned standards, the aircraft class system relates to maneuverability alone, rather than a correlation between weight and designed G-loading. The 1976 document defines Class 1 to cover mini UAVs, and Classes 2 through 4 to encompass UAVs with low, medium, and high maneuverability, respectively. The document argues that comparing weight and maneuverability is not as useful, because unmanned aircraft with very similar weights can offer wide ranging levels of maneuverability. Comparing aircraft weight and mission alone, is also troublesome, because this would create too many categories [3].

Appropriately classifying unmanned aircraft is vital to specifying flying qualities requirements. The reason manned aircraft are grouped together based on gross weight and designed G-loading, is because this method of categorization highly relates to mission type, which in turn relates to design requirements for aircraft dynamic response. Categorizations of unmanned aircraft based solely on size, weight, or mission parameters is problematic, because for UAVs, these characteristics may not relate to system dynamic response.

To address this concern, a study in 2010 [29] suggested the categorization of UAVs based on Reynolds number and gross weight. This is because Reynolds number relates to the "lift, drag, and pitching moment coefficients that in turn have a large impact on short period and phugoid natural frequency and damping ratio." Gross weight serves as the second variable of correlation because of its relationship with aircraft range and performance. The 42 aircraft that were compared can be seen in Figure 17.

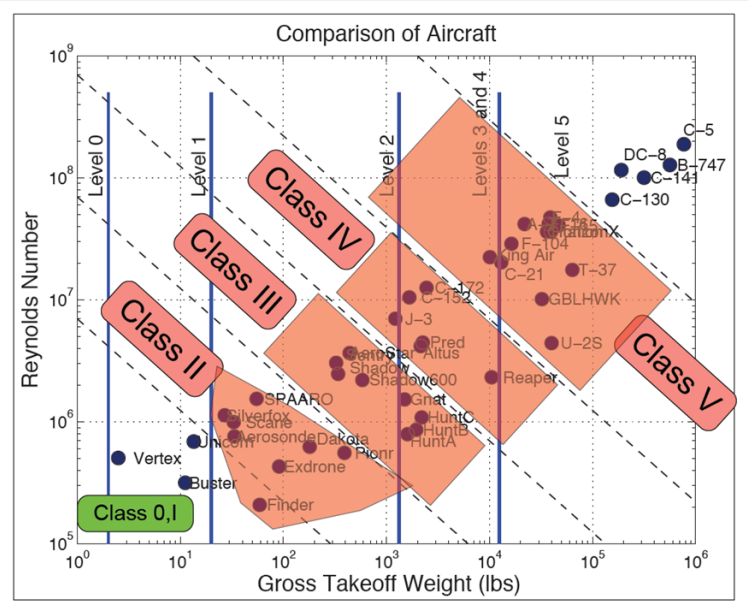

Figure 17. UAV Classification System Based on Reynolds Number and Weight [29]

AFFDL-TR-76-125 [3] goes further to introduce a fourth flight phase category

to the three phases discussed in current manned standards. Category D flight was designated to describe terminal area operations that involve launch and recovery techniques different from classical aircraft takeoff and landing. This is explained to allow for more precise requirements that would entail UAVs being launched from other aircraft, or being recovered under parachute.

It was suggested that perhaps a mission-based standard, such as this, is more effective for specifying flying qualities for UAVs [39]. This technique is actually widely accepted for manned rotary-wing aircraft, and is detailed in ADS-33E-PRF "Aeronautical Design Standard Performance Specification Handling Qualities Requirements for Military Rotorcraft" [5]. The Army rotorcraft document specifies requirements for flying qualities as they relate to specific Mission-Task-Elements (MTEs). Further along these lines, a technical report from HOH Aeronautics and Systems Technology [48] details how these MTEs should be incorporated into fixed-wing standards, which would prove to be particularly useful for UAVs. The report presented the MTEs that would fall under flight phase categories based on maneuvering precision and aggressiveness, as shown in Table 2.

Table 2. Categorization of Mission-Task-Elements [48]

Non-Precision Tasks		Precision Tasks	
Non-Aggressive Category B	Aggressive Category D	Non-Aggressive Category C	Aggressive Category A
Reconnaissance	Gross Acquisition	Aerial Recovery	Tracking
Climb	Anti-submarine	Close Formation	Ground Attack
Takeoff	Max G Turn	Approach	Terrain Following
Non-precision Landing	"Herbst" Turn	Precision Landing	Precision Aerobatics

In terms of literal factors, like phugoid and short period frequencies, a 2005 study proposes that current manned aircraft parameters can be modified to fit UAVs, through a process known as dynamic scaling [33]. The concept is exceedingly simple in that the short period natural frequency for a UAV, for example, can be determined

by multiplying the short period natural frequency of a larger, manned aircraft by a numerical factor. The method has been shown to work [24], however, the drawback is that it requires data taken from a manned aircraft which is representative of the smaller scale UAV. This may be possible when comparing the U-2 to the RQ-4, but is not possible in the case of many existing UAVs today.

The discussion up to this point details objectively measurable or calculable UAV stability characteristics as they relate to levels of flying qualities determined from flight testing with manned aircraft. There is still the question of assessing operator workload and performance with UAVs. In his research published in 2010, M. Christopher Cotting suggests the use of a similar, but modified Cooper-Harper rating scale, pictured in Figure 18, for use with UAVs [29]. Instead of focusing on the pilot and aircraft, this scale considers the entire UAV system, from operator, to ground station, to aircraft, and then back to the operator.

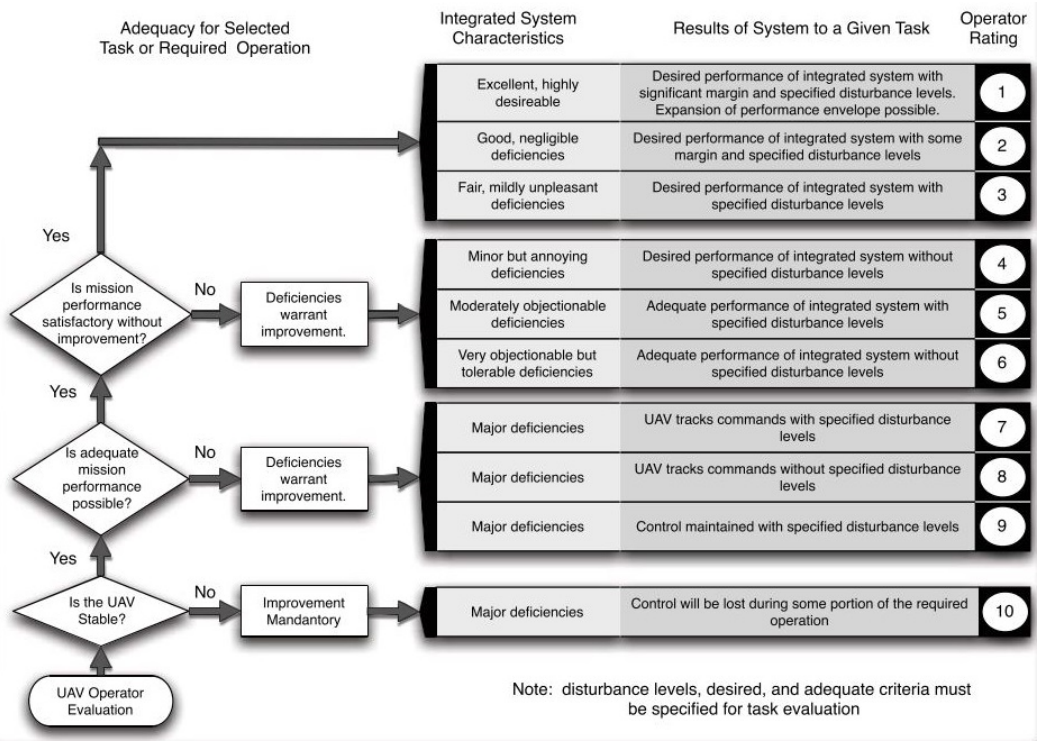

Figure 18. Modified Cooper-Harper Rating Scale for UAVs [29]

Applying manned aircraft flying qualities standards to UAVs may prove to be too restrictive, and thus hinder the potential for designing an unmanned aircraft with more superior capabilities. In order to properly uncover the aircraft flying qualities which are specific to unmanned aircraft, it is necessary to collect a large amount of data produced through extensive flight testing. This is precisely what was done with the variable stability NT-33 in gathering invaluable insights through the creation of the Neal-Smith database [52], in which aircraft stability and control characteristics were varied and then correlated to pilot opinion through the Cooper-Harper rating scale.

While many UAVs are remotely piloted, like the MQ-9 [72], some are operated in a more autonomous fashion, like the RQ-4, which draws its inputs from human generated task-lists rather than direct control surface inputs [8]. A modified Cooper-Harper rating scale for UAVs [29], as previously shown in Figure 18, provides a subjective means of rating UAV/operator workload as it relates to achieving desired maneuvering performance. Perhaps more objective metrics can also be used to evaluate these system parameters.

Research presented in 2016, addressing the design of control systems for small UAVs flying in turbulent environments, had several interesting findings. Specific servo motors were selected for their cost effectiveness and quick response time. When the test UAV was flown in heavy turbulence, using control laws optimized for rapid rejection of flight path angle disturbances, it was found that the servo motors were operating close to their rate saturation levels. Continuous operation in these conditions, on the order of just minutes, would result in the servo motors burning out, and rendering them ineffective [13].

In light of these results, and UAV concepts of operations trending toward autonomous control, as opposed to remotely piloted control, perhaps metrics can be

devised that correlate the workload of an aircraft, itself, to its performance throughout a designated maneuver.

Previous research [43] used such metrics to evaluate the workload and performance of a simulated T-41 single-engine piston aircraft as it performed a climbing spiral turn, a non-precision, non-aggressive mission task. When the results were analyzed relative to flying qualities assessments, using established manned aircraft criteria, there were several cases that suggested manned criteria may simply not be a good indicator of how hard an autonomous aircraft would have to work to achieve desired tracking performance throughout a given maneuver.

There are another three categories of MTEs into which further research can be conducted. Ultimately, there is no complete substitute for live flight testing. It is, however, a costly undertaking, and, thus, before taking to the runway, it is important to run computer simulations. The data gained from these trials can be analyzed to assess the applicability of specific aircraft workload and performance metrics. A particular mission task can also be evaluated for its usefulness in providing insight into unmanned aircraft flying qualities.

2.6 Flying Qualities Research Using Computer Simulation

By the same token, computer simulations, themselves, can prove to be quite expensive. Computing power requirements, and complex proprietary software can easily make things cost prohibitive. Fortunately, there are open-source and high fidelity software tools available, like JSBSim.

The software package [21], named after its creator, Jon S. Berndt, exists as a compilation of mostly C++ code . The C++ classes constitute flight dynamics model elements like the atmosphere, engines, and flight control systems. The software combines these constructs with control inputs and calculates resultant aircraft forces and

moments. These values are then integrated to advance vehicle states, like velocity and attitude, in set time increments.

Originally conceived in 1996, JSBSim has been used in several notable aircraft design projects. One such example is the DuPont Aerospace DP-1 vertical takeoff jet aircraft [20]. The company successfully used the JSBSim flight dynamics model in order to conduct flying qualities research with flight actuators operating in the control loop. When other software tools were deemed inadequate, JSBSim proved itself as a robust design tool, in allowing for accurate, six degree-of-freedom, non-linear, simulation of the aerodynamic forces that hovering flight entails. Using this software tool, DuPont Aerospace was finally able to design an aircraft that could takeoff and hover, while completely under autopilot control.

Other research efforts that leveraged JSBSim, include projects like the Aerocross Echo Hawk UAV [20]. The flight dynamics library worked seamlessly with flight hardware and was used extensively to train operators. JSBSim was even used in official projects carried out with the US Department of Transportation, in the development of a mathematical model for a human pilot [20]. Further details as to how JSBSim works, and how it will be used in this research effort, will be presented in Chapter III.

2.7 Summary

The preceding discussion began by providing evidence for the assertion that flying qualities research is vitally important to the design of safe and well-performing aircraft. The flying qualities of an aircraft are directly related to its geometry and control systems. Once a purely empirical art, aircraft design evolved into an analytical science. Only then, were engineers finally able to perform calculations that could predict how well an aircraft would fly, before having to cut materials and build

full-scale models. By using tools like the variable stability aircraft, engineers were able to verify calculated assumptions and gather extensive data relating specific aircraft stability characteristics to levels of flying qualities. To this day, the resulting flying qualities database provides an understanding as to how design parameters relate to pilots' perceived workload in maneuvering their aircraft to achieve desired performance objectives.

UAVs stem from a history as deep as their manned counterpart. However, the two technologies vastly diverged in popularity in the early years. With the advent of automatic flight control and remote communication systems, UAVs became prevalent in both military and civil applications. The rich knowledge-base of manned aircraft flying qualities serves to provide a boost for similar research with UAVs. However, it is still not fully understood which techniques are most relevant, or how best they can be applied to these unmanned systems. Various solutions to this challenge were suggested by previous research in the field. Regardless of the specific techniques that were presented in these efforts, they all came to the similar conclusion that advocates the creation of an unmanned flying qualities database. This would ultimately inform the future design of new UAVs and the techniques that can be used to augment current systems. In beginning this process, computer simulation is a cost effective tool that should be leveraged as a preface for real-world flight testing with variable stability aircraft. The following chapter will serve to detail the methodology of using these tools for such an effort.

III Research Methodology

The research findings and recommendations discussed in the previous chapter represent a diverse subset of areas for further flying qualities investigations. Regardless of the specific item of interest explored in these studies, they were all in accord in advocating the establishment of a UAV flying qualities database. A compendium of information, such as this, would shed light on the stability and control characteristics that are most desirable for achieving unmanned aircraft performance benchmarks, during set tasks, without overburdening on-board computer processing systems or the actuators and flight surfaces which they command.

This chapter begins with a discussion of the metrics to be used in assessing aircraft workload and performance. Next, the fundamentals of computer simulation are described in detail and the process by which JSBSim is configured to model the flight of an F-16 is outlined. The discussion continues by identifying relevant calculations for selected methods of flying qualities assessments from MIL-STD-1797 [4]. The final part of this section explains the design of the two aircraft longitudinal-axis autopilots to be used for this research.

3.1 Aircraft Performance and Workload Metrics

Flying qualities assessments of manned aircraft rely on pilot opinions of aircraft handling by use of the Cooper-Harper scale. Since the human is out of the loop in the scenarios presented here, evaluation metrics must quantify the performance and workload of the aircraft alone.

A measurement of the disparity between aircraft command inputs and actual achieved aircraft states, in simulation, can serve as an accurate metric for aircraft performance. The time history of aircraft commands can be compared to the time

history of actual aircraft states by calculating Theil's Inequality Coefficient (TIC). While the TIC metric traces its origins to financial market forecasting [76], it has successfully been used in the aerospace industry [42] to evaluate differences between the time histories of aircraft states during real-world flight, and computer simulation. In a study at the University of Minnesota [31], which used a UAV platform, TIC was shown to be an applicable metric for both linear and non-linear control systems. The coefficient is given by the relationship expressed in Equation 1

$$TIC = \frac{\sqrt{\frac{1}{n}\sum_{i=1}^{n}(x_i - \tilde{x}_i)^2}}{\sqrt{\frac{1}{n}\sum_{i=1}^{n}x_i^2} + \sqrt{\frac{1}{n}\sum_{i=1}^{n}\tilde{x}_i^2}} \tag{1}$$

where x_i is the command input to the aircraft at a given instant in simulation, $\tilde{x}_i$ is the actual aircraft state at that instant, and n is the number of instances that occur throughout the duration of the time history.

TIC values can fluctuate between zero and unity. A value of zero indicates perfect performance, in that the aircraft followed commands exactly. Values closer to one represent large deviations between the two time histories being compared, which indicates poor performance. Typically, values around 0.25 or higher are indicative of significantly degraded performance. Or in other words, significant disparity between commands and achieved aircraft states [31].

In order to evaluate the workload of the aircraft, the deviation of flight control surfaces away from their trimmed configuration can be measured. Larger, and for that matter, more frequent movements of a control surface from its initial, trimmed, configuration require actuators to work harder in driving control surfaces, and require computer systems to work harder in calculating new control inputs, all while responding to rapidly changing aircraft states.

JSBSim, the computer simulation software of choice, outputs control surface po-

sition in units of radians, degrees, or as a normalized value. For example, if a control surface can deflect between negative ten degrees and positive ten degrees, and at a given instant the control surface is deflected at positive five degrees, JSBSim gives its normalized position as positive 0.50, indicating that the control surface is deflected to half of its maximum amount. Because of this native software capability, it was suggested in previous research [43] that the $\mathcal{L}_2$ error norm be used as a metric to describe the workload of the aircraft in deflecting control surfaces away from their trimmed position. This metric is given by Equation 2

$$\mathcal{L}_2 = \sqrt{\frac{1}{n}\sum_{i=1}(x_1(i) - x_2(i))^2} \tag{2}$$

where $x_1(i)$ is the normalized control surface deflection at a given instant, $x_2(i)$ is the constant normalized control surface deflection in the trimmed configuration, and n is the number of instances.

The $\mathcal{L}_2$ norm represents the average difference between actual and trimmed control surface deflections throughout a given maneuver. Values closer to unity are indicative of control surfaces having to deflect further from their trimmed position throughout a given maneuver, and thereby signify higher aircraft workload.

Now that the metrics have been established, it is necessary to generate actual flight simulation data. This requires an explanation of how JSBSim is configured, and how it operates. Toward this understanding, it is first necessary to review the mathematics which explain flight dynamics.

3.2 Fundamentals of Computer Simulation

As mentioned previously, the mathematical secrets of aircraft dynamics were unlocked when Bryan applied first principles, authored by Euler and Newton, to air vehicles, in 1911. The result of his research manifested as a system of first-order dif-

ferential equations, describing the rates of change of aircraft states. Flight simulators are founded upon these very equations. Given a set of initial conditions, the rates of changes of aircraft states (pitch-rate, velocity, etc.) at a given time step in simulation, are integrated to yield the new aircraft states occurring in the following time step. This propagation of aircraft states is what constitutes the flight simulation.

In developing these equations, the first step is to define the appropriate aircraft reference frames. The body-fixed, stability, wind, and earth-fixed reference frames are delineated in Figure 19.

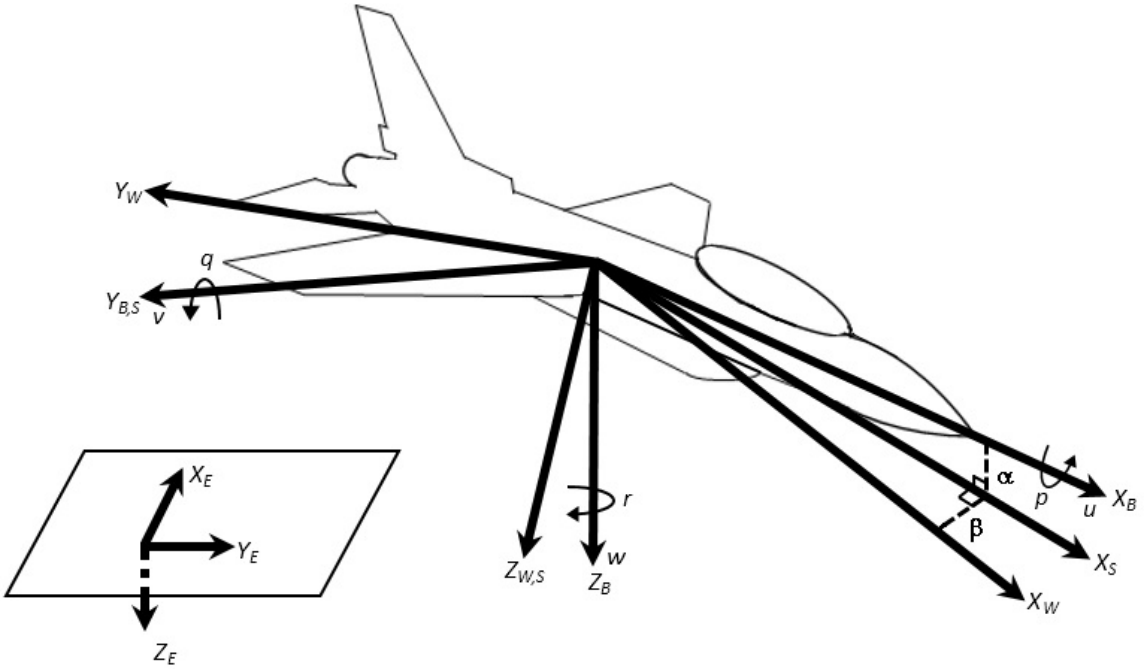

Figure 19. Diagram of Aircraft Body, Stability, and Wind Axes, and Earth Fixed Reference Frame

With the exception of the earth-fixed reference frame, shown in the bottom left corner of Figure 19, all other reference frames have their origin at the aircraft center of gravity (CG). The body-fixed reference frame is right-handed and orthogonal, and has its three axes denoted as X_B, Y_B, and Z_B. The X_B-axis points forward, through the nose of the aircraft, the Y_B-axis points outward through the right wing, and the Z_B-axis points downward. The aircraft can translate forward and aft along,

and rotate about the X_B axis with linear velocity, u, and roll-rate, p, respectively. The aircraft can also translate laterally along, and rotate about the Y_B-axis, with linear velocity, v, and pitch-rate, q, respectively. Finally, the aircraft can translate upward and downward along, and rotate about the Z_B axis with linear velocity, w, and yaw-rate, r. Now, the first simplifying assumption must be made. The aircraft is considered to be a rigid body, meaning that all particles that make up the airframe are rigidly attached to the particle at the aircraft CG. The particle at the aircraft CG, and in turn the entire aircraft, has freedom of motion which is limited to translation in three dimensions, and rotation in three dimensions. The three translations and three rotations constitute the aircraft's six degrees-of-freedom.

The next reference frame is the stability-axes frame, denoted by X_S, Y_S, and Z_S. This frame is used for calculating the effect of perturbations on the aircraft from its steady, level, unaccelerated state in equilibrium flight. Its orientation is defined by a left-handed Euler rotation about the Y_B-axis through the angle of attack, α. Thus, converting from the body-fixed reference frame to the stability reference frame requires the rotation matrix expressed in Equation 3.

$$C^{SB} = \begin{bmatrix} \cos\alpha & 0 & \sin\alpha \\ 0 & 1 & 0 \\ -\sin\alpha & 0 & \cos\alpha \end{bmatrix} \tag{3}$$

The aerodynamic lift, drag, and side forces are defined in the wind-axes reference frame denoted by X_W, Y_W, and Z_W. This reference frame is obtained from the stability-axes frame by a Z-axis rotation through the sideslip angle, β. This is described by the rotation matrix in Equation 4.

$$C^{WS} = \begin{bmatrix} \cos\beta & \sin\beta & 0 \\ -\sin\beta & \cos\beta & 0 \\ 0 & 0 & 1 \end{bmatrix} \tag{4}$$

Concatenating these two rotation matrices, yields Equation 5, which is the rotation matrix required to transform from the body-fixed frame to the wind-axes frame.

$$C^{WB} = \begin{bmatrix} \cos\alpha\cos\beta & \sin\beta & \sin\alpha\cos\beta \\ -\cos\alpha\sin\beta & \cos\beta & -\sin\alpha\cos\beta \\ -\sin\alpha & 0 & \cos\alpha \end{bmatrix} \tag{5}$$

The second assumption in deriving aircraft equations of motion, is establishing that the earth-fixed reference frame is a non-rotating (i.e. inertial) reference frame. This is required for the calculations described by Newton's Second Law, which necessitate that derivatives be taken relative to an inertial reference frame. The aircraft's dynamics must now be defined by its position, velocity, orientation, and angular velocity relative to the earth-fixed reference frame.

Figure 20 introduces the aircraft Euler angles, roll (ϕ), pitch (θ), and yaw (ψ), along with the previously defined angular rates, p, q, and r. The three Euler angles constitute the three-dimensional Euler orientation vector, $\vec{\Phi}$. The three-dimensional angular rates constitute the three-dimensional angular velocity vector, $\vec{\omega}$.

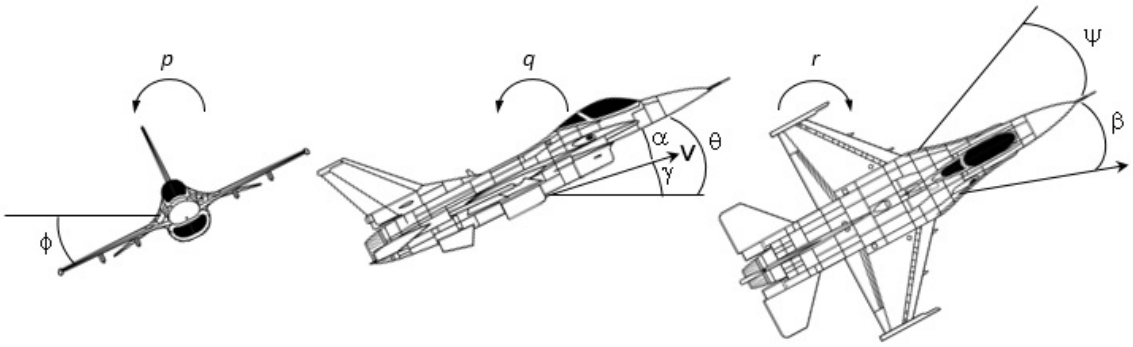

Figure 20. Diagram of Aircraft Orientation Angles (ϕ, θ, ψ), Angular Rates (p, q, r), Aerodynamic Angles (α, β), and Flight Path Angle (γ)

The aircraft's body-fixed reference frame can be related to the inertial, earth-fixed, reference frame through a direction cosine matrix. This rotation matrix, shown in Equation 6, is a concatenation of a Z-axis rotation with angle ψ, then a Y-axis rotation with angle θ, and, finally, an X-axis rotation with angle ϕ.

$$C^{BE} = \begin{bmatrix} 1 & 0 & 0 \\ 0 & \cos\phi & \sin\phi \\ 0 & -\sin\phi & \cos\phi \end{bmatrix} \begin{bmatrix} \cos\theta & 0 & -\sin\theta \\ 0 & 1 & 0 \\ \sin\theta & 0 & \cos\theta \end{bmatrix} \begin{bmatrix} \cos\psi & \sin\psi & 0 \\ -\sin\psi & \cos\psi & 0 \\ 0 & 0 & 1 \end{bmatrix} \tag{6}$$

This set of Euler rotations gives way for the rotation matrix that transforms body-fixed rotation rates to Euler angle rates. Shown in Equation 7, the body-fixed rotation vector $\vec{\omega} = [p\ q\ r]^T$ can be transformed to the Euler angle rate vector $\dot{\vec{\Phi}} = [\dot{\phi}\ \dot{\theta}\ \dot{\psi}]^T$.

$$C^{\dot{\Phi}\omega} = \begin{bmatrix} 1 & \sin\phi\tan\theta & \cos\phi\tan\theta \\ 0 & \cos\phi & -\sin\phi \\ 0 & \frac{\sin\phi}{\cos\theta} & \frac{\cos\phi}{\cos\theta} \end{bmatrix} \tag{7}$$

It is important to note that this Euler rotation method can be problematic in some special cases. If the pitch angle, θ, passes through 90 degrees or 270 degrees, the differential equations encounter a singularity. In order to avoid this problem, aircraft orientation can be represented using the four-valued quaternion system. JSBSim will

in fact use quaternions to propogate the equations of motion [21]. While useful, and in many cases, completely necessary for use in computer simulations of vehicle dynamics, quaternions are more difficult when trying to understand vehicle orientation intuitively. Nonetheless, a detailed explanation of this derivation is readily available in many textbooks, including *Aircraft Control and Simulation* [64].

Returning to developing the Euler equations, the total aircraft velocity in the body-frame, V_T, is made up of the three-dimensional velocity components u, v, and w, as shown in Equation 8.

$$V_T = \sqrt{u^2 + v^2 + w^2} \tag{8}$$

The angle of attack can be determined by Equation 9.

$$\alpha = \arctan \frac{w}{u} \tag{9}$$

The side-slip angle, β, is defined by Equation 10.

$$\beta = \arctan \frac{v}{V_T} \tag{10}$$

When both the side-slip angle, β, and the roll angle ϕ are zero, the flight path angle, γ, is given by Equation 11.

$$\gamma = \theta - \alpha \tag{11}$$

Now that the relationships between reference frames have been established using Euler's principles, the fundamentals of Newton can be applied. The linear motion that occurs along the three translational degrees of freedom can be calculated by using Newton's Second Law. Shown in Equation 12, the sum of all the external forces, $\vec{F}$, is equal to the time rate of change of linear momentum, $\vec{p}$.

$$\sum \vec{F} = \frac{d\vec{p}}{dt} \tag{12}$$

where the linear momentum is given by Equation 13.

$$\vec{p} = m\vec{v} \tag{13}$$

Making another simplifying assumption, that the mass of the aircraft is constant, and applying the transport theorem, which allows inertial derivatives of vectors to be taken in their native (non-inertial) reference frame, yields Equation 14.

$$\frac{d\vec{p}}{dt} = m\frac{d\vec{v}}{dt} + \vec{\omega} \times m\vec{v} \tag{14}$$

Vector Equations 12 and 14 can now be combined to yield Equation 15.

$$\sum \vec{F} = \begin{bmatrix} m(\dot{u} + qw - rv) \\ m(\dot{v} + ru - pw) \\ m(\dot{w} + pv - qu) \end{bmatrix} \tag{15}$$

The external forces that the aircraft experiences in all three directions, include the force of thrust, $\vec{F}_T$, force of gravity, $\vec{F}_g$, and aerodynamic forces, $\vec{F}_A$. For most aircraft, the force of thrust acts solely in the X-direction and the thrust vector can be represented by Equation 16.

$$\vec{F}_T = \begin{bmatrix} F_{T_x} \\ 0 \\ 0 \end{bmatrix} \tag{16}$$

The weight vector acts normal to the local horizontal plane of the Earth-fixed reference frame. Using the transformation matrix shown in Equation 6, the weight

vector is calculated as follows.

$$\vec{F}_g = \begin{bmatrix} -mg\sin\theta \\ mg\sin\phi\cos\theta \\ mg\cos\phi\cos\theta \end{bmatrix} \tag{17}$$

The aerodynamic forces that the aircraft experiences are the lift, drag, and cross-wind forces. These forces are originally defined in the wind axis, but after being multiplied by the inverse of Equation 5, they can be described in the body frame as follows.

$$\vec{F}_A = \begin{bmatrix} \bar{X} \\ \bar{Y} \\ \bar{Z} \end{bmatrix} = \begin{bmatrix} \bar{q}SC_X \\ \bar{q}SC_Y \\ \bar{q}SC_Z \end{bmatrix} \tag{18}$$

where S is the wing area, and the dynamic pressure, $\bar{q}$, is a function of air density, ρ, and is equal to $\frac{1}{2}\rho V_T^2$. The coefficients are complex functions that depend on the two aerodynamic angles, Mach number, Reynolds number, control surface deflections, $\delta_{elev,ail,rud}$, and the thrust coefficient, T_C. These coefficients are empirically determined in wind tunnel testing.

Combining Equations 15, 17, and 18 yields the body-axes force equations.

$$\bar{X} + F_T - mg\sin\theta = m(\dot{u} + qw - rv) \tag{19}$$

$$\bar{Y} + mg\sin\phi\cos\theta = m(\dot{v} + ru - pw) \tag{20}$$

$$\bar{Z} + mg\cos\phi\sin\theta = m(\dot{w} + pv - qu) \tag{21}$$

The aircraft's angular motion about the three body axes, is described by the rotational analog to Newton's Second Law. Equation 22 states that the sum of

all externally applied torques, $\vec{M}$, is equal to the time rate of change of angular momentum, $\vec{H}$.

$$\sum \vec{M} = \frac{d\vec{H}}{dt} \tag{22}$$

where $\vec{H}$ is given by

$$\vec{H} = [I]\vec{\omega} \tag{23}$$

Here, a fourth assumption is made. The mass distribution of the aircraft is assumed to be symmetric about the X_B-Z_B plane. Thus, the products of inertia I_{xy}, I_{yx}, I_{yz}, and I_{zy} are zero. The moment of inertia matrix, $[I]$, can then be expressed by Equation 24.

$$[I] = \begin{bmatrix} I_x & 0 & -I_{xz} \\ 0 & I_y & 0 \\ -I_{xz} & 0 & I_z \end{bmatrix} \tag{24}$$

Again applying the transport theorem, yields Equation 25, which describes the time rate of change of angular momentum.

$$\frac{d\vec{H}}{dt} = [I]\frac{d\vec{\omega}}{dt} + \vec{\omega} \times [I]\vec{\omega} \tag{25}$$

Combining Equations 22 through 25 yields the moment equation as follows.

$$\sum \vec{M} = \begin{bmatrix} \dot{p}I_{xx} - \dot{r}I_{xz} + qr(I_{zz} - I_{yy}) - pqI_{xz} \\ \dot{q}I_{yy} + pr(I_{xx} + I_{zz} - r^2I_{xz} + p^2I_{xz}) \\ \dot{r}I_{zz} - \dot{p}I_{xz} + pq(I_{yy} - I_{xx}) - qrI_{xz} \end{bmatrix} \tag{26}$$

The aircraft experiences external moments due to thrust and aerodynamics. If

the engine is mounted such that the thrust line lies in the X_B-Z_B plane, and is offset from the CG, along the Z_B-axis, by a distance z, the moment due to thrust can be expressed by Equation 27.

$$\vec{M}_T = \begin{bmatrix} 0 \\ F_T z \\ 0 \end{bmatrix} \tag{27}$$

The aerodynamic moments are described in Equation 28, in similar fashion to the aerodynamics forces

$$\vec{M}_A = \begin{bmatrix} \bar{L} \\ \bar{M} \\ \bar{N} \end{bmatrix} = \begin{bmatrix} \bar{q}SbC_l \\ \bar{q}S\bar{c}C_m \\ \bar{q}SbC_n \end{bmatrix} \tag{28}$$

where $\vec{M}_A$ is the vector sum of the aerodynamic moments in all three axes, $\bar{L}$, $\bar{M}$, and $\bar{N}$. The wingspan is given by b, and $\bar{c}$ is the mean aerodynamic chord. The moment coefficients C_l, C_m, and C_n are, again, complex functions that depend on the two aerodynamic angles, Mach number, Reynolds number, control surface deflections, and the thrust coefficient.

Combining Equations 26, 27, and 28 yields the body-axes moment equations.

$$\bar{L} + L_T = \dot{p}I_{xx} - \dot{r}I_{xz} + qr(I_{zz} - I_{yy}) - pqI_{xz} \tag{29}$$

$$\bar{M} + M_T = \dot{q}I_{yy} + pr(I_{xx} + I_{zz} - r^2 I_{xz} + p^2 I_{xz}) \tag{30}$$

$$\bar{N} + N_T = \dot{r}I_{zz} - \dot{p}I_{xz} + pq(I_{yy} - I_{xx}) - qrI_{xz} \tag{31}$$

As long as the engine is mounted at the center of the aircraft, and all thrust acts on the aircraft centerline, the thrust moments, L_T, and N_T are zero. The derived equations describing the motion in the six degrees-of-freedom are now written as a

system of 12, scalar, first-order equations.

Force Equations

$$\dot{u} = rv - qw - g\sin\theta + \frac{F_X + F_T}{m} \tag{32}$$

$$\dot{v} = -ru + pw - g\sin\phi\cos\theta + \frac{F_Y}{m} \tag{33}$$

$$\dot{w} = qu - pv + g\cos\phi\cos\theta + \frac{F_Z}{m} \tag{34}$$

Moment Equations

$$\dot{p} = \frac{1}{\Gamma}\left[I_{xz}[I_x - I_y + I_z]pq - [I_z(I_z - I_y) + I_{xz}^2]qr + I_z\bar{L} + I_{xy}\bar{N}\right] \tag{35}$$

$$\dot{q} = \frac{1}{I_y}\left[(I_z - I_x)pr - I_{xz}(p^2 + r^2) + \bar{M}\right] \tag{36}$$

$$\dot{r} = \frac{1}{\Gamma}\left[[(I_x - I_y)I_x + I_{xz}^2]pq - I_{xz}[I_x - I_y + I_z]qr + I_{xz}\bar{L} + I_x\bar{N}\right] \tag{37}$$

where

$$\Gamma = I_x I_z - I_{xz}^2 \tag{38}$$

Kinematic Equations

$$\dot{\phi} = p + \tan\theta(q\sin\phi + r\cos\phi) \tag{39}$$

$$\dot{\theta} = q + \cos\phi - r\sin\phi \tag{40}$$

$$\dot{\psi} = \frac{1}{\cos\theta}(q\sin\phi + r\cos\phi) \tag{41}$$

Navigation Equations

$$\dot{p}_N = u\cos\theta\cos\psi + v(-\cos\phi\sin\psi + \sin\phi\sin\theta\cos\psi) \tag{42}$$
$$+ w(\sin\phi\sin\psi + \cos\phi\sin\theta\cos\psi)$$

$$\dot{p}_E = u\cos\theta\sin\psi + v(\cos\phi\cos\psi + \sin\phi\sin\theta\sin\psi) \tag{43}$$
$$+ w(-\sin\phi\cos\psi + \cos\phi\sin\theta\sin\psi)$$

$$\dot{h} = u\sin\theta - v\sin\phi\cos\theta - w\cos\phi\cos\theta \tag{44}$$

Recalling Equations 8, 9, and 10, u, v, and w can be defined as functions of V_T and the aerodynamic angles, as shown in Equation 45.

$$\begin{bmatrix} u \\ v \\ w \end{bmatrix} = \begin{bmatrix} V_T\cos\alpha\cos\beta \\ V_T\sin\beta \\ V_T\sin\alpha\cos\beta \end{bmatrix} \tag{45}$$

These values can now be differentiated and arranged to yield three new state equations as shown.

$$\dot{V}_T = \frac{u\dot{u} + v\dot{v} + w\dot{w}}{V_T} \tag{46}$$

$$\dot{\alpha} = \frac{u\dot{w} - w\dot{u}}{u^2 + w^2} \tag{47}$$

$$\dot{\beta} = \frac{\dot{v}V_T - v\dot{V}_T}{V_T^2\cos\beta} \tag{48}$$

Computer based flight simulators numerically integrate each of these scalar, first-order, differential equations. Thus, aircraft states are propagated throughout the duration of the simulation.

3.3 Configuring JSBSim

While JSBSim is a platform-independent software package, Linux was the chosen operating system for this research effort. The software source code is available online for free download. In addition to the code, the JSBSim reference manual [21] can also be downloaded at no charge, and is particularly useful in understanding the inner workings of the software. Once the software package is downloaded and extracted, it can be built using operating system specific tools. After it is installed, the software's hierarchical file structure will be revealed under the JSBSim directory, as illustrated in Figure 21. This is perhaps the best place to start when understanding how JSBSim flight simulations can be configured.

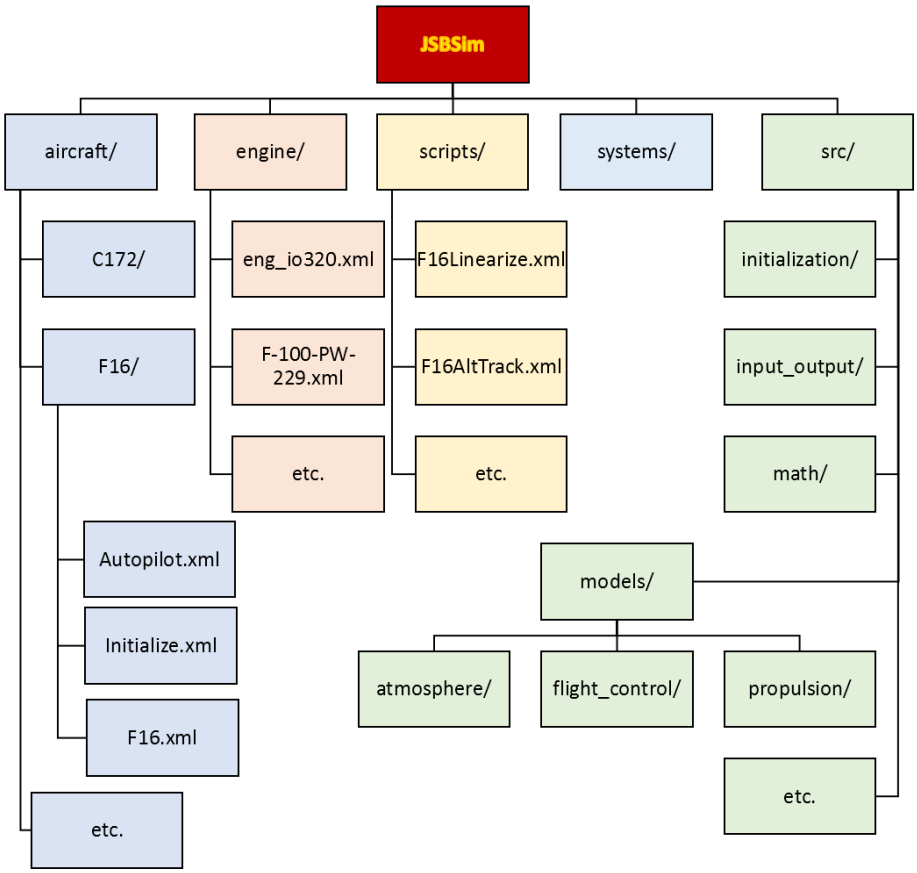

Figure 21. JSBSim Hierarchical File Structure

The folder titled 'src' contains about 70 C++ classes that comprise JSBSim's source code [21]. These are the functions that calculate forces and moments acting on an aircraft model, and propagate its dynamics over a given period of time, based on specific inputs. Examples of this code include files that model different types of engines that are electric, piston, rocket, turbine, or turboprop type. Along with different engine types, the 'Force' class is used to calculate thrust using equations specific to nozzles, propellers, or rotors. The 'Model' class incorporates aircraft mass and aerodynamic properties, along with ground reactions and atmospherics. Other classes feed these calculations by determining aircraft orientation, using the quaternion method, and executing commands specified in aircraft scripts, among other important simulation functions. This source code is also the basis for flight control components, like mathematical functions and control system gains, summers and Proportional, Integral, Derivative (PID) controllers.

The folders labeled 'aircraft', 'engine', 'scripts', and 'systems', under the root directory, are prepopulated with sample eXtensible Markup Language (XML) files. These files can be used as-is, or modified to suit research needs. All of these files are essentially compilations of inputs to the corresponding classes contained in the JSBSim source code.

The aircraft folder contains configuration files for a number of different vehicles, like the Cessna 172 or the Boeing 747. It is in these aircraft files that airframe specific measurements (e.g. wing-span), mass properties (e.g. moments and products of inertia), flight control surfaces, propulsion systems, and aerodynamic coefficients are defined. In addition to these files, the aircraft folder can also include initialization files, which specify any relevant aircraft initial conditions (e.g. initial altitude and initial velocity).

The engine folder contains files that detail specific propulsion systems, their type

(e.g. turbine or piston), the amount of thrust they produce, if they have nozzles or propellers, and so forth.

The scripts folder contains a series of commands which, when executed, command JSBSim to simulate a given aircraft executing certain maneuvers, like entering a climb, or attaining trimmed flight, for example.

The systems folder contains guidance and navigation utilities files. It can also contain autopilot files, although, they can just as easily be placed in the specific aircraft's folder and used from there without issue.

To reiterate, these files can be thought of as the inputs to the JSBSim source code. Once they are populated with aircraft data, designed control systems, and scripted maneuvers, a simulation can be run on JSBSim, using the corresponding mathematical functions, or classes, of the source code. The XML files which are pre-populated in the JSBSim distribution, are compiled by various authors who made use of open source aircraft information. According to the descriptions written by some authors, many of the models were verified solely by running simulations to subjectively evaluate if they could "fly right".

3.3.1 F-16 Aircraft Model

In the interest of performing higher fidelity simulations, verified aerodynamic data of the F-16 was used for this research effort. This data was obtained from low-speed ($0.1 \leq M \leq 0.6$) wind-tunnel tests, conducted using small-scale F-16 models at NASA Ames and NASA Langley [55]. The study analyzed the maneuverability of the F-16 in the stall and poststall regions of flight, and therefore contains data corresponding to angles of attack ranging from negative 20 degrees to positive 90 degrees. Unfortunately, it is difficult to create accurate dynamic models in the poststall region, and the F-16 does not have adequate pitch moment control at angles of attack beyond 25

degrees [64]. For these reasons, only the data from angles of attack ranging from negative 10 degrees to positive 45 degrees were extracted from the data tables presented in the original study.

Most aircraft are optimized for cruise conditions. The F-16 was intended as a high speed fighter aircraft. In turn, the wings were designed to provide adequate lift, while mitigating induced drag at the high airspeeds that the F-16 would most commonly experience. Consequently, the wings cannot provide sufficient lift at lower speeds. The operational F-16 features leading-edge flaps that mitigate this issue, by automatically varying wing camber based on angle of attack at low Mach numbers. In the subsonic speed range, for which the wind-tunnel data is valid, the leading edge flap deployment angle is only minimally related to Mach number. As a result, the model [64] used in this research approximates the leading edge flaps to vary only as a function of angle of attack. Furthermore, the leading edge flap actuator dynamics are ignored. These approximations do not significantly sacrifice model accuracy. They also allow for less computationally intensive simulations, as they do not require the 50 lookup tables presented in the initial study.

Although the aircraft maneuvers to be performed will be explained later, it is important to mention that one of the maneuvers most closely resembles air-to-air refueling. Thus, the F-16 will be initialized at the specified altitude of 30,000 feet and true airspeed of 315 knots (Mach 0.53) [12]. The same altitude and airspeed will be used for both of aircraft maneuvers.

The F-16 model [55] has a gross weight of 20,500 pounds. A nominal drag index of 50 can be assumed, if the aircraft is configured for only one pod mounted on the undercarriage, and no wing-mounted munitions or sensors. Given these details, the F-16 falls well within the bounds of its flight envelope as shown in Figure 22 [44].

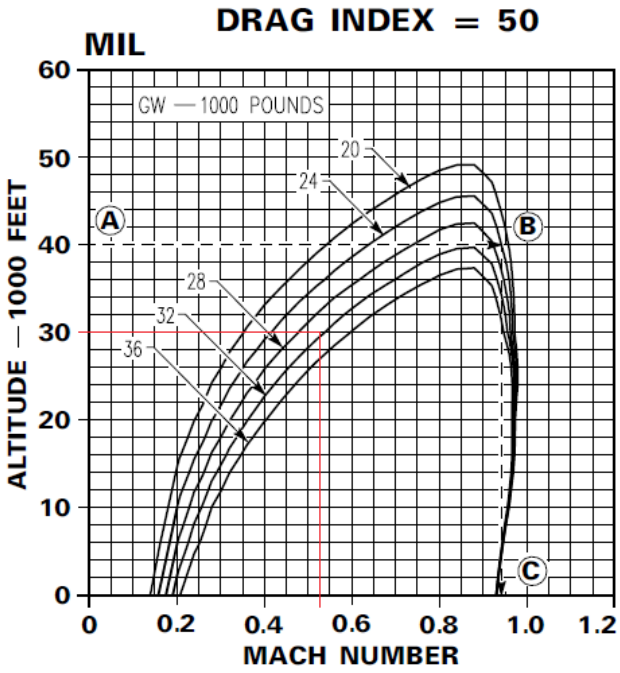

Figure 22. F-16 Flight Envelope with Nominal Drag Index [44]

3.3.2 Configuring the Aircraft File

The XML aircraft file written for this analysis details the wing area, wing span, and mean aerodynamic chord of the F-16. In addition, it contains the moments and products of inertia, along with the empty weight, and CG locations. The simulations performed will use a nominal F-16 CG position located at $0.35\bar{c}$, or at 35% of the aircraft's mean aerodynamic chord length. This information is readily found in the appendix of *Aircraft Control and Simulation* [64].

After these properties are specified, the aircraft file is organized to contain flight control information configurations in the pitch, roll, and yaw channels. JSBSim is capable of trimming an aircraft for steady, level, unaccelerated flight. This trim calculation, to be detailed later, is used to determine the control surface deflections required for an aircraft to maintain flight equilibrium. The trim function of JSBSim outputs trimmed control surface deflections as normalized values that range from negative one to positive one. For example, the position limits of the F-16 elevator

range from negative 25 degrees to positive 25 degrees. If full negative control deflection is required, the normalized trim value is given as negative one. If the elevator is deflected negative 12.5 degrees, the normalized trim value is negative 0.5. The normalized trim value can then be expanded to elevator deflection in degrees or radians using an aerosurface scale element [21].

Once the trimmed elevator deflection is determined in degrees, it can be added to elevator deflection commands that originate from an autopilot, using a summer element. This is known as the pitch command sum, and is sent to an actuator element which models the lag, bias, rate, and position limits of the elevator actuator. To analyze the aircraft workload ($\mathcal{L}_2$ norm), this final elevator deflection, in degrees, is normalized again. An example of this code is shown as follows.

```
<!--
================================================================
                        PITCH CHANNEL
================================================================
-->
<channel name="Pitch">

        <summer name="Pitch Trim Sum">
                <input>fcs/elevator-cmd-norm</input>
                <input>fcs/pitch-trim-cmd-norm</input>
                <clipto>
                        <min>-1</min>
                        <max> 1</max>
                </clipto>
                <output>fcs/pitch-trim-sum</output>
        </summer>

        <aerosurface_scale name="Elevator Control">
                <input>fcs/pitch-trim-sum</input>
                <range>
                        <min>-25</min>
                        <max> 25</max>
                </range>
                <output>fcs/elevator-pos-deg</output>
        </aerosurface_scale>

        <aerosurface_scale name="Elevator Position Normalized">
                <input>fcs/elevator-pos-deg</input>
                <domain>
                        <min>-25</min>
                        <max> 25</max>
                </domain>
                <range>
                        <min>-1</min>
                        <max> 1</max>
                </range>
                <output>fcs/elevator-pos-norm</output>
        </aerosurface_scale>

</channel>
```

After these elements are configured in their respective channels, the aircraft file details aerodynamic functions and coefficients. The X-component of Equation 18, for example, is specified as a mathematical function in JSBSim. This function depends on the X-axis force coefficient, C_X, which is dependent on angle of attack, α, and elevator deflection, δ_e, in degrees. Therefore, the corresponding lookup table is included in this aerodynamics section of the aircraft file. JSBSim will linearly interpolate any values that are not discretely specified. An excerpt of this data is shown in Table 3.

Table 3. Excerpt of X-axis Force Coefficient (C_X) Look-up

		δ_e (deg)				
		-24.0	-12.0	0.0	12.0	24.0
α (deg)	-10.0	-0.099	-0.048	-0.022	-0.040	-0.083
	...	...	...	...	...	...
	45.0	0.166	0.167	0.138	0.091	0.040

Another example of an aerodynamic element in the aircraft configuration file is the calculation of the pitching moment about the Y-axis, $\bar{M}_\alpha$, which is defined in Equation 26. The calculation depends on the pitch stiffness stability derivative, or non-dimensional coefficient, C_{m_α}, which is a function of angle of attack, α, and, elevator position, δ_e, in degrees. The pitching moment about the Y-axis is shown in Equation 49.

$$M_\alpha = \bar{q}S\bar{c}C_{m_\alpha} \tag{49}$$

The equation is calculated using the XML code as shown.

```
<function name="aero/coefficient/CM">
  <description>Moment about the Y axis</description>
  <product>
    <property>aero/qbar-psf</property>
    <property>metrics/Sw-sqft</property>
    <property>metrics/cbarw-ft</property>
    <property>aero/function/CM</property>
  </product>
</function>
```

An excerpt from the pitch stiffness coefficient lookup is shown in Table 4.

Table 4. Excerpt of Pitch Stiffness Coefficient (C_{m_α}) Look-up

		δ_e (deg)				
		-24.0	-12.0	0.0	12.0	24.0
α (deg)	-10.0	0.205	0.081	-0.046	-0.174	-0.259
	...	...	...	...	...	...
	45.0	0.192	0.093	0.032	-0.006	-0.005

The aircraft configuration file concludes with XML code that specifies values to be written to an output file.

3.3.3 Configuring the Engine File

As previously mentioned, engine files can be configured for a variety of propulsion systems. In addition to the aerodynamic coefficients, the NASA study [55] contains data for the F100-PW-229 engine. The Pratt and Whitney afterburning turbofan engine has its thrust response modeled as a first-order lag, which is a function of actual engine power level, and commanded power [64]. Due to limitations with JSBSim, this engine lag was not readily modeled for this research. In addition, this is not the same engine used in the F-16 VISTA. However, the two engine models are close in specifications, and coarse comparisons with simulation results obtained in MATLAB did not indicate significant discrepancies by omitting the thrust lag.

The engine file contains three data lookup tables which indicate thrust at three different power settings: idle, military, and augmented. These two-dimensional lookup tables provide thrust as a function of Mach number and density altitude. Just as with aerodynamic coefficient tables in the aircraft file, JSBSim is able to linearly interpolate dependent variables (i.e. thrust) as they correspond to the independent variables (i.e. Mach number, density altitude).

3.3.4 Configuring the Script File

The final XML file required for running simulations is the script file. These files begin with identifying the aircraft to be used for the simulation, and calling an initialization file, which is included in the aircraft folder, and is used to specify the initial states of an aircraft at the start of a simulation.

Next, the simulation start and end times are specified, along with the desired time-step size. The script file continues forward to call a set of time-triggered 'events'. Examples of these events include trimming the aircraft for equilibrium flight at the initial conditions, linearizing the aircraft state-space model, or toggling auto-pilot switches and set points.

3.4 Initial Flying Qualities Assessment

Techniques for assessing aircraft flying qualities were introduced in Chapter II. These methods represent the current state of the art and are espoused by authoritative documents like MIL-STD-1797B [6], as well as the many legacy documents on which its requirements are based. Adequate control in all three aircraft axes is necessary to accomplish precision-aggressive tasks like aerial refueling and gun tracking. However, this research focuses on the longitudinal flying qualities. As such, two techniques from MIL-STD-1797B [6] will be used to assess the baseline longitudinal flying qualities of the simulated F-16.

The first technique predicts flying qualities by analyzing aircraft short-period natural frequency, ω_{sp}, short-period damping coefficient, ζ_{sp}, high-frequency numerator time constant, T_{θ_2}, and time delay, τ_θ. The second technique predicts flying qualities by determining aircraft bandwidth, ω_{BW}, and phase delay τ_{θ_p}. Both methods rely on the 'lower-order equivalent systems' (LOES) concept.

3.4.1 Aircraft Equations in State-Variable Form

To understand this concept, it is necessary to discuss the derived aircraft equations of motion in light of classical control systems. Flight simulation software, like JSBSim, model the fully non-linear dynamics of aircraft motion. The non-linear aircraft equations of motion are organized in state variable form, as shown in Equation 50,

$$\dot{\vec{\mathbf{x}}}_{n\times 1} = [\mathbf{A}]_{n\times n}\, \vec{\mathbf{x}}_{n\times 1} + [\mathbf{B}]_{n\times p}\, \vec{\mathbf{u}}_{p\times 1} \tag{50}$$

where $\dot{\vec{x}}$ is the state derivative vector, $[A]$ is the plant matrix, n is the number of states, $[B]$ is the control matrix, p is the number of control inputs, $\vec{x}$ is the state vector, and $\vec{u}$ is the control vector.

Equations 32 through 48 are condensed and organized in state variable form to yield twelve state derivatives ($n = 12$) and four control inputs ($p = 4$). Once these equations are put in the state variable representation, the plant matrix, $[A]$, is made up of aircraft dimensional properties (e.g. mass, moments of inertia, wing surface area, etc.) and aircraft force and moment coefficients. The control matrix, $[B]$, is formed by control derivatives, and the control vector, $\vec{u}$, is comprised of control inputs (i.e. control surface deflections and throttle setting). JSBSim organizes these states and controls as shown in Equations 51 and 52.

$$\vec{x} = [V_T\ \alpha\ \theta\ q\ \beta\ \phi\ p\ r\ p_{lat}\ p_{long}\ \psi\ h]^T \tag{51}$$

$$\vec{u} = [\delta_t\ \delta_a\ \delta_e\ \delta_r]^T \tag{52}$$

The output vector, $\vec{\mathbf{y}}$ is represented by Equation 53.

$$\vec{\mathbf{y}}_{q\times 1} = [\mathbf{C}]_{q\times n}\, \vec{\mathbf{x}}_{n\times 1} + [\mathbf{D}]_{q\times p}\, \vec{\mathbf{u}}_{p\times 1} \tag{53}$$

where q is the number of outputs, $[C]$ is the output matrix, and $[D]$ is the feed-through, or feed-forward matrix. The $[C]$ and $[D]$ matrices can be configured for any desired output. For this research, the aircraft pitch-attitude, θ, pitch-rate, q, and altitude, h are important output values.

3.4.2 Aircraft Trim and Linearization

It is apparent upon examining the equations of motion, that non-linear terms exist (e.g. trigonometric functions and exponents). This will prove problematic when designing controllers using linear control systems techniques. Thus, these non-linear equations must be linearized. The first step toward this process is using the equations of motion to determine a system equilibrium point. Pilots will find this point by feel and commonly refer to this condition as 'trimmed flight'.

Aircraft equilibrium occurs when the vehicle is in steady, level, un-accelerated flight. In other words, equilibrium occurs when the state derivative vector, $\dot{\vec{x}}$, is zero. This can be determined by minimizing the scalar cost function, shown in Equation 54, subject to constraint Equations 55 and 56 [64].

$$J = \dot{V}_T^2 + \dot{\alpha}^2 + \dot{\beta}^2 + \dot{p}^2 + \dot{q}^2 + \dot{r}^2 \tag{54}$$

$$\tan\theta = \frac{ab + \sin\gamma\sqrt{a^2 - \sin^2\gamma + b^2}}{a^2 - sin^2\gamma} \tag{55}$$

where

$$\theta \neq \pm\pi/2$$

$$a = \cos\alpha\cos\beta$$

$$b = \sin\phi\sin\beta + \cos\phi\sin\alpha\cos\beta$$

$$\tan\phi = \Gamma\frac{\cos\beta}{\cos\alpha} \times \frac{a - b^2 + \tan\alpha\sqrt{c(1-b^2) + \Gamma^2\sin^2\beta}}{a^2 - b^2(1 + c\tan^2\alpha)} \tag{56}$$

where

$$\Gamma = \frac{\dot{\psi}V_T}{g}$$

$$a = 1 - \Gamma\tan\alpha\sin\beta$$

$$b = \frac{\sin\gamma}{\cos\beta}$$

$$c = 1 + \Gamma^2\cos^2\beta$$

These constraint equations are greatly simplified in steady, level, un-accelerated, flight, where side-slip angle, β, roll angle, ϕ, and yaw-rate, $\dot{\psi}$, are all zero.

JSBSim performs the minimization of the cost function, shown in Equation 54, using the Nelder Mead Simplex method [38]. There are a number of benefits to using this technique. For one, it does not require the computation of derivatives or the Jacobian of the equations of motion. On the other hand, the technique heavily relies on 'good' initial guesses for the values contributing to the cost function. Unsuitable entries for these initial values could lead the Nelder Mead Simplex search to fixate on local minimum values, rather than global minima, which may yield nonsensical results. Some trial and error must be exercised, along with reality checks, in obtaining final answers.

Since the aircraft simulation will begin in the trimmed-state, and not rolling, yawing, or slipping, there are exact guesses that can be made for several cost function values. The Nelder Mead Simplex method will return the normalized throttle setting, δ_t, and elevator position, δ_e, along with the aircraft angle of attack, α, and pitch angle, θ, that result in trimmed flight.

Once this equilibrium point is determined, JSBSim uses one of its C++ classes to perform the system linearization. This computation uses the trimmed state values, normalized input vectors, and state derivatives to yield the linearized state-space representation of the aircraft equations of motion. This function outputs the plant matrix, $[A]$, and the control matrix, $[B]$. It also yields the output matrix, $[C]$, which is simply the identity matrix. Finally, it outputs the feed forward matrix, $[D]$ as a null matrix. These outputs can now be read in MATLAB for flying qualities analysis and control systems design.

3.4.3 Lower Order Equivalent System Calculation

The linearized equations of motion can then be converted to transfer functions in the Laplace domain. In the pitch axis, this transfer function can represent the relationship between aircraft pitch angle, or pitch rate, and elevator deflection angle. This longitudinal axis transfer function is used to analyze the aircraft's dominant flight response modes (i.e. the short period and phugoid mode).

However, for complex aircraft, like the F-16, these transfer functions can exhibit "higher-order modes plus arbitrary shaping of responses" [48]. For this reason, the Lower Order Equivalent System (LOES) model must be calculated. This allows designers to analyze aircraft dynamics as they would relate to flying qualities of classical aircraft. Once the LOES model is obtained, "well established boundaries [of flying qualities] generated from classical airplane data" can be applied [4].

The classical aircraft transfer function from elevator deflection angle to pitch angle, shown in Equation 57, can be obtained by minimizing the cost function represented in Equation 58.

$$\frac{\theta(s)}{\delta_e(s)} = \frac{K_\theta(s+\frac{1}{T_{\theta_1}})(s+\frac{1}{T_{\theta_2}})e^{-\tau_\theta s}}{(s^2+2\zeta_p\omega_p+\omega_p^2)(s^2+2\zeta_{sp}\omega_{sp}+\omega_{sp}^2)} \tag{57}$$

where s is the Laplace operator, K_θ is the pitch-attitude gain, $1/T_{\theta_1}$ and $1/T_{\theta_2}$ are the low-frequency and high-frequency pitch-attitude zeros, respectively, ζ_p and ζ_{sp} are the phugoid and short period damping ratios, respectively, ω_p and ω_{sp} are the phugoid and short period natural frequencies, respectively, and τ_θ is the system equivalent time delay.

$$J = \frac{20}{n}\sum_{\omega_1}^{\omega_n}[(G_{HOS}-G_{LOES})^2 + 0.01745(\phi_{HOS}-\phi_{LOES})^2] \tag{58}$$

where, J is the cost, n is the number of discrete frequencies, G_{HOS} and G_{LOES} are the higher-order and lower-order system gains in decibels, respectively, and ϕ_{HOS} and ϕ_{LOES} are the higher-order and lower order phase angles in degrees, respectively.

It goes without saying, that the LOES calculation is an estimate of the actual aircraft higher-order dynamics model. Therefore, the LOES system will have some degree of mismatch to the higher-order model. To determine if these mismatches are allowable, the error between the gains and the phases must fit inside envelopes as described in Equations 59 through 62, and delineated in Figure 23.

Upper Gain Envelope

$$\frac{3.16s^2+31.61s+22.79}{s^2+27.14s+1.84} \tag{59}$$

Lower Gain Envelope

$$\frac{0.095s^2+9.92s+2.15}{s^2+11.6s+4.95} \tag{60}$$

Upper Phase Envelope

$$\frac{68.89s^2 + 1100.12s + 275.22}{s^2 + 39.94s + 9.99} e^{0.006s} \tag{61}$$

Lower Phase Envelope

$$\frac{475.32s^2 + 184100.12s - 29460}{s^2 + 11.66s + 0.039} e^{-0.0072s} \tag{62}$$

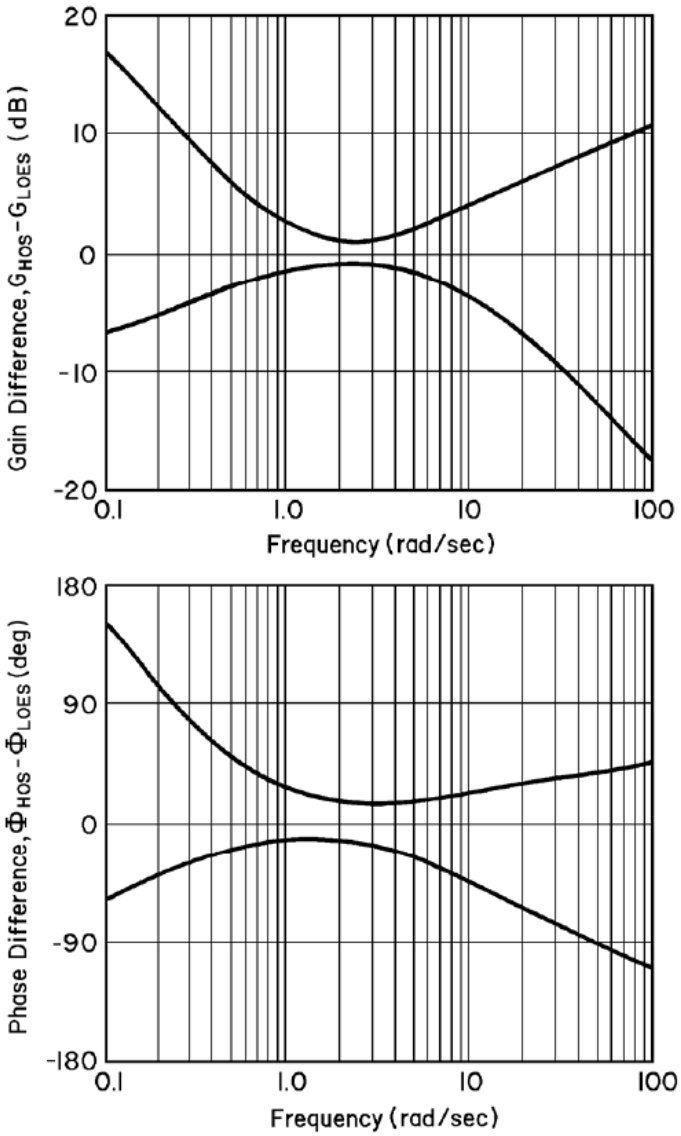

Figure 23. Envelopes within which Gain and Phase Mismatches Must Fit for Valid LOES Approximation [6]

3.4.4 Short-Term Response to Pitch Control Criteria

MIL-STD-1797B [6] cites short-term response requirements that can be applied to the stability values obtained from determining the pitch controller transfer function, represented by Equation 57. These requirements were formulated as an alternative to measuring the Control Anticipation Parameter (CAP), which was discussed in the preceding chapter. The short period natural frequency, ω_{sp}, was found to be related to

the "normal acceleration response to attitude changes" [4]. For classical aircraft, the product of the short period natural frequency, and the high frequency pitch-attitude zero, $\omega_{sp}T_{\theta_2}$, represents a phase lag between aircraft pitch and path attitude response.

If $1/T_{\theta_2}$ is much larger than ω_{sp}, the values may not have enough seperation from one another, and the pitch and path response to elevator deflection may occur simultaneously. This results in difficulty controlling the aircraft, as is evident by pilot comments like "trim hard to find" or "pilot effort produces oscillations" [4]. Conversely, if the two values are too far apart, it could result in large overshoots in pitch or oscillations during closed-loop tracking. It was found that the correlation of $\omega_{sp}T_{\theta_2}$ with the short period damping coefficient, ζ_{sp}, defines the shape of the pitch-attitude frequency response [4]. Figure 24 shows the 'thumbprint' plots that were generated by defining these values with respect to levels of flying qualities, for flight Categories A, B, and C. In addition to these criteria, the equivalent time delay, τ_θ, must fall within the boundaries represented in Table 5. Finally, the equivalent phugoid damping coefficient, ζ_p, must fall within the ranges shown in Table 6.

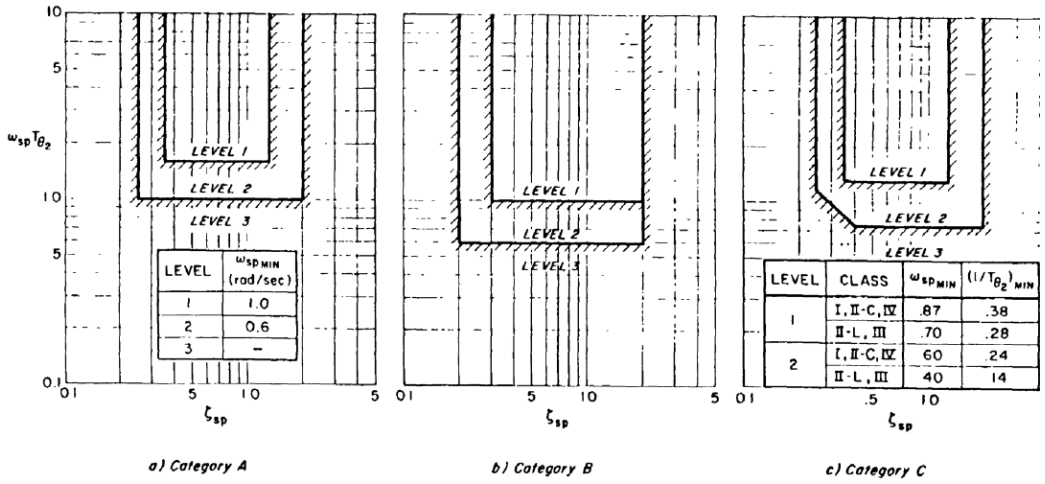

Figure 24. Short-Term Pitch Response Requirements ($\omega_{sp}T_{\theta_2}$ vs ζ_{sp}) [4]

Table 5. Flying Qualities and Allowable Time Delays [4]

Level	Time Delay (sec)
1	0.10
2	0.20
3	0.25

Table 6. Flying Qualities and Allowable Phugoid Damping Coefficients [4]

Level 1	$\zeta_p > 0.04$
Level 2	$\zeta_p > 0.00$
Level 3	$T_2 > 55$ seconds

3.4.5 Bandwidth and Time Delay Criteria

An aircraft's longitudinal flying qualities can also be determined via the bandwidth and phase delay criteria, as shown in Figure 25.

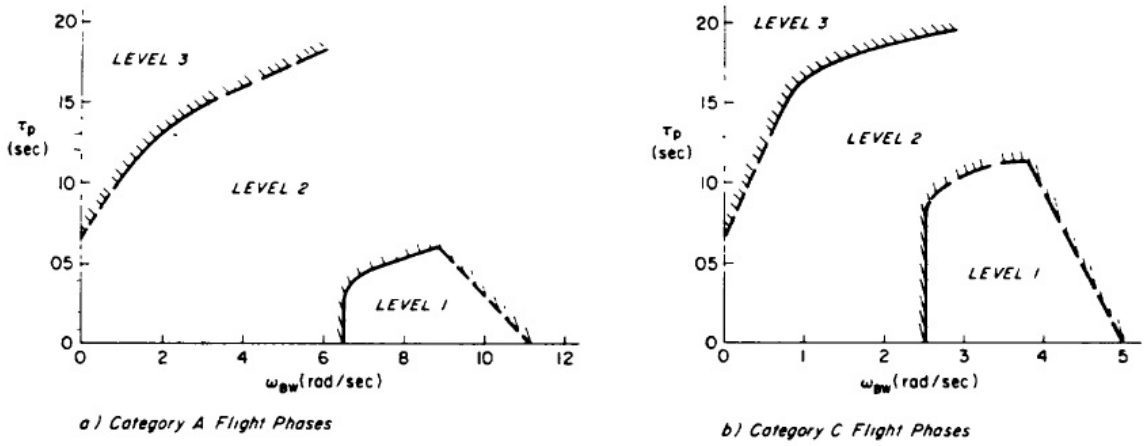

Figure 25. Bandwidth Requirements [4]

The maximum frequency at which an aircraft is capable of performing a tracking task, without becoming unstable, is known as the bandwidth, ω_{BW}. The larger the bandwidth, the easier it is for the pilot to control the aircraft, in making fine corrections, during refueling, gun tracking, or when exposed to turbulence.

In control theory, a system is driven unstable when the gain tends to zero decibels, or the phase tends to 180 degrees. For flying qualities, margins of safety are introduced. The phase margin is 45 degrees, and the gain margin is six decibels. Once the

pitch control transfer function is graphed on a Bode plot, the frequency at which the phase is negative 135 degrees is first determined. This frequency is known as $\omega_{BW_{phase}}$. Then the amplitude at which the phase is negative 180 degrees is determined, and six decibels of gain is added. The frequency corresponding to this amplitude is known as $\omega_{BW_{gain}}$. The lesser of these two values is the bandwidth, ω_{BW}. In addition to the bandwidth, the phase delay, τ_{θ_p}, can be determined via Equation 63.

$$\tau_{\theta_p} = -\frac{\phi_{2_{\omega_{180}}} + 180^\circ}{57.3 \times 2\omega_{180}} \tag{63}$$

where ω_{180} is the frequency that occurs at the 180 degree phase angle, and $\phi_{2_{\omega_{180}}}$ is the phase angle that occurs at twice that frequency [6].

3.5 Maneuvers to be Performed

The report produced by HOH Aeronautics and Systems Technology [48] advocated a mission-oriented evaluation of flying qualities that would be applicable to UAVs. Criteria for this type of flying qualities evaluation would be based on levels of precision and aggressiveness for specific flight maneuvers. A list of examples of the four proposed categories of MTEs was detailed in Table 2.

Previous research [43] examined the climbing spiral turn, a non-precision, non-aggressive task. In order to further contribute to the knowledge-base of UAV flying qualities, this research effort will focus on two precision-aggressive tasks, both of which are longitudinal aircraft maneuvers. The first MTE is a pitch-attitude tracking task, which would most resemble gun or sensor tracking. The second MTE that will be performed is the altitude-tracking task. This most closely resembles the maneuvers that a receiver aircraft has to perform when tracking a refueling boom during air-to-air refueling.

These tasks are considered by MIL-STD-1797B [6] to fall under flight phase Cat-

egory A. As such, the manned flying qualities assessments that will be carried out on the simulated F-16 aircraft, will reference Category A standards.

The pitch-attitude tracking and altitude tracking commands will be generated as a multisine input in the form of Equation 64,

$$\theta_{CMD} \text{ -or- } h_{CMD} = A_1 \sin(\omega_1 t + \phi_1) + A_2 \sin(\omega_2 t + \phi_2) + A_3 \sin(\omega_3 t + \phi_3) \qquad (64)$$

where $A_{1,2,3}$ refer to amplitude, $\omega_{1,2,3}$ refer to frequency, $\phi_{1,2,3}$ refer to phase, and t refers to simulation time.

For both maneuvers the first set of commands will hold frequency and phase constant. Thus, the command will consist of only a single sinusoidal input, with varying amplitude. Commands generated for subsequent trials will vary frequency and phase, and will be true multisine inputs. Once a baseline is established for the workload ($\mathcal{L}_2$ norm) and performance (TIC) metrics, a combination amplitude, frequency, and phase-varied maneuver will be performed.

3.6 Control Systems Design

Many of the aircraft today feature at least one of three types of control systems. Stability Augmentation Systems (SASs) are those control systems which augment aircraft response modes that are unstable, or too lightly damped, creating undesired oscillations. Control Augmentation Systems (CASs) are those systems that translate specific control inputs into particular aircraft responses (e.g. stick deflection rate causing a particular roll rate). The third, and most well-known control system is the autopilot.

As previously mentioned, UAVs like the MQ-9 can be maneuvered by a pilot at

a ground station, using conventional control inputs like the stick and rudder. These systems are prone to instability as a result of excessive time delay. Other UAVs like the RQ-4 are commanded via mission task lists generated by keyboard and mouse. This research precludes the analysis of direct human inputs and time delay effects, because the focus is on aircraft workload and performance, alone. Thus, two autopilots must be designed to allow the aircraft to perform the two longitudinal tracking tasks.

3.6.1 Pitch-Attitude Tracking Autopilot

The pitch-attitude tracking autopilot function can be used for longitudinal tracking tasks such as 'gun-tracking' or pointing relevant sensors at air or ground targets. A schematic of such an autopilot is provided in Figure 26.

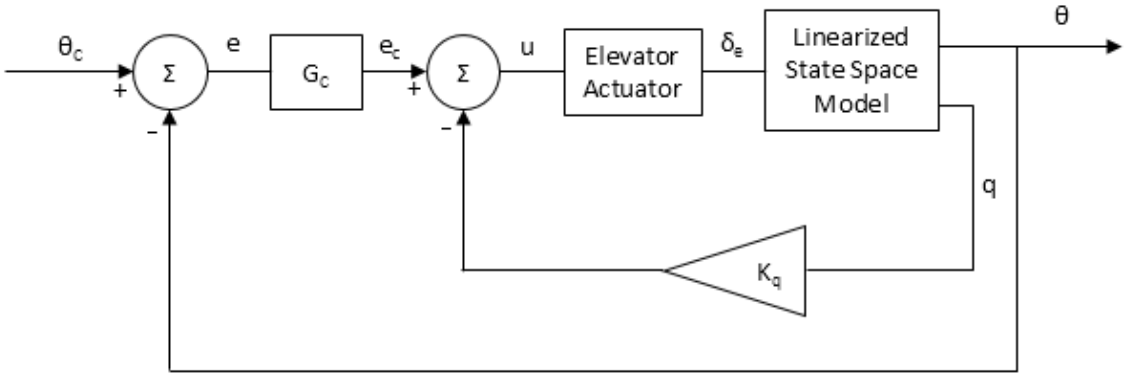

Figure 26. Block Diagram of Pitch-Attitude Tracking Autopilot

This autopilot is designed using classical controls concepts. It begins with the linearized state space model obtained from JSBSim via the procedures described in the Aircraft Trim and Linearization section. The outputs of the model include the pitch angle, θ, and the pitch-rate, q. This autopilot contains two control loops. The inner loop feeds back the pitch-rate, after multiplying it by a simple gain. The outer-loop feeds back the aircraft pitch angle. This is then differenced by the commanded pitch angle, θ_C. The difference constitutes the pitch error, e, which is then sent

to a compensator. The compensated error signal, e_c, is then differenced with the compensated pitch-rate, and thus produces the control signal, u. The control signal is sent to the elevator actuator, which is modeled as a first order lag, shown in Equation 65 [64].

$$\frac{\delta_e}{u} = \frac{20.2}{s + 20.2} \tag{65}$$

The output of the elevator actuator is the elevator deflection command, δ_e, which command is then fed as an input to the aircraft linearized state space model.

Instead of using proportional control, which simply multiplies the error signal by a gain, the system response can be greatly improved by changing G_C to a dynamic compensator. Proportional-Integral-Derivative (PID) control, as its name implies, also integrates and differentiates the error signal, e. A PID controller can be mathematically represented by Equation 66.

$$K_p e(t) + K_i \int_0^t e(\tau)d\tau + K_d \frac{de(t)}{dt} \tag{66}$$

where K_p, K_i, and K_d are the proportional, integral, and derivative gains, respectively, $e(t)$ is the error signal as a function of time, τ is the variable of integration, and time, t, is greater than or equal to zero. The result of increasing the gains is given in Table 7.

Table 7. Effect of Increasing PID Gains on System Response [21]

Parameter	Rise Time	Overshoot	Settling Time	Steady State Error
K_p	Decrease	Increase	Small Change	Decrease
K_i	Decrease	Increase	Increase	Eliminate
K_d	Small Decrease	Decrease	Decrease	None

The ideal system response would have a short rise time, minimal overshoot, short settling time, and zero steady state error.

The controls system design was be done using the linearized aircraft state space model obtained from JSBSim, and MATLAB. Once the controller was designed, it was translated to XML code and written to a JSBSim autopilot file. It is important to understand that the control system, designed using linear systems theory, will not work without modifications, when integrated into a non-linear simulation. Other elements must still be added. For one, there are the position limitations and rate saturation, which must be added to the elevator actuator. This must be appended to the aircraft configuration file as shown in the following XML code.

```
<actuator name="Elevator Actuator">-->
        <input> fcs/pitch-trim-cmd-sum-deg </input>
        <lag>20.2</lag>                          <!--Actuator TF is 20.2 / (s + 20.2)      -->
        <rate_limit>60</rate_limit>              <!-- Rate Limit is 60 deg/s -->
        <clipto>
                <min>-25</min>                   <!-- Position Limits of Elevator are  -->
                <max> 25</max>                   <!-- +/- 25 degrees      -->
      </clipto>
      <output>fcs/elevator-pos-deg</output>
    </actuator>
```

In addition to adding the non-linear elements in the actuator dynamics, steady state values must be added to the autopilot functions, and careful attention must be paid to the units of the state values being fed back. These values are added to the block diagram representation of the pitch-attitude control system in Figure 27.

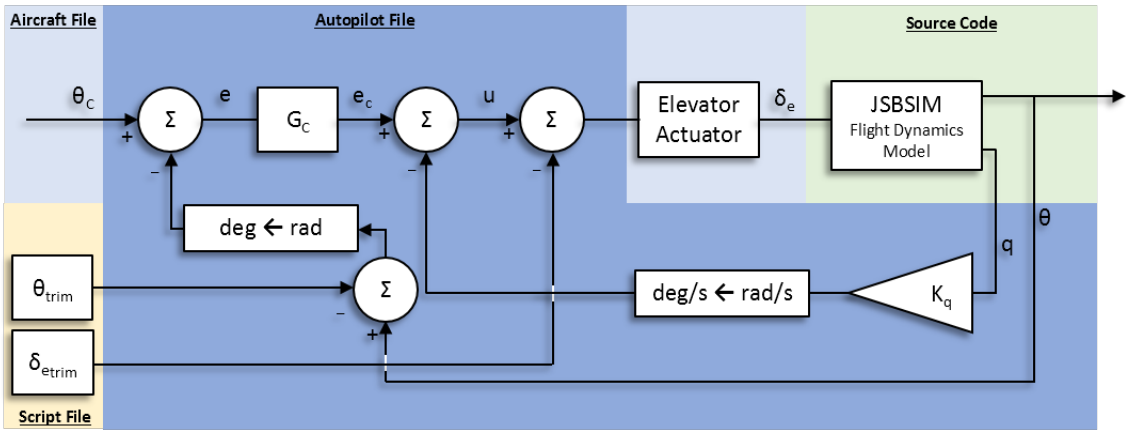

Figure 27. Block Diagram of Non-linear Pitch-Attitude Tracking Autopilot

The aircraft file will contain the multisine command generator which will create

the pitch-attitude command, θ_c. It also contains the actuator dynamics as mentioned.

The elevator deflection required to maintain trimmed flight, $\delta_{e_{trim}}$, at the trimmed pitch angle, θ_{trim}, will be determined from the results of the trim script. These values must be specified to a separate XML file that will allow JSBSim to execute the flight simulation. This file should be stored in the 'scripts' folder. The file should also include all of the other equilibrium states that the aircraft experiences during trimmed flight. These are the aircraft's initial conditions, which are important to successfully running the non-linear simulation.

The autopilot file contains the specified block diagram elements, according to Figure 27. These elements are configured using the XML script as follows.

```
<channel name ="Pitch Altitude Hold">

  <summer name="Pitch Angle Steady State Summer">
    <input> attitude/pitch-rad      </input>            <!-- theta (radians)               -->
    <input>-attitude/pitch-trim-rad </input>            <!-- subtract theta_trim (radians) -->
    <output>ap/pitch-minus-pitch-trim-rad </output>     <!-- theta - theta_trim  (radians) -->
  </summer>

  <pure_gain name="Radians to Degrees">                 <!-- convert radians to degrees    -->
    <input>  ap/pitch-minus-pitch-trim-rad </input>
    <gain>   57.2957795131 </gain>
    <output> ap/pitch-minus-pitch-trim-deg </output>    <!-- theta - theta_trim (degrees)  -->
  </pure_gain>

  <summer name="Pitch Loop Summer">
    <input>  ap/pitch_setpoint  </input>                <!-- theta_c (degrees)              -->
    <input> -ap/pitch-minus-pitch-trim-deg </input>     <!-- subtract (theta - theta_trim) (degrees)  -->
    <output> ap/pitch-error    </output>                <!-- error (e)                      -->
  </summer>

  <pid name ="fcs/pitch-ap-error-pid">                  <!-- G_c                            -->
    <input> ap/pitch-error </input>
    <kp> ???   </kp>
    <ki> ???  </ki>
    <kd> ???   </kd>
  </pid>

  <pure_gain name="Pitchrate Gain">                     <!-- Multiply q by gain             -->
    <input> velocities/q-rad_sec </input>
    <gain> ??? </gain>                                  <!-- K_q                            -->
    <output>ap/q-rad_sec-gain</output>
  </pure_gain>

  <pure_gain name="Radians per Sec to Degrees per Sec"> <!-- convert radians/s to degrees/s -->
    <input> ap/q-rad_sec-gain </input>
    <gain>  57.2957795131  </gain>
    <output>ap/q-deg_sec-gain</output>                  <!-- Kq*q  (degrees/s)              -->
  </pure_gain>

  <summer name="Primary Loop Summer">
    <input>fcs/pitch-ap-error-pid</input>               <!-- e_c-->
    <input> -ap/q-deg_sec-gain</input>                  <!-- subtract Kq*q (degrees/s)      -->
    <output> ap/elevator-cmd-deg </output>              <!-- u                              -->
  </summer>

  <summer name="Input Summer">
    <input> ap/elevator-cmd-deg         </input>
    <input> -fcs/elevator-trim-pos-deg  </input>
    <output> ap/elevator-cmd-deg        </output>      <!-- Command to Actuator  -->
  </summer>
```

3.6.2 Altitude Tracking Autopilot

In order to simulate the aircraft attempting to match the altitude of a refueling boom, an altitude tracking autopilot must be designed. A schematic of this autopilot is given in Figure 28

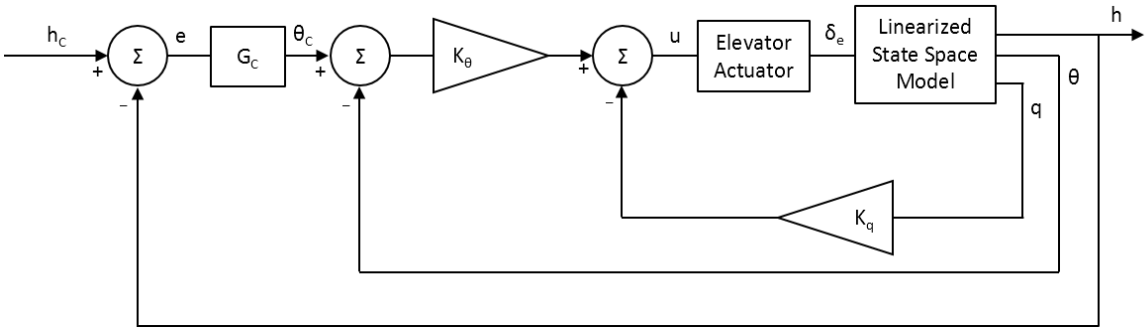

Figure 28. Pitch-Attitude PID Controller Response to Step Input

The pitch-rate and pitch-attitude feedback loops are configured to use the same proportional gains, K_q, and K_θ, that will be determined from the initial pitch-attitude autopilot design. Similar techniques, will be used for the design of the altitude tracking autopilot, with the addition of one extra feedback loop, as shown.

3.7 Aircraft Stability Variation

Once the aircraft workload and performance have been evaluated in its nominal configuration, the same pitch-attitude tracking and altitude tracking maneuvers will be repeated. This time, they will be performed on the F-16 model with varied stability. As mentioned, an aircraft's stability can be augmented by changing the feedback gains in the control system design. The stability can also be varied by changing the aircraft's stability derivatives. In the real-world, this would be done by physically varying the geometry or configuration of the aircraft wings, or control surfaces. The power of computer simulation, however, affords the ability to artificially change these values, simply by adding a multiplication factor to selected coefficients.

In JSBSim, this can be done by modifying relevant moment equations. For example, the pitching moment about Y-axis, M_α, shown in Equation 49, can be modified by adding a multiplication factor, of 1/4 or 2, for instance.

As both mission tasks are longitudinal maneuvers, the relevant stability derivatives

are listed in order of importance, in Table 8.

Table 8. Importance of Longitudinal Stability Derivatives [64]

Derivative	Importance
Lift-Curve Slope (C_{L_α})	Determines Response to Turbulence
Pitch Stiffness (C_{m_α})	< 0 for Static Stability
Pitch Damping (C_{m_q})	< 0 for Short Period Damping
Tuck (C_{m_V})	< 0 Gives Unstable Tuck
Alpha-dot ($C_{m_{\dot{\alpha}}}$)	Less Important than C_{m_q}

The F-16 model [55] gives easy access to varying the pitch stiffness derivative,C_{m_α}, and the pitch damping derivative, C_{m_q}. Thus these are the two values that will be varied to change the stability of the simulated F-16. Increasing the pitch stiffness derivative primarily increases the short period natural frequency, ω_{sp}. Whereas, increasing the pitch damping derivative primarily increases the short period damping, ζ_{sp} [23].

Once the stability derivatives are varied, a JSBSim script will be run to re-trim the modified aircraft, and re-linearize its equations of motion. The linearized model will be used to perform a new LOES approximation, and the aircraft's flying qualities will be re-evaluated. It will then be determined which stability derivative variations resulted in the largest variations to the aircraft's level of flying qualities. Two of the most extreme cases from each stability derivative variation will be selected to then re-evaluate the aircraft workload and performance in carrying out the two mission tasks. The autopilot design will not be changed.

3.8 Summary

Chapter III began by describing the metrics to be used for assessing autonomous aircraft workload and performance. Several sets of flight simulation tests must be completed in order to generate the data on which these metrics can be applied. To better understand how computer-based flight simulation works, aircraft equations of

motion were derived from first principles. Next, the inner workings of JSBSim were explained, by walking through the description of the F-16 simulation model, and the process by which software specific XML files are written. After detailing the JSBSim configuration, the trim and linearization functions were described. These native features of JSBSim make it possible to apply relevant techniques for aircraft flying qualities evaluation. After delineating the short-term pitch response requirements, and bandwidth and phase delay criteria, the pitch-attitude and altitude tracking, precision-aggressive, mission tasks were described. The penultimate section detailed the process to be followed for the design of the pitch-attitude and altitude tracking autopilots, which will allow the F-16 to perform the designated mission tasks. Finally, it was explained how the F-16 model's stability could be varied, by changing its stability derivatives. The resulting flight simulation data will be presented and analyzed in the following chapter.

IV Results

The previous chapter detailed computer-based flight simulation at a conceptual level, and highlighted specific information pertinent to the JSBSim software package, and the F-16 aircraft model used in this research effort. Two precision-aggressive mission task elements were selected for evaluation, including the aircraft pitch-attitude tracking and altitude tracking maneuvers. The following chapter is a comprehensive analysis of the results of the F-16 flight simulations, using the established criteria for manned aircraft flying qualities and the proposed metrics for unmanned aircraft workload and performance.

4.1 F-16 Trim Results

Since the altitude tracking task most closely resembles an air-to-air refueling maneuver, the F-16 was initialized in JSBSim at the specified aerial refueling airspeed of 315 knots (531.66 ft/sec), and altitude of 30,000 feet [12]. These values were first written to an XML initialization file. Next, a JSBSim script was run to establish the aircraft in trimmed flight at the specified conditions. The aircraft successfully attained steady, level, un-accelerated flight, as summarized in the following output file.

F16trim.txt

```
aircraft state
        vt, ft/s    : 531.66
        alpha, rad  : 0.1216
        theta, rad  : 0.1216
        q, rad/s    : 0.000
        thrust, lbf : 2118.6
        beta, deg   : 0.000
```

```
        phi, deg    : 0.000
        p, rad/s    : 0.000
        r, rad/s    : 0.000
        mass, lbm   : 20500
actuator state
        throttle, %  : 61.445
        elevator, %  : -2.24
        aileron, %   : 0.000
        rudder, %    : 0.000
nav state
        altitude, ft : 30000
        psi, deg     : 0.000
        lat, deg     : 0.000
        lon, deg     : 0.000
aircraft d/dt state
        d/dt alpha, deg/s   : 0.000
        d/dt theta, deg/s   : 0.000
        d/dt q, rad/s^2     : 9.63e-17
        d/dt beta, deg/s    : 0.00
        d/dt phi, deg/s     : 0.00
        d/dt p, rad/s^2     : 1.97e-16
        d/dt r, rad/s^2     : -1.23e-32
d/dt nav state
        d/dt altitude, ft/s : 0.000
        d/dt psi, deg/s     : 0.000
```

4.2 Initial Flying Qualities Evaluation

Once the trimmed configuration was determined, a script was run to linearize the aircraft equations of motion. This process outputs the $[A]$, $[B]$, $[C]$, and $[D]$

matrices which correspond to state space Equations 50 and 53. The equations of longitudinal aircraft dynamics were then extracted from these matrices. Next, the Higher Order System (HOS) transfer function of the bare airframe dynamics, relating elevator deflection angle, δ_e, to pitch angle, θ, was extracted, and is shown in Equation 67.

$$\frac{\theta}{\delta_e} = \frac{-1.8414(s+0.406)(s+0.01408)}{(s+0.4345 \pm 0.2893i)(s+0.0037 \pm 0.0467i)} \tag{67}$$

4.2.1 Lower Order Equivalent System Approximation

The Lower Order Equivalent System (LOES) transfer function was then determined in the form of Equation 57 by minimizing the cost function represented by Equation 58. The error between the HOS and LOES gain and phase values were plotted, and found to fit well within the error envelopes specified in MIL-STD-1797B, as can be seen in Figure 29.

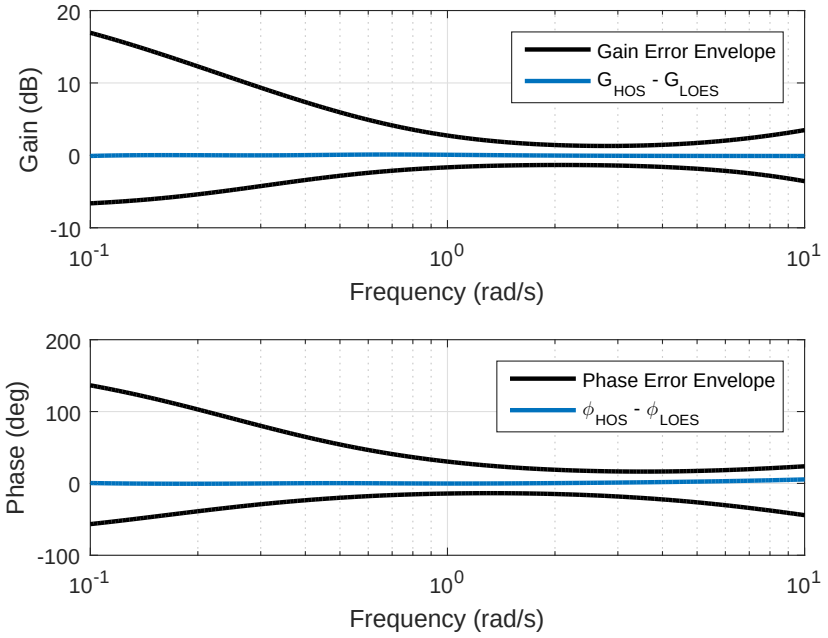

Figure 29. HOS-LOES Gain and Phase Mismatch Errors and Mismatch Envelopes

For added confirmation that the LOES approximation was precise, the higher order and lower order elevator deflection to pitch angle transfer functions were plotted on the same Bode plot, as shown in Figure 30. Based on how well the LOES approximation fits on top of the HOS plot, it is evident that the LOES model can accurately be used to predict the F-16 bare airframe flying qualities.

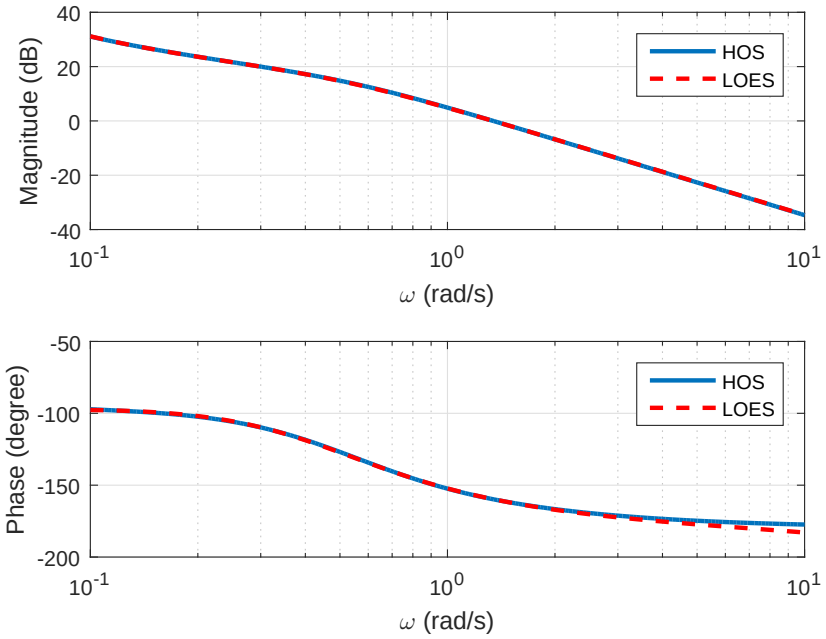

Figure 30. Bode Plot Comparing HOS and LOES Pitch Angle to Elevator Deflection Transfer Functions

The literal factors that were determined from the lower order approximation are shown in Table 9. These values were then compared to the flying qualities criteria specified in MIL-STD-1797B [6].

Table 9. Lower Order Equivalent System Approximation Results

K_θ	T_{θ_1}	T_{θ_2}	τ_θ	ω_p	ω_{sp}	ζ_p	ζ_{sp}
1.86	111.03	3.000	0.01	0.0494	0.4822	0.0163	0.8582

4.2.2 F-16 Short Term Response to Pitch Control

Examining the LOES time delay, τ_θ, against Table 5, it was found that the F-16 shows Level 1 flying qualities, since the equivalent time delay was less than 0.1 seconds. Comparing the calculated LOES value for the phugoid damping coefficient, ζ_p, with Table 6, the F-16 would be predicted to exhibit Level 2 flying qualities, because ζ_p is less than 0.04.

However, the aircraft is predicted to exhibit Level 2 flying qualities, when plotting the value for $\omega_{sp}T_{\theta_2}$, against the short period damping coefficient, ζ_{sp}, as shown in Figure 31.

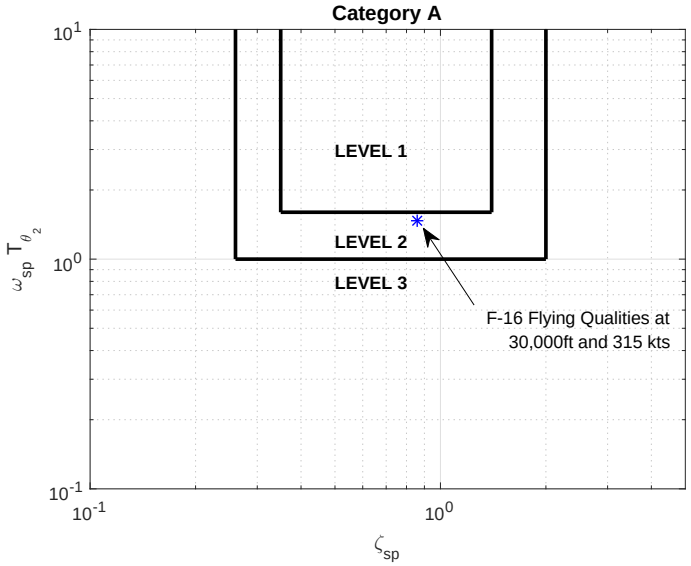

Figure 31. Calculated Flying Qualities Level for F-16 according to MIL-STD-1797A Short-Term Pitch Response Requirements [4]

4.2.3 F-16 Bandwidth and Time Delay

In order to determine the bandwidth and time delay of the F-16 bare airframe, in the given flight configuration, the higher order elevator deflection to pitch angle transfer function was re-examined on a Bode plot, as illustrated in Figure 32.

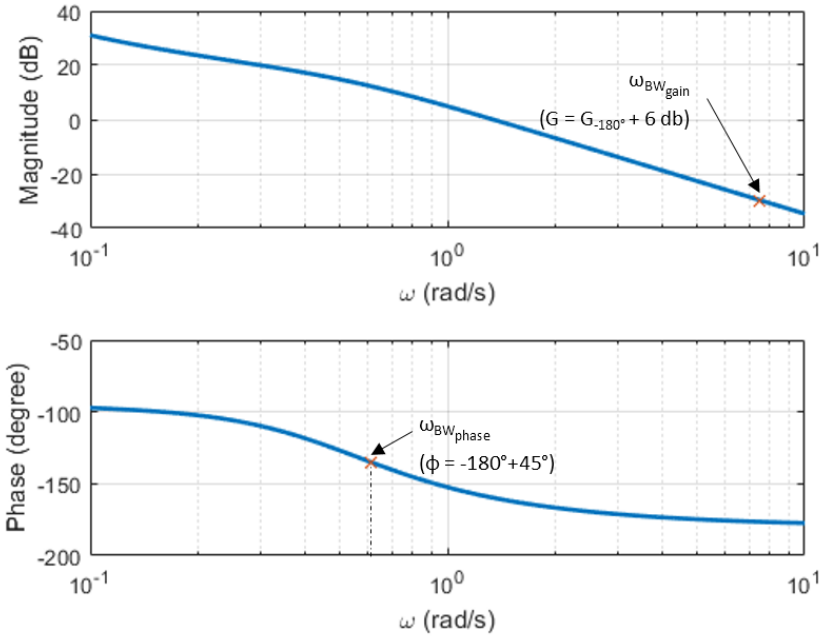

Figure 32. F-16 Pitch Attitude Bandwidth Determination

It appears that the system is phase limited ($\omega_{BW_{phase}} < \omega_{BW_{gain}}$), and the bandwidth was determined to be 0.612 radians per second. After calculating Equation 63, the phase delay was found to be 0.01 seconds. These values were plotted against the requirements for Category A flight, specified in MIL-STD-1797B [6]. The plot in Figure 33, further confirmed that the F-16 is predicted to handle with Level 2 flying qualities.

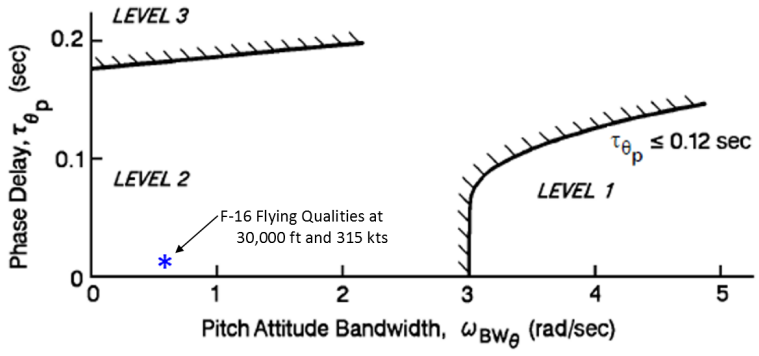

Figure 33. F-16 Flying Qualities based on Bandwidth Criteria for Category A Flight

The overall results of the initial flying qualities evaluation, using the methods from MIL-STD-1797B [6], indicate that the bare airframe F-16 will handle as a Level 2 aircraft, at this specific flight configuration. This was expected since the F-16 was designed with relaxed longitudinal stability, and relies on complex stability and control augmentation systems for sustained flight [55].

4.3 Autopilot Design

Since the aim of this research effort is to evaluate the workload and performance of the aircraft, as it maneuvers through two precision-aggressive mission task elements, two types of autopilots were designed. The first was a pitch-attitude tracking autopilot, and the second was an altitude tracking autopilot.

4.3.1 Pitch-Attitude Tracking Autopilot

The design of the pitch-attitude tracking autopilot began by adding the altitude state to the linearized aircraft longitudinal equations of motion. Once the altitude state was added, the elevator actuator, represented by the first-order lag, in Equation 65, was also incorporated into the state space equations. Then, the higher order elevator deflection to pitch angle transfer function was calculated, as shown in Equation 68.

$$\frac{\theta}{\delta_e} = \frac{-105.51(s+0.406)(s+0.01408)}{(s+0.4345 \pm 0.2893i)(s+0.0037 \pm 0.0467i)} \tag{68}$$

It is evident that the system is stable, since all zeros and poles are negative. This was expected, because while the initial flying qualities evaluation identified the aircraft as Level 2, it did not indicate any serious instability issues. From the transfer function, it can be determined that the short period damping coefficient, ζ_{sp}, is 0.832, which means that the short period mode is adequately damped. The phugoid mode

is also adequately damped, according to Table 6, with the value for ζ_p being 0.0522.

The initial pitch-attitude tracking autopilot design started by considering the compensator, G_C, represented in Figure 26, as simple gain (i.e. $G_C = K_\theta$). The pitch-rate loop was closed, and the root locus of the open pitch-attitude loop was plotted as shown in Figure 34. Values for both gains were found by iteratively assigning a value for K_q, such that the root locus of the open pitch-attitude loop passed through the point associated with a damping coefficient of 0.707 (-2, 2i). Once the root locus was found to pass through this point, the gain, K_θ, was determined such that the short period roots would be a complex conjugate pair of $s = -2 \pm 2i$.

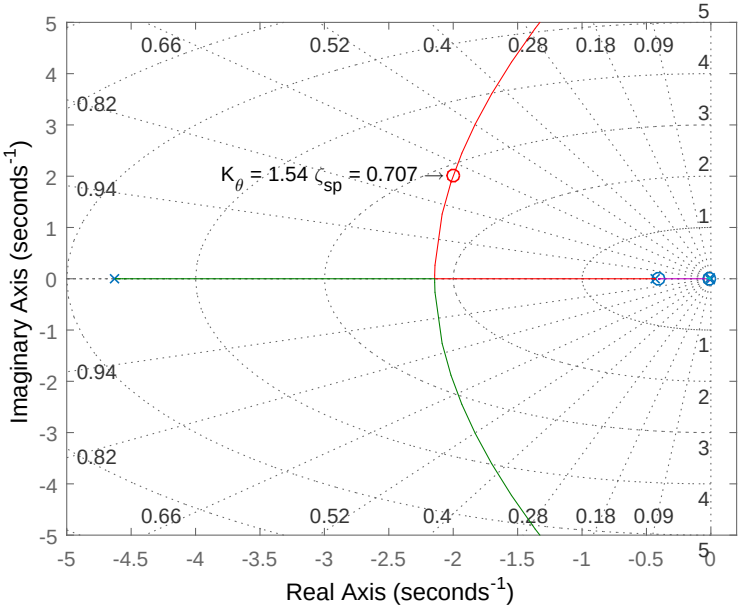

Figure 34. Root Locus for Open Pitch-Attitude Loop with Pitch-Rate Feedback

A damping coefficient of 0.707 was chosen, because systems with less damping tend to oscillate more, while systems with more damping do not oscillate as much, but are generally slower in response. After several iterations, K_q was determined to be -0.7643 elevator degrees per degree per second of pitch-rate. Then, by examining the resulting root locus, shown in Figure 34, K_θ was determined to be 1.54 elevator

degrees per degree of pitch.

The controller's response to a step input, in the time domain, is illustrated in Figure 35. Relevant control system values are presented in Table 10

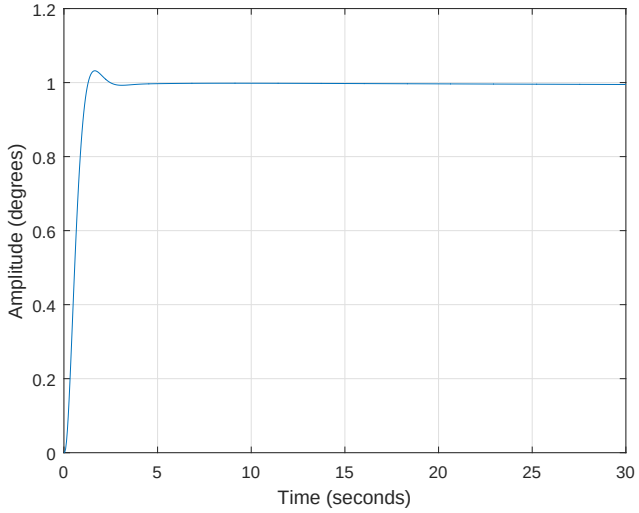

Figure 35. Pitch-Attitude Controller Response to Step Input

Table 10. Pitch-Attitude Proportional Controller Performance

Rise Time (sec)	Settling Time (sec)	Overshoot (%)	Gain Margin (dB)	Phase Margin (deg)
0.7627	2.4349	5.1408	21.4	65.2

In order to improve the response, G_C was made into a PID compensator, rather than a simple the static gain (K_θ). Using Table 7 as a guide, several design iterations yielded the PID gains summarized in Table 11.

Table 11. Pitch-Attitude Controller PID Gains

Parameter	Value
K_p	-1.9428
K_i	-0.071276
K_d	-0.29927

The system response to a step input is shown in Figure 36, and the PID control system performance values are given in Table 12.

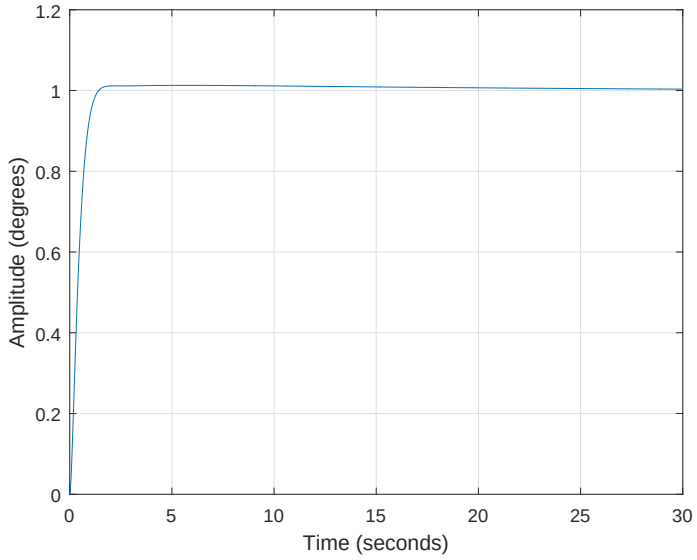

Figure 36. Pitch-Attitude PID Controller Response to Step Input

Table 12. Pitch-Attitude PID Controller Performance

Rise Time (sec)	Settling Time (sec)	Overshoot (%)	Gain Margin (dB)	Phase Margin (deg)
0.768	1.2	1.28	∞	75.7

These values indicate minimal rise time, and settling time, which means that the autopilot would cause the F-16 to attain the and settle on the commanded pitch attitude quickly. Additionally, the percent overshoot is relatively low, indicating that the aircraft would not significantly overshoot the commanded attitude, upon executing the pitching maneuver. Finally, the gain and phase margins are favorable, indicating that the autopilot control system is stable.

4.3.2 Altitude Tracking Autopilot

The altitude tracking autopilot was designed to simulate the aircraft performing the second precision-aggressive mission task element. A block diagram of this control system was shown in Figure 28.

The pitch-rate and pitch-attitude feedback loops of the autopilot were configured

to use the same proportional gains, K_q, and K_θ, that were determined from the initial pitch-attitude autopilot design. After closing the pitch-attitude, θ, loop, the resulting transfer function between θ_c and altitude, h, is shown in Equation 69, and the corresponding root locus diagram is shown in Figure 37.

$$\frac{h}{\theta_c} = \frac{-14.238(s-7.402)(s+4.7)(s-0.005639)}{s(s+16.66)(s+0.4006)(s+0.01235)(s+2.0015 \pm 2.001)} \tag{69}$$

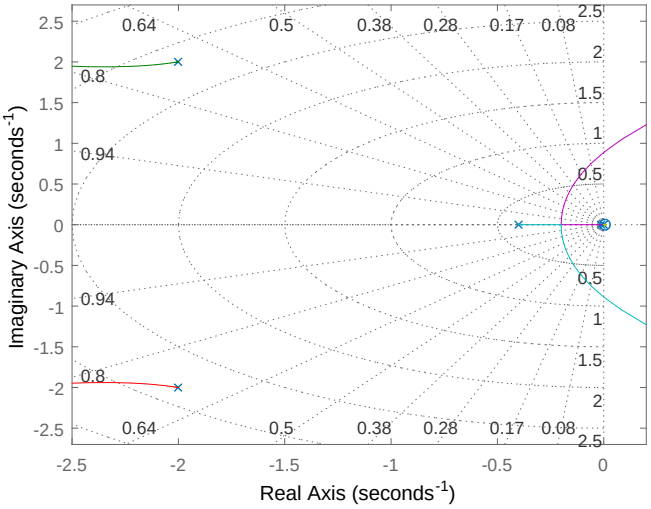

Figure 37. Root Locus for Altitude Loop with Pitch-Rate and Pitch-Attitude Loops Closed

The transfer function reveals a free integrator, $\frac{1}{s}$, which eliminates the concern for any steady state error. The root locus shows that the short period roots are already damped favorably ($\zeta_{sp} = 0.707$). When increasing the gain, the poles at $s = -0.0124$ and $s = -0.4006$ will break away from the real axis to form phugoid poles. The short period poles will move left, while the phugoid poles will move toward the right-half plane. To improve the gain and phase margins, a lead-lag compensator was designed. First, a lead compensator was iterated upon, with a zero chosen close to the pole, $s = -0.4006$, and a pole chosen using an initial pole-to-zero ratio of around 10. The gain was varied to yield a desirable gain and phase margin. Next, a lag compensator

was designed to boost low frequency gain, without adding significant phase-lag. The final compensator design is shown in Equation 70.

$$G_c = 1.5625 \left(\frac{s + 0.4}{s + 10} \right) \left(\frac{s + 0.04}{s + 0.01} \right) \tag{70}$$

The altitude tracking autopilot's response to a step input is illustrated in Figure 38, with control system performance values listed in Table 13.

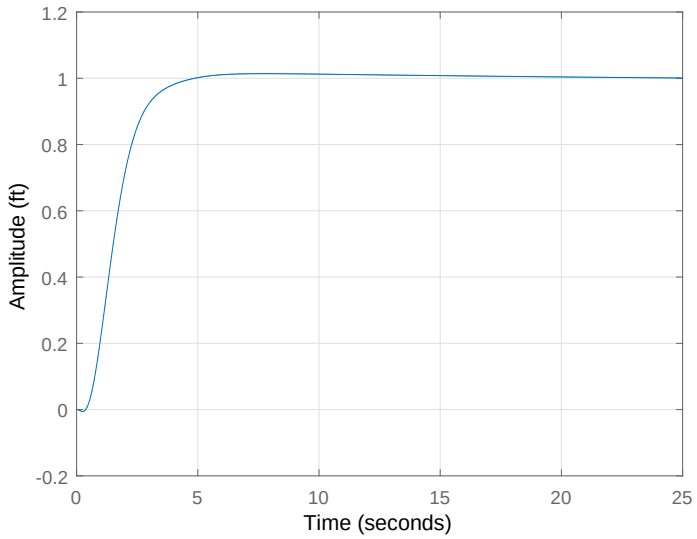

Figure 38. Altitude Tracking Controller Response to Step Input

Table 13. Altitude Tracking Controller Performance

Rise Time (sec)	Settling Time (sec)	Overshoot (%)	Gain Margin (dB)	Phase Margin (deg)
2.04	3.96	1.38	10.9	160

Just as with the pitch-attitude autopilot, the altitude tracking autopilot would cause the F-16 to attain and settle on the commanded altitude quickly. The autopilot would also not cause the aircraft to significantly overshoot the commanded altitude. Finally, the gain and phase margins indicate that the autopilot is an inherently stable control system.

Once the autopilots were configured, a baseline set of maneuvers was executed

in JSBSim. The generated flight simulation data was then analyzed to establish how sensitive the $\mathcal{L}_2$ norm and TIC metrics were to aircraft workload and aircraft performance throughout the accomplishment of specific mission tasks.

4.4 Pitch-Attitude Tracking Task

The first simulated precision-aggressive maneuver most closely resembles the rapid changes in pitch-attitude that an aircraft would execute in a task such as gun or optical sensor tracking. Three different sets of pitch-attitude tracking tasks were constructed by varying the multisine input represented by Equation 64. The results of each task are discussed below.

4.4.1 Amplitude Variation

The pitch-attitude command inputs for the first set of tracking tasks were constructed by varying only the amplitude of a sinusoidal input. Thus in this case, rather than input commands taking the form of a multisine input, they take the form of only a single sinusoidal input. The amplitude was first set at two degrees, then five degrees, and finally 10 degrees. The frequency was held at a constant 0.1 radians per second, with the phase at a constant zero radians. The results of the first amplitude variation are shown in Figure 39.

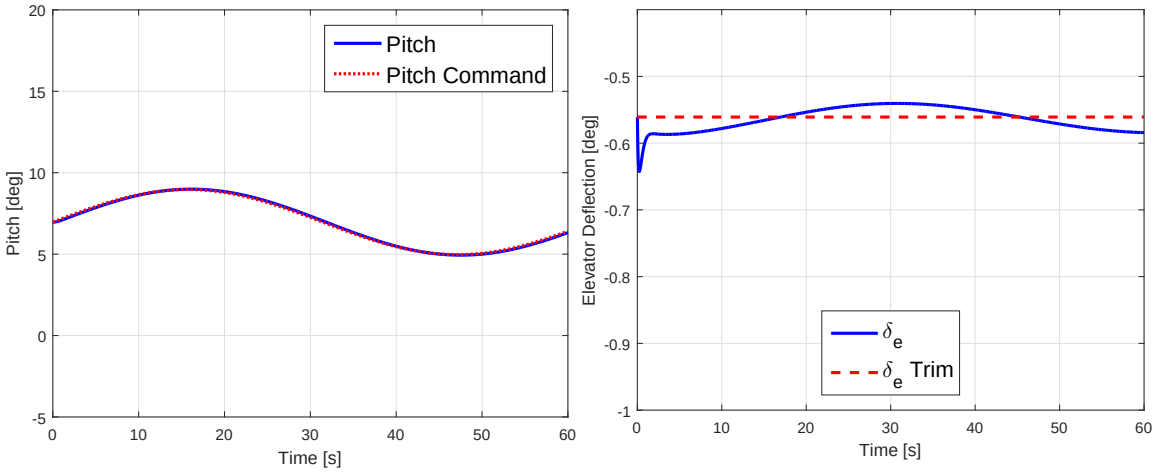

(a) Pitch vs. Command **(b) Elevator Deflection vs. Trim**

Figure 39. Pitch and Elevator Deflection for Amplitude = 2°

Figure 39a shows what appears to be perfect, or near perfect tracking. An initially larger elevator deflection, seen in Figure 39b, is indicative of the control system's quick response to attaining the commanded pitch angle. The relatively small elevator deflection angles, thereafter, are consistent with the small amplitude of the pitch angle command.

For the second amplitude variation, a pitch command amplitude of five degrees was used. The results are presented in Figure 40.

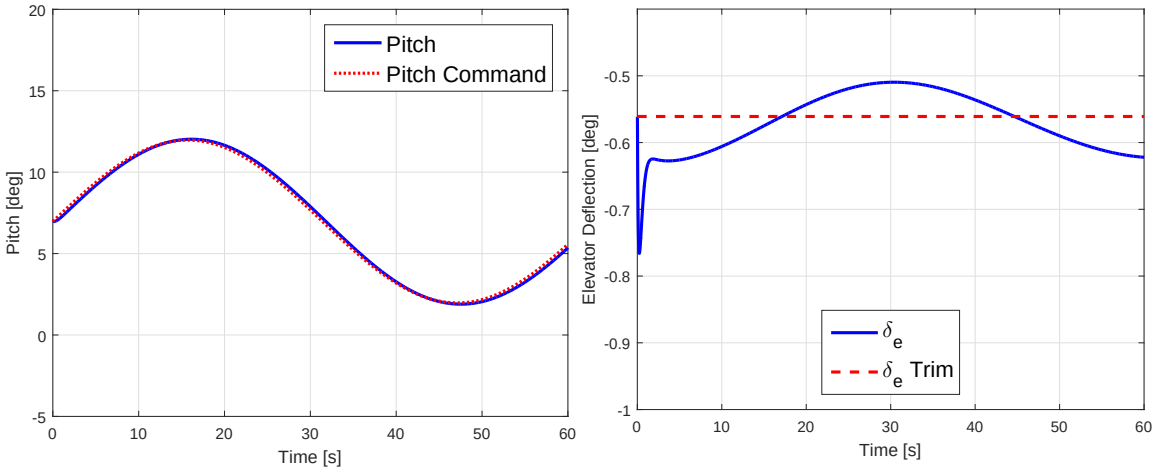

(a) Pitch vs. Command **(b) Elevator Deflection vs. Trim**

Figure 40. Pitch and Elevator Deflection for Amplitude = 5°

When increasing amplitude, the pitch-tracking performance seems almost equivalent to that in the first amplitude variation. The same goes for the shape of the elevator deflection curve in Figure 40b, with the exception of the larger elevator deflections that are consistent with the higher amplitude maneuver.

The final trial varied the pitch command amplitude to 10 degrees. Figure 41 shows the resulting pitch-attitudes and elevator deflections.

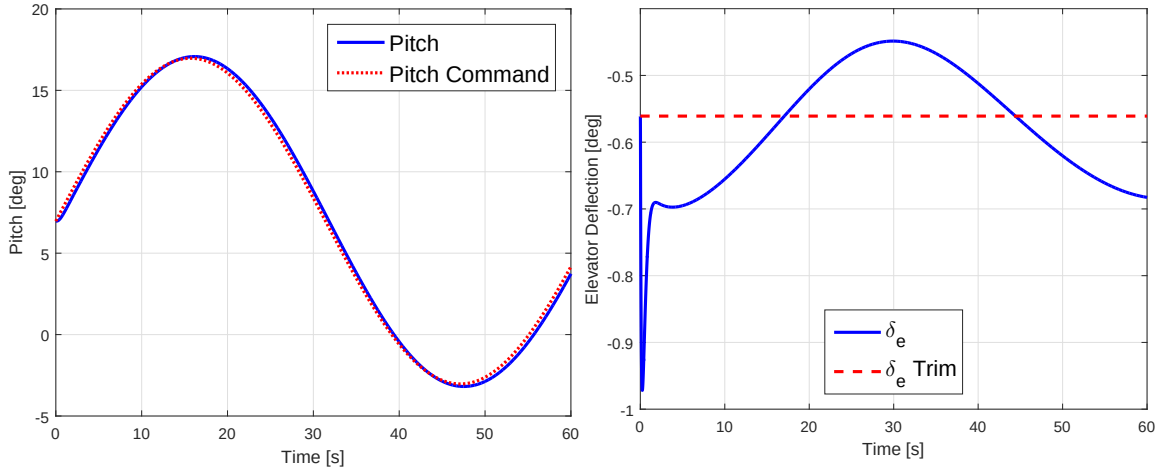

(a) Pitch vs. Command **(b) Elevator Deflection vs. Trim**

Figure 41. Pitch and Elevator Deflection for Amplitude = 10°

A glance at Figure 41a continues to show almost perfect tracking, just as with the previous trials using lower pitch command amplitudes. While the shape of the elevator deflection curve is only varied in amplitude, with respect to the other trials, the steeper change in elevator deflection may be indicative of actuator rate saturation.

Calculated values for the $\mathcal{L}_2$, norm, measuring aircraft workload, and TIC, measuring aircraft performance, are shown in Figure 42.

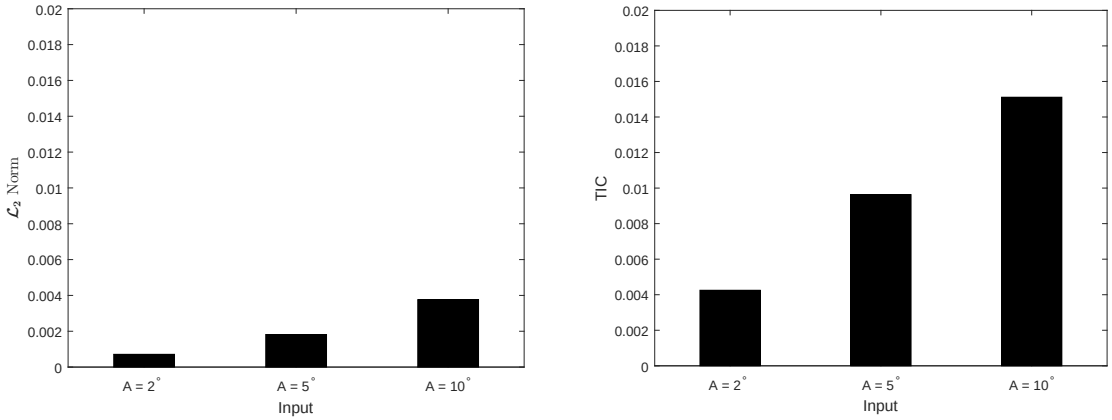

(a) Aircraft Workload **(b) Aircraft Performance**

Figure 42. Pitch-Tracking Workload and Performance for Amplitude Variation

Figure 42a, depicts the increasing elevator workload, as the amplitude of the command inputs increase. This is consistent with the larger elevator deflections seen as the tasks became progressively more challenging.

In terms of tracking performance, all plots comparing the aircraft's pitch-attitude to its commanded pitch-attitude input, make it seem as if the aircraft continues perfect tracking regardless of command amplitude. However, the increasing TIC values, shown in Figure 42b, call attention to the fact that performance does slightly degrade with tracking commands of increasing difficulty. Again, the TIC value is a measure of disparity between two values. Thus, as tracking degrades, the disparity between achieved aircraft states and command inputs increases. TIC values increase as performance decreases.

4.4.2 Phase Variation

For the phase variation task, a true multisine pitch-tracking input, was constructed by holding amplitude at a constant two degrees, and frequency at a constant 0.1 radians per second. Only the phase angles of the input were varied for each trial, as shown in Table 14.

Table 14. Pitch-Tracking Phase Variations in Degrees

Phase Variation	ϕ_1	ϕ_2	ϕ_3
1	5	10	20
2	10	30	50
3	20	50	90

While the phase angles were entered into JSBSim in radians, they are shown here, in degrees, for ease of understanding. The results of the first phase variation trial are presented in Figure 43.

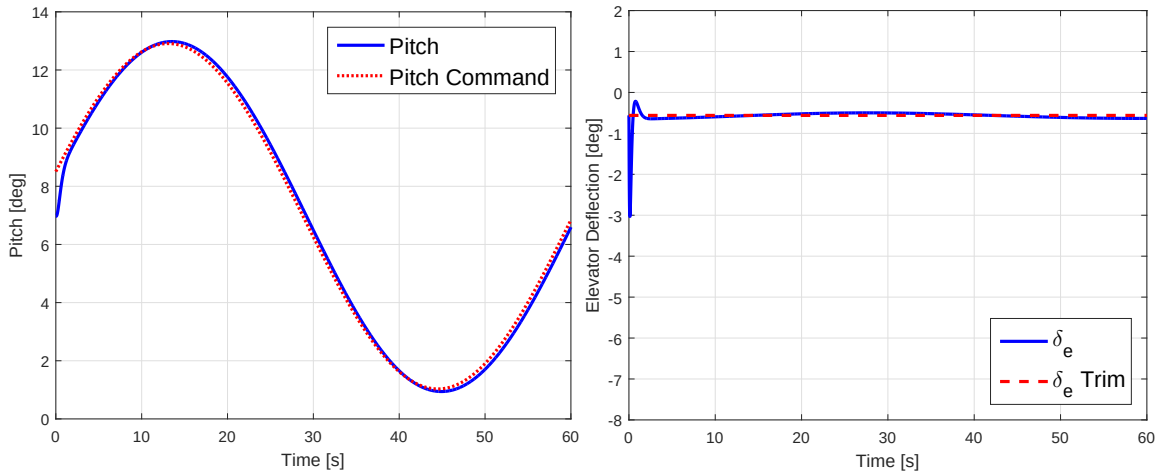

(a) Pitch vs. Command **(b) Elevator Deflection vs. Trim**

Figure 43. Pitch and Elevator Deflection for Phase Variation 1

Figure 43a indicates the initial phase mismatch between the pitch command and the aircraft pitch. However, it appears that the aircraft has no difficulty in quickly matching the command. During the maneuver, the elevator barely deflects, even though the pitch angle changes from plus and minus almost six degrees from the initial trimmed position. It is interesting to note, that while the amplitude of the pitch maneuver almost parallels that of the second amplitude variation trial, the elevator deflects noticeably less.

The results of the second phase variation are shown in Figure 44.

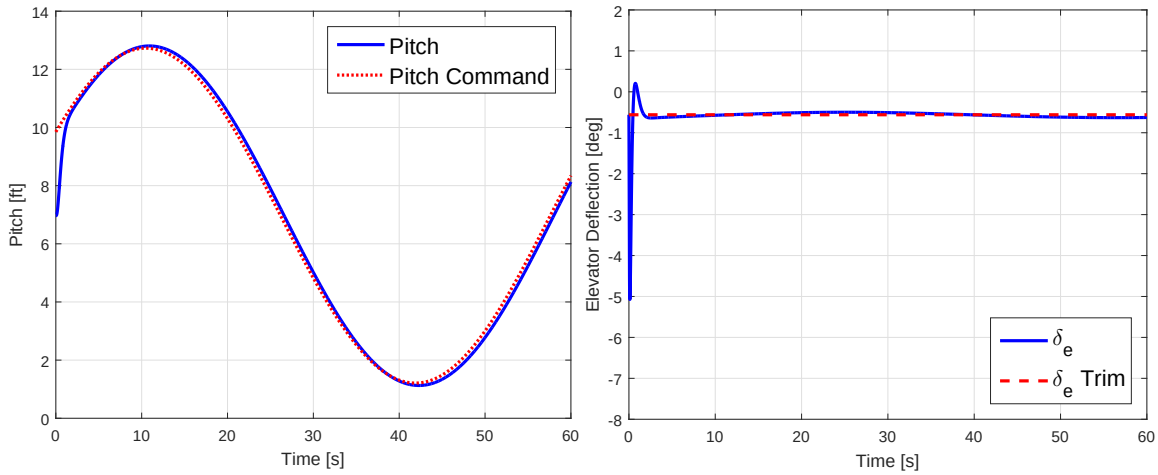

(a) Pitch vs. Command **(b) Elevator Deflection vs. Trim**

Figure 44. Pitch and Elevator Deflection for Phase Variation 2

It is clearly seen in Figure 44a, that there is a larger mismatch between the commanded pitch-attitude and the initial pitch-attitude of the aircraft. In order to compensate for this error, the elevator clearly has to work harder. While there is an initial sharp elevator deflection, it is only deflecting by about 0.2 degrees from the initial trimmed elevator position. Even if this deflection occurs on the order of one hundredth of a second, the elevator deflection rate is still on the order of 20 degrees per second, thereby not causing the elevator to hit its rate saturation limit of 60 degrees per second.

The final phase variation trial is shown in Figure 45. The most stressing phase variation case yielded the largest difference between trimmed pitch angle and initial pitch-attitude command. At first glance, it appears as if the aircraft had no trouble adjusting to this command.

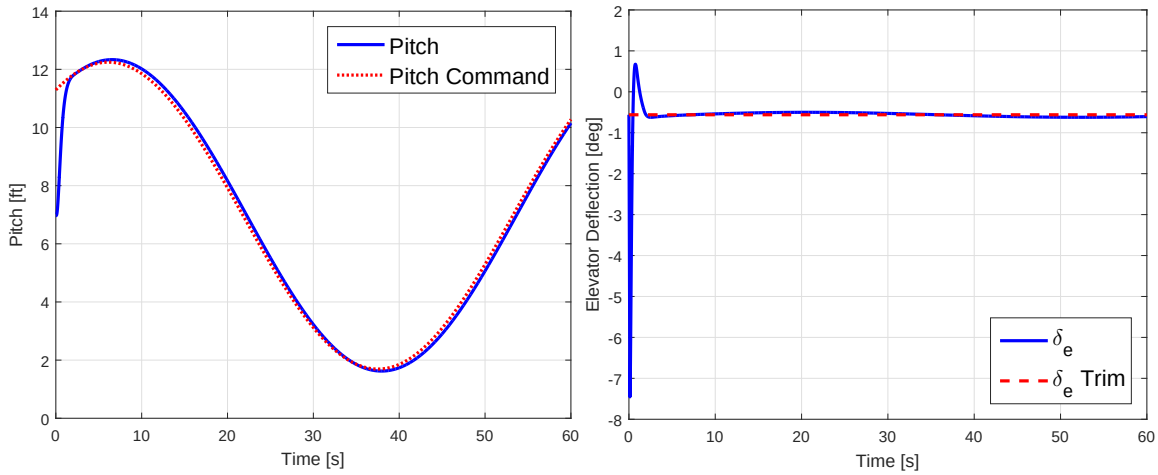

(a) Pitch vs. Command **(b) Elevator Deflection vs. Trim**

Figure 45. Pitch and Elevator Deflection for Phase Variation 3

However, examining the slope of the initial elevator deflection from the initial trim deflection, in Figure 45b, it appears as if the elevator deflects almost half a degree. Since this appears to happen in about a hundredth of a second, the elevator deflection rate is almost 50 degrees per second, thereby almost approaches its rate limit of 60 degrees per second.

The overall workload and performance of the aircraft throughout the three pitch-attitude tasks, with phase variations, are detailed in Figure 46.

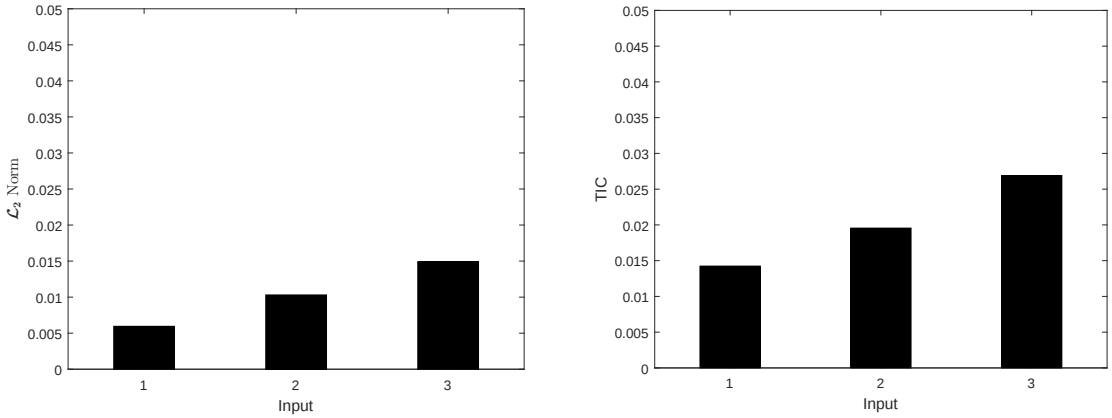

(a) Aircraft Workload **(b) Aircraft Performance**

Figure 46. Altitude Tracking Workload and Performance for Amplitude Variation

The workload of the aircraft clearly increased as the phase values were varied to greater degrees. Following the trend of increased workload, the aircraft performance also degraded, as is shown with the increasing TIC values in Figure 46b. It appears as if the workload and performance metrics are more sensitive to phase differences in commands, than they are to variations in input amplitude alone.

4.4.3 Frequency Variation

The final pitch-attitude tracking variation was done using a multisine input, built by holding amplitude at a constant pitch angle of two degrees, a constant phase input of zero degrees, and varying only the frequencies, according to Table 15.

Table 15. Pitch-Attitude Tracking Frequency Variations in Radians Per Second

Frequency Variation	ω_1	ω_2	ω_3
1	0.1	0.2	0.3
2	0.1	0.4	0.6
3	0.1	0.5	1.0

The results of the first frequency variation are shown in Figure 47.

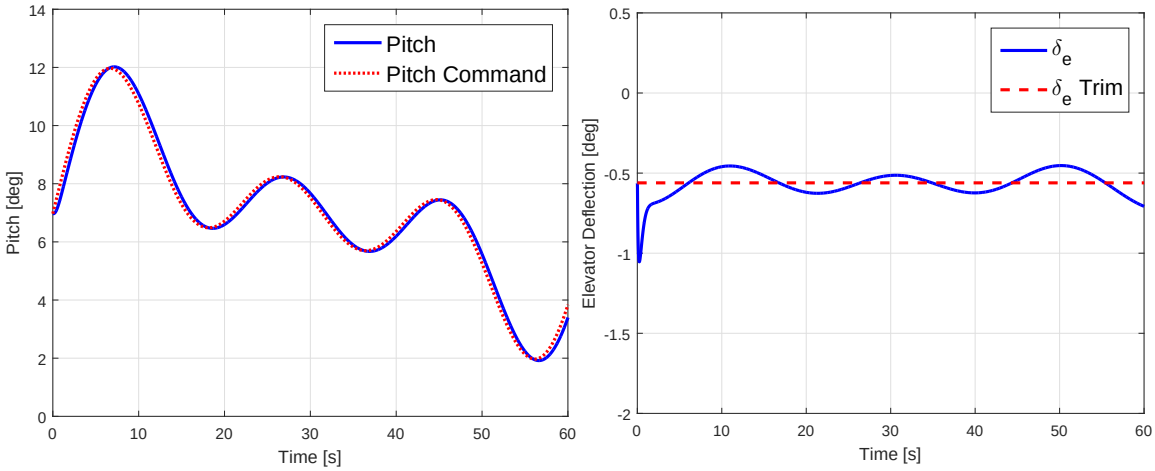

(a) Pitch vs. Command **(b) Elevator Deflection vs. Trim**

Figure 47. Pitch and Elevator Deflection for Frequency Variation 1

Consistent with its performance in the trials varying only amplitude, the pitch-

attitude controller seems to afford the aircraft almost perfect tracking. The relatively larger initial elevator deflection is consistent with the first peak in aircraft pitch-attitude. It is interesting to see a more gradual elevator deflection toward the end of the maneuver, despite the fact that the command amplitudes seem to be equal and opposite to that in the beginning of the maneuver.

The frequency variation was made slightly more rigorous for the second trial. The results of the simulation are plotted in Figure 48.

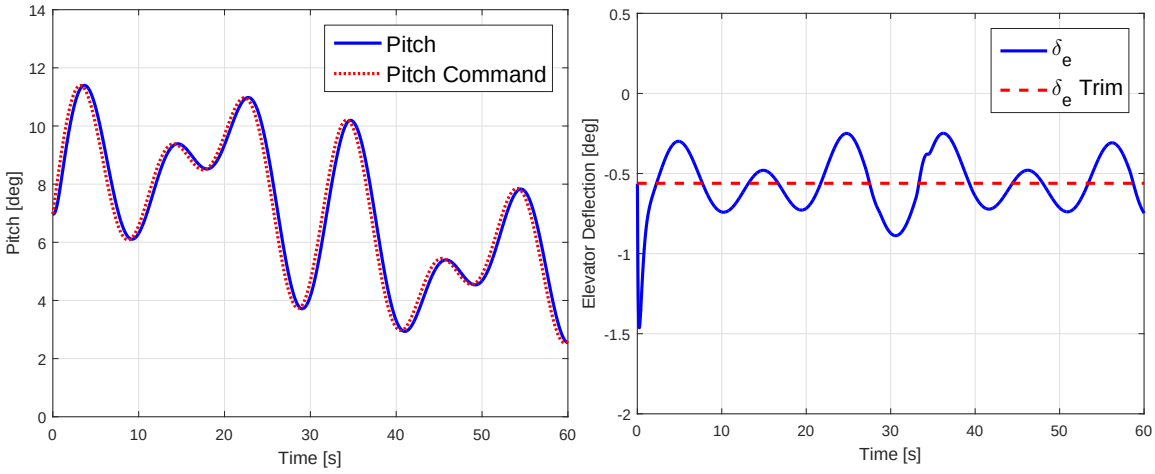

(a) Pitch vs. Command **(b) Elevator Deflection vs. Trim**

Figure 48. Pitch and Elevator Deflection for Frequency Variation 2

It can be alluded from Figure 48a, that the aircraft is now beginning to lag slightly behind the pitch-attitude commands. The plot in Figure 48b depicts an interesting flat spot that occurs between 30 and 40 seconds in the simulation. The slope of the elevator deflection curve does not immediately indicate the possibility of rate saturation. Rate saturation could, however, be one explanation as to the reason for the elevator failing to change deflection angle at that instance.

The results of the final, and most stressing, frequency variation to the pitch-attitude task, are plotted in Figure 49.

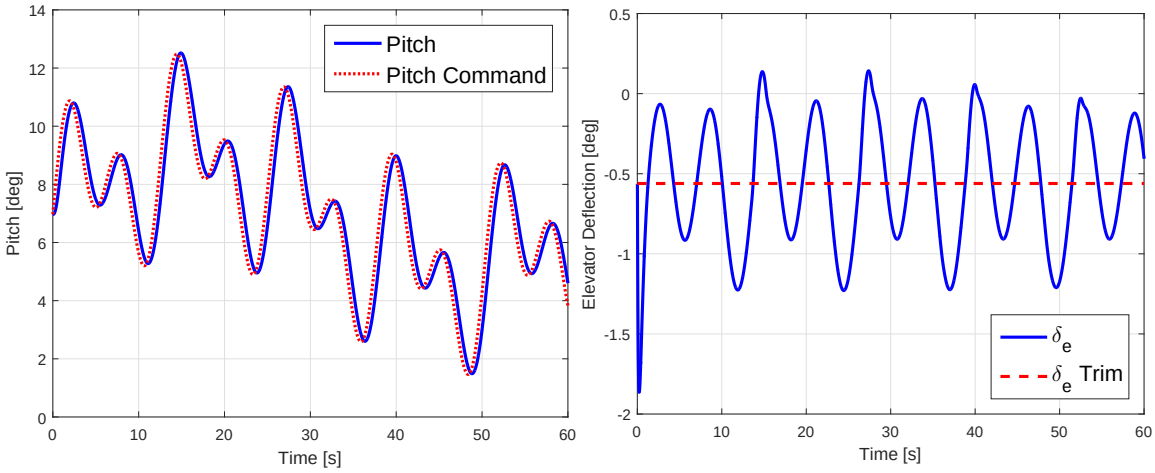

(a) Pitch vs. Command **(b) Elevator Deflection vs. Trim**

Figure 49. Pitch and Elevator Deflection for Frequency Variation 3

In the pitch versus pitch command plot, depicted in Figure 49a, it is now clear that the aircraft appears to trail the pitch commands. The elevator deflection graph, in Figure 49b, does begin to show an interesting response shape, with very flat areas, that may be indications of actuator rate saturation.

The overall results of the pitch-attitude frequency variations are captured in Figure 50.

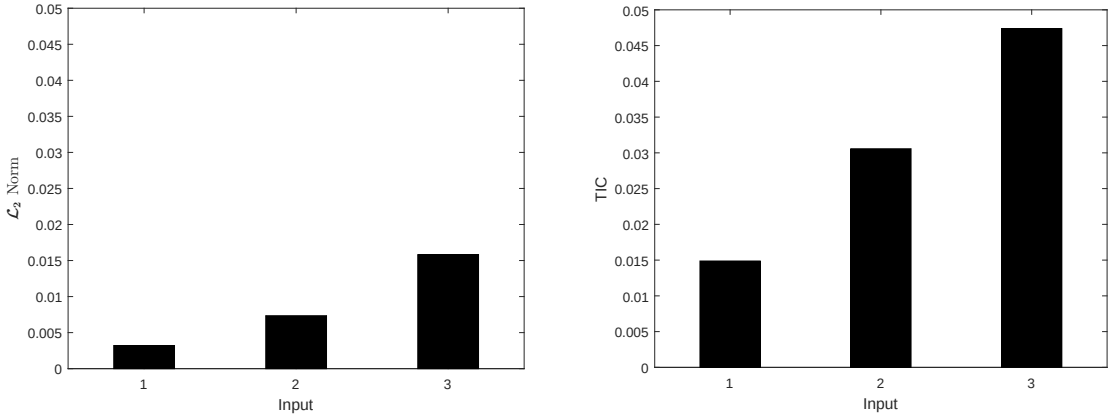

(a) Aircraft Workload **(b) Aircraft Performance**

Figure 50. Pitch-Attitude Tracking Workload and Performance for Frequency Variation

As frequency variations were increased, the workload of the elevator increased, and

performance decreased. The third, and most stressing frequency variation resulted in the most degraded aircraft performance, as can be seen with the relatively larger TIC value in Figure 50b.

4.5 Altitude Tracking Task

Just as with the pitch-attitude tracking task, there were three cases in which the performance and workload of the F-16 were evaluated, while performing the altitude tracking task. The first case varied the amplitude of a single sinusoidal input, and the second and third cases varied multisine input phase angles and frequencies, respectively.

4.5.1 Amplitude Variation

The sinusoidal altitude command input was set at a constant frequency of 0.1 radians per second, and a phase of 0 radians, with only the amplitude varied. The amplitudes of the three cases were set at 5, 10 and 25 feet. A relatively small altitude variation was chosen, because this most replicates the fine tracking required during aerial refueling.

Figure 51a shows the aircraft altitude response for the first commanded altitude input. The elevator deflection is shown relative to the trimmed elevator position in Figure 51b.

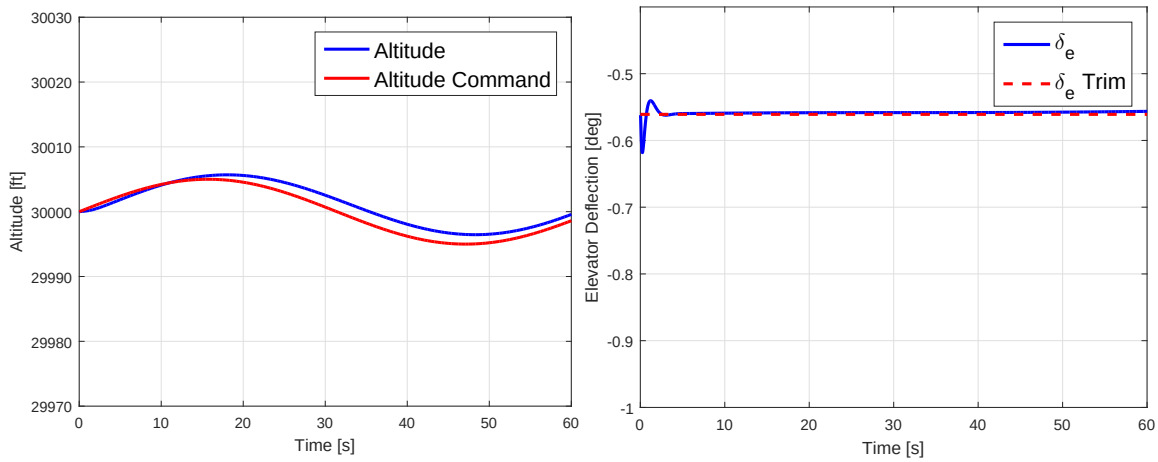

(a) Altitude vs. Command **(b) Elevator Deflection vs. Trim**

Figure 51. Altitude and Elevator Deflection for Amplitude = 5 ft

Figure 51 is important because it establishes that the autopilot is working correctly. The aircraft appears to generally follow the command altitude input, climbing and descending in a sinusoidal fashion. It should be explained that there is a relatively larger initial elevator deflection in the beginning of the maneuver, as the aircraft receives an immediate input to increase altitude by five feet.

The next case was carried out by varying the amplitude to 10 feet. The results of this simulation are shown in Figure 52.

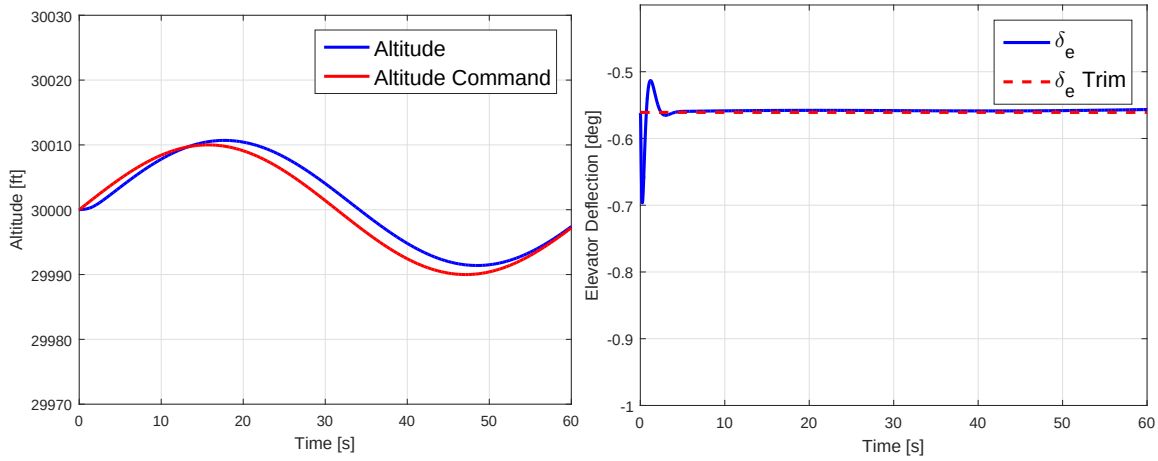

(a) Altitude vs. Command **(b) Elevator Deflection vs. Trim**

Figure 52. Altitude and Elevator Deflection for Amplitude = 10 ft

It is confirmed, through Figure 52a, that the aircraft is indeed tracking to increase and decrease the aircraft altitude by 10 feet. In addition, Figure 52b is indicative of slightly more elevator deflection in the beginning of the maneuver.

The third amplitude variation case increased altitude to 25 feet. The results of the simulation are shown in Figure 53.

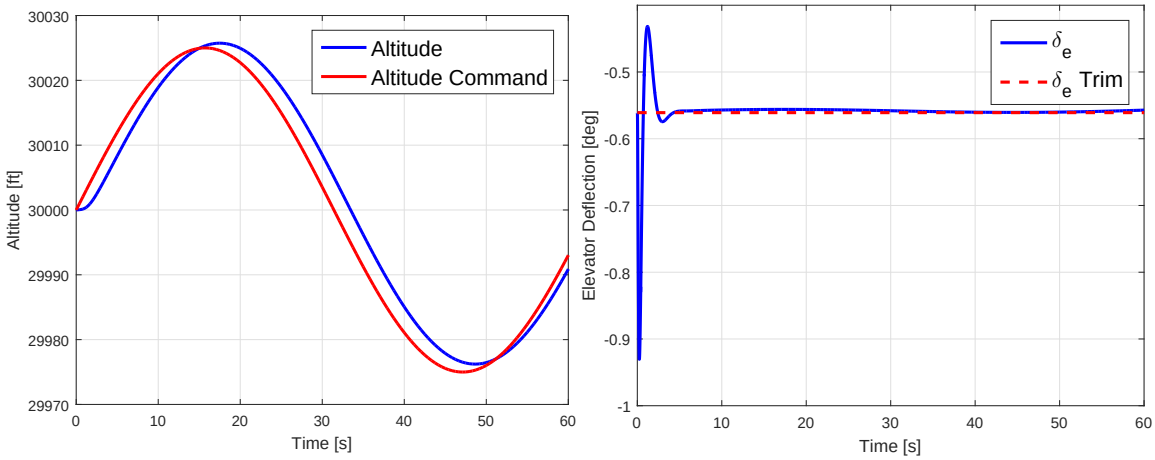

(a) Altitude vs. Command **(b) Elevator Deflection vs. Trim**

Figure 53. Altitude and Elevator Deflection for Amplitude = 25 ft

The aircraft is clearly able to achieve the 25 foot increase and decrease in altitude. However, a noticeable lag is evident with the aircraft attaining the commanded altitude slightly after said attitude is commanded. This slight decrease in performance is quantified through the TIC metric. As amplitude was increased, the initial elevator deflection was also larger, which is captured by the $\mathcal{L}_2$ metric. The final results of the aircraft's performance and workload are graphically summarized in Figure 54.

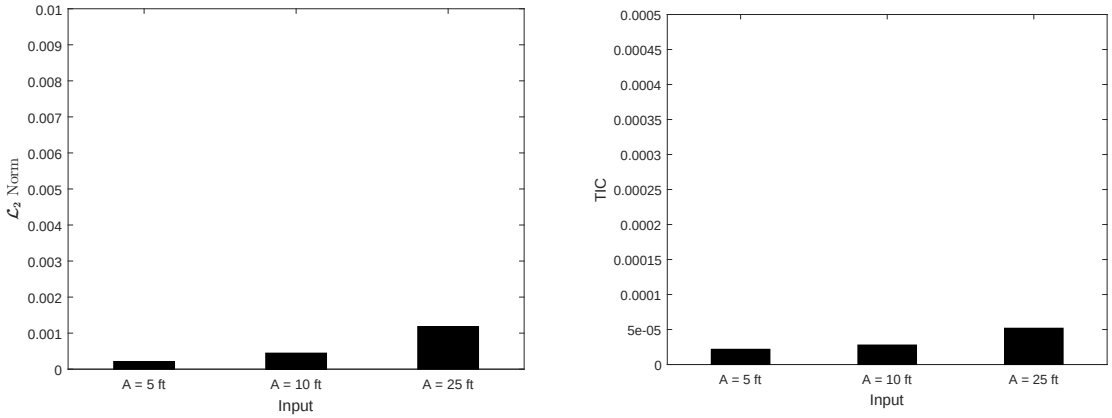

(a) Aircraft Workload **(b) Aircraft Performance**

Figure 54. Altitude Tracking Workload and Performance for Amplitude Variation

From the results above, it should go without saying that the amplitude variation maneuver was very benign, and the aircraft had no trouble following altitude commands. The results were in accord with intuition, in that it is clearly seen that as amplitude increases, the workload of the aircraft increases, and the performance of the aircraft decreases. While Figure 54b does show an increase in TIC values, the numbers are still extremely low. It is suggested from this data, that varying amplitude alone, at least for these small altitude ranges, does not present a stressing task for the control system.

4.5.2 Phase Variation

After the amplitudes were varied, a multisine input was generated by holding a constant amplitude at five feet, a constant frequency at 0.1 radians per second, and varying only phase. These variations are listed in Table 16.

Table 16. Altitude Tracking Phase Variations in Degrees

Phase Variation	ϕ_1	ϕ_2	ϕ_3
1	5	10	20
2	10	30	50
3	20	50	90

The results of the first phase variation are given in Figure 55, which again confirms that the autopilot is able to track, and shows only an initial, relatively larger, jump in elevator deflection.

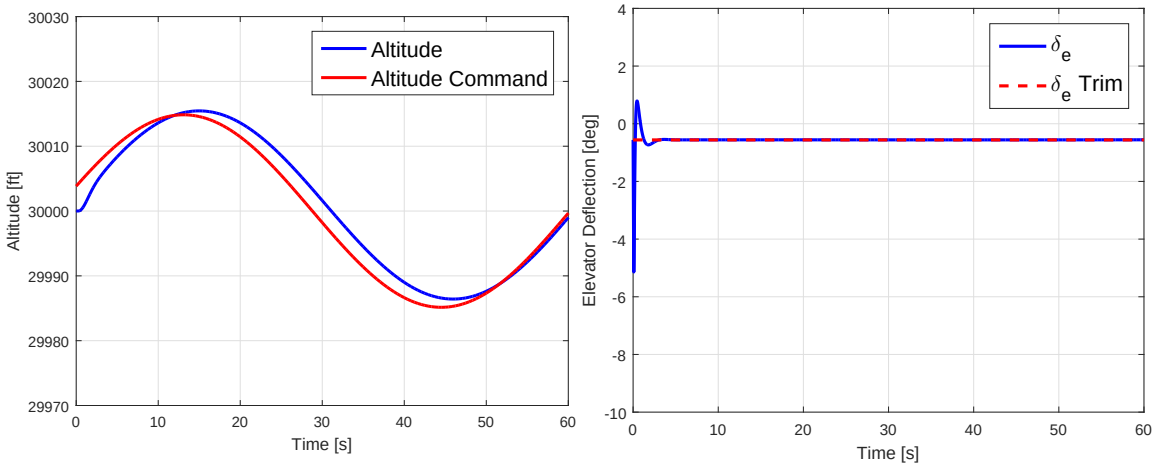

(a) Altitude vs. Command **(b) Elevator Deflection vs. Trim**

Figure 55. Altitude and Elevator Deflection for Phase Variation 1

The results of the second phase variation are shown in Figure 56.

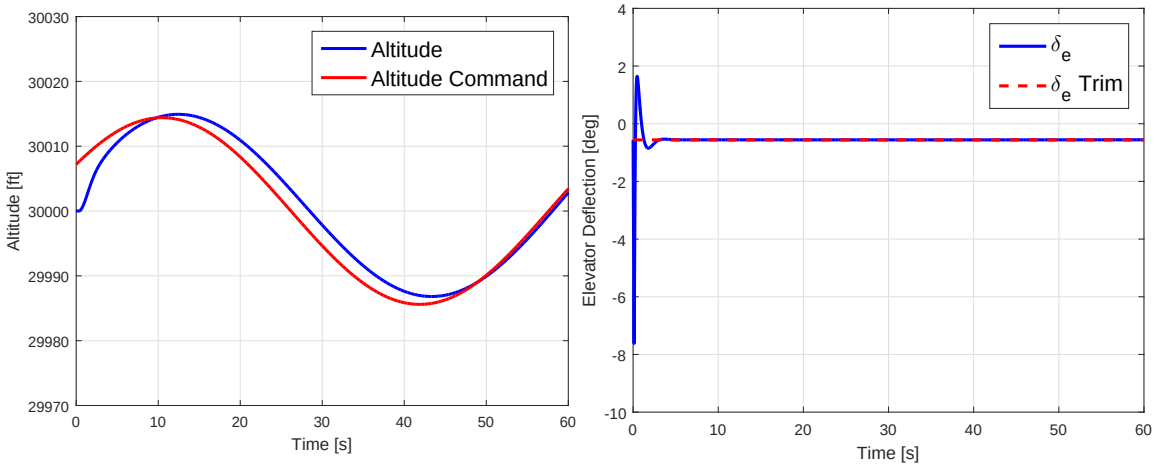

(a) Altitude vs. Command **(b) Elevator Deflection vs. Trim**

Figure 56. Altitude and Elevator Deflection for Phase Variation 2

Figure 56a delineates a larger difference between the aircraft's initial altitude and the initial commanded altitude. These results are consistent with the increased phase

angle variations of the multisine input command. Figure 56b also shows a larger initial elevator deflection, relative to that required when tracking the first phase variation input.

The final phase variation is shown in Figure 57.

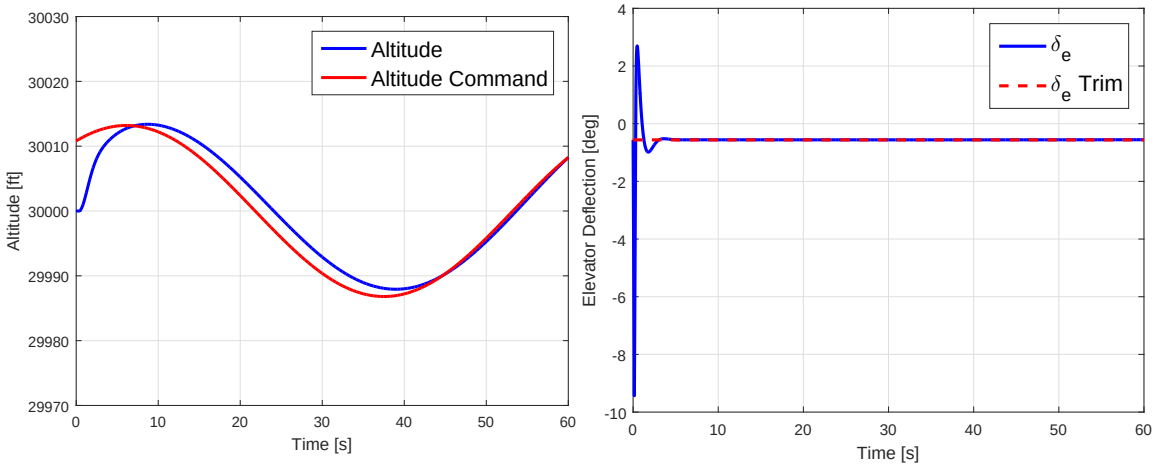

(a) Altitude vs. Command **(b) Elevator Deflection vs. Trim**

Figure 57. Altitude and Elevator Deflection for Phase Variation 3

The results of the third phase variation follow a similar trend, in that the yet larger, and more varied phase angles, cause a larger difference between initial aircraft altitude and commanded altitude input. The elevator deflection angle stays true to this trend, with greater deflections required for tracking, as the task becomes more stressing. Figure 58 shows a summary of the workload and performance of the aircraft throughout all three phase variations.

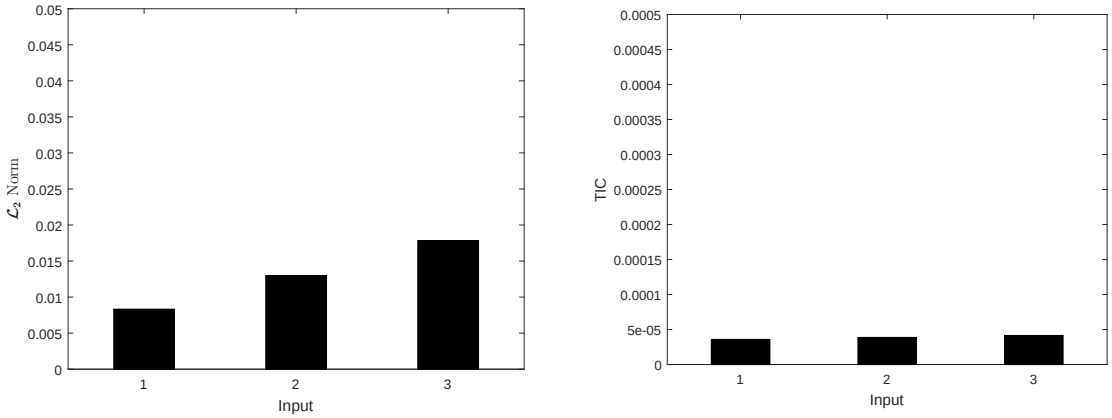

(a) Aircraft Workload **(b) Aircraft Performance**

Figure 58. Pitch-Attiude Tracking Workload and Performance for Phase Variation

The phase variation maneuver had a greater effect on aircraft workload, than it did on performance. The workload of the aircraft, in keeping up with the phase varied sine inputs, was noticeably greater than the workload in keeping up with the amplitude maneuvers. The difference between aircraft performance throughout the three cases was negligible. Overall, while the aircraft worked harder as the cases became more stressing, the performance did not decrease appreciably.

4.5.3 Frequency Variation

The third type of multisine input was constructed by holding a constant amplitude at five feet, a phase angle of zero radians, and only varying input frequency. These frequency values were varied in the order listed in Table 17.

Table 17. Frequency Variations in Radians Per Second

Frequency Variation	ω_1	ω_2	ω_3
1	0.1	0.2	0.3
2	0.1	0.4	0.6
3	0.1	0.5	1.0

The results of the first frequency variation are represented in Figure 59.

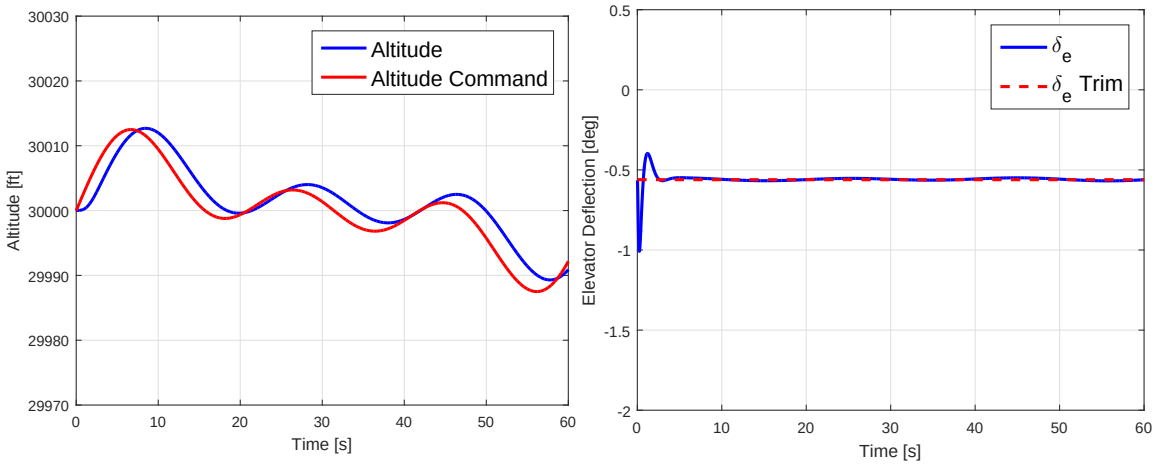

(a) Altitude vs. Command **(b) Elevator Deflection vs. Trim**

Figure 59. Altitude and Elevator Deflection for Frequency Variation 1

In examining Figure 60a, it initially appears as if the aircraft is simply losing altitude over time. While this is true, it is only losing altitude because the commanded altitude is guiding the aircraft to do so. When comparing Figure 60b to other figures, representing elevator deflection in previous altitude trials, it is noticed that elevator deflections after the initial jump are finally becoming visible.

The second frequency variation is shown in Figure 60.

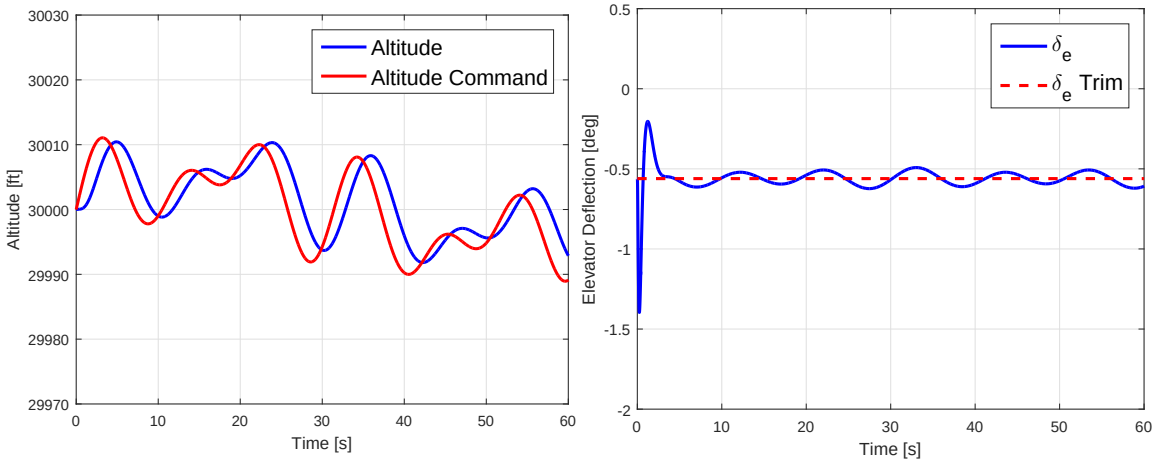

(a) Altitude vs. Command **(b) Elevator Deflection vs. Trim**

Figure 60. Altitude and Elevator Deflection for Frequency Variation 2

Figure 60a clearly shows the complexity of the task, as the frequency variation

becomes slightly more stressing. In addition, the oscillatory changes in elevator deflection are also more distinctly visible in Figure 60b.

The third and final frequency variation is shown in Figure 61.

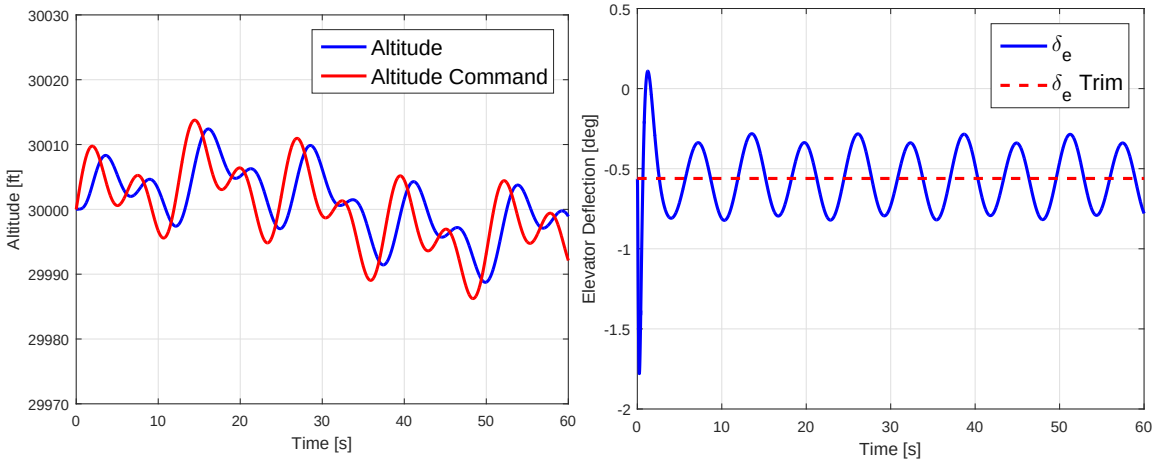

(a) Altitude vs. Command **(b) Elevator Deflection vs. Trim**

Figure 61. Altitude and Elevator Deflection for Frequency Variation 3

It is clear that varying the frequencies of the multisine input yield the most complex altitude tracking task, just as seen with the frequency variation in pitch tracking. Figure 61b depicts oscillations in elevator deflection, more clearly than in any other case. Figure 62 summarizes the results the frequency-varied altitude tracking tasks.

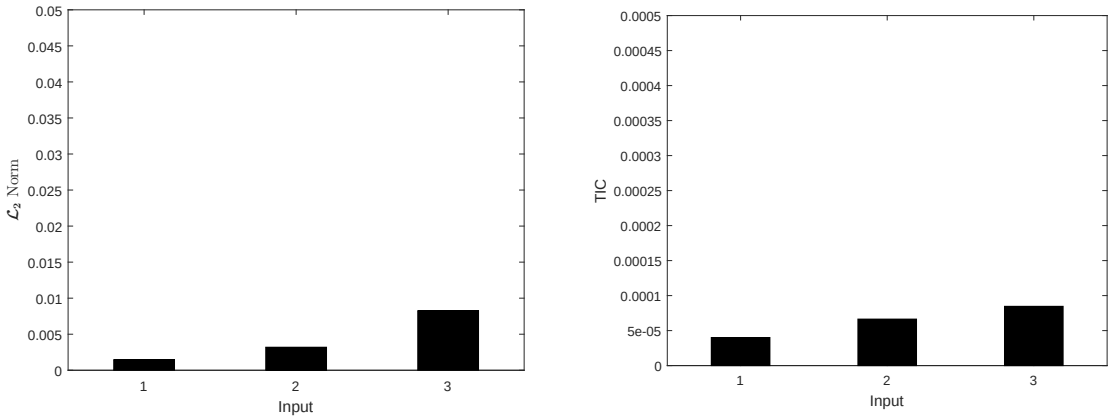

(a) Aircraft Workload **(b) Aircraft Performance**

Figure 62. Altitude Tracking Workload and Performance for Frequency Variation

Even the most stressing case presented to the aircraft, in terms of frequency, did not show an increase to aircraft workload as much as the phase variations did. This is a testament to the control design, as the frequency of the tracking task was almost double that of the bandwidth of the bare airframe. The final frequency variation did however cause slightly degraded aircraft performance, when compared to the most stressing cases of amplitude and phase variation.

4.6 Sensitivity of Workload and Performance Metrics to Mission Task

The workload and performance for each of the three types of maneuver variations, conducted with each of the two tracking tasks, are shown in Figure 63.

According to Figure 63a, for pitch-attitude tracking, the workload metric ($\mathcal{L}_2$ norm) had the most sensitivity to multisine command inputs with increasing frequency variations. The aircraft's workload was almost as high when tasked with tracking multisine inputs with increasing phase variations. However, in terms of performance, Figure 63b clearly shows increasing TIC values, or in other words, decreasing aircraft performance, in tracking multisine input commands with larger frequency variation.

Figure 63c clearly identifies the $\mathcal{L}_2$ norm to be most sensitive to the increased workload of the altitude tracking autopilot when following altitude commands of increasing amplitude. When the amplitude of the altitude command increases, it requires more elevator deflection, and therefore greater workload. It is hypothesized that if elevator deflection rate could be examined as a native output of JSBSim, altitude tracking commands of increased frequency would be causing actuator rate saturation. This would allow insights to be drawn as to how taxing inputs with frequency variations are to the altitude tracking autopilot.

For the altitude tracking task, increasing amplitude caused the strongest increase

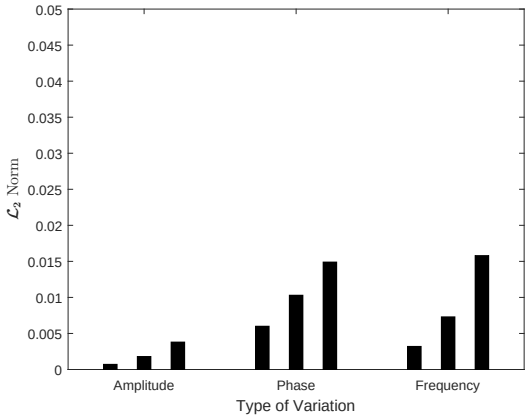

(a) Pitch Tracking Workload

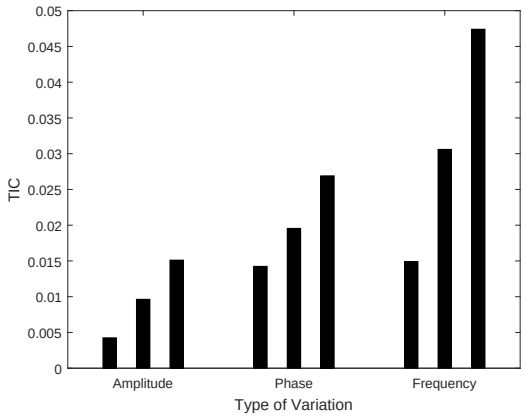

(b) Pitch Tracking Performance

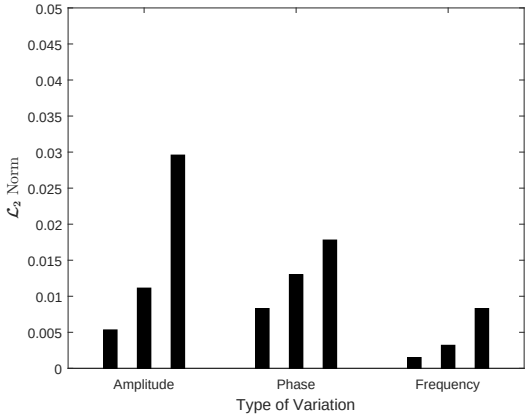

(c) Altitude Tracking Workload

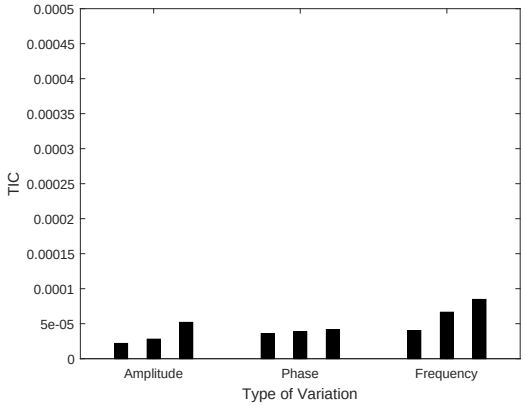

(d) Altitude Tracking Performance

Figure 63. Workload and Performance for Each Variation of Pitch-Attitude Tracking and Altitude Tracking Tasks

in aircraft workload. However, Figure 63d shows that increasing command frequency was most detrimental to aircraft performance. By the same token, it is important to note that the TIC values calculated from altitude tracking data, are two orders of magnitude less than those calculated from pitch-attitude tracking simulations.

Overall, as the multisine input commands were varied to increasing levels of difficulty, the workload of the aircraft increased, while the performance decreased. The pitch-attitude task that required the most workload, resulted in the worst performance, a direct correlation.

On the other hand, the altitude tracking task requiring the most workload, resulted in almost the best performance. This is a testament to the suggestion that emphasis be placed on particular mission task elements when defining aircraft design requirements. In addition, it aligns with results from other studies which found that robustly designed control systems can afford an aircraft excellent tracking, but may do so at the expense of overworked control surface actuators [13].

4.7 Stability Derivative Variations

Once the baseline study was completed, identifying the sensitivities of the $\mathcal{L}_2$ norm and TIC metrics to aircraft workload and performance, throughout the two mission tasks, with varying degrees of complexity, the F-16's stability derivatives were varied. The predicted effects of varying these aircraft design parameters were discussed in the previous chapter. The following is an analysis of the results of varying the pitch stiffness derivative, C_{m_α}, and the pitch damping derivative, C_{m_q}.

4.7.1 Pitch Stiffness Derivative (C_{m_α}) Variation

The pitch stiffness derivative was varied by several different multiples ranging from 1/4 to 4. For each modification of C_{m_α}, the aircraft trim and linearization scripts

were run to yield the linearized aircraft equations of motion. From these equations of motion, the longitudinal LOES models were approximated using the same techniques employed in the initial flying qualities analysis. The values obtained from the LOES approximations are shown in Table 18.

Table 18. Lower Order Equivalent System Approximation with C_{m_α} Variations

C_{m_α} Variation	K_θ	T_{θ_1}	T_{θ_2}	τ_θ	ω_p	ω_{sp}	ζ_p	ζ_{sp}
1/4	0.46	156.55	5.141	0.01	0.0331	0.3257	0.0100	1.0457
1/2	0.93	143.73	3.578	0.01	0.0401	0.4071	0.0100	0.9493
3/4	1.39	129.68	3.178	0.01	0.0453	0.4505	0.0100	0.8963
Original	1.86	111.03	3.000	0.01	0.0494	0.4822	0.0163	0.8582
2	3.72	81.21	2.753	0.01	0.0596	0.5743	0.0330	0.7487
3	5.59	66.51	2.690	0.01	0.0654	0.6454	0.0504	0.6751
4	7.45	74.99	2.627	0.01	0.0688	0.7100	0.0436	0.6175

Just as specified by Blakelock [23], increasing the pitch stiffness derivative had the greatest effect on the short period natural frequency, ω_{sp}. It is clearly seen that, indeed, increasing C_{m_α} increased ω_{sp}. The results of the C_{m_α} variations were plotted in Figure 64, against the MIL-STD-1797A [4] short-term pitch response requirements for Category A flight.

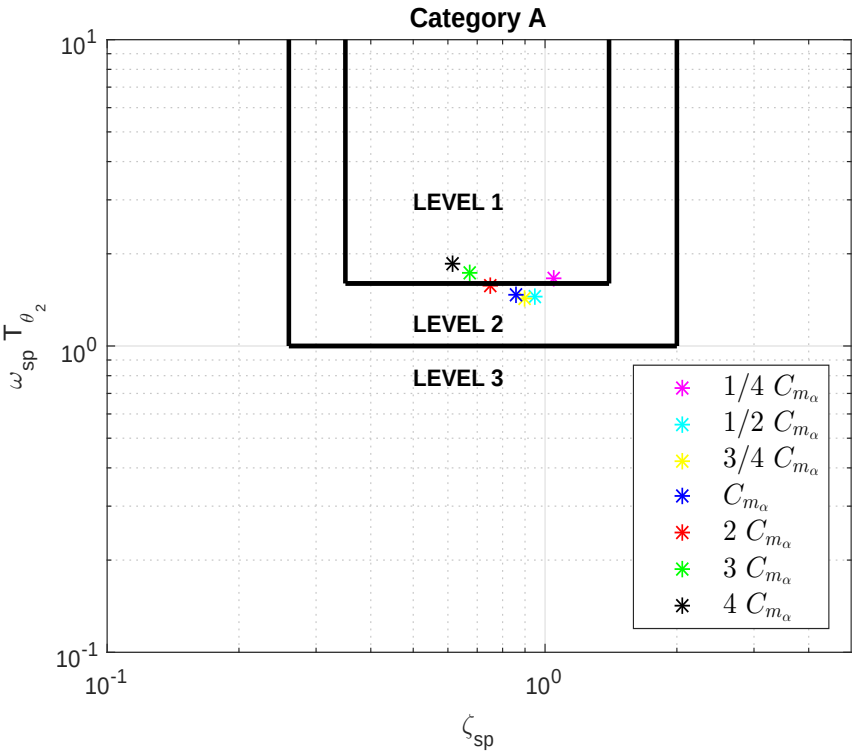

Figure 64. Calculated Flying Qualities Levels for C_{m_α} Variations, According to MIL-STD-1797A [4] Short-Term Pitch Response Requirements

Using the bandwidth and phase delay criteria [6], the appropriate values were calculated for each variation of C_{m_α}. The results are presented in Table 19

Table 19. Bandwidth and Phase Delay for C_{m_α} Variations

C_{m_α} Variation	τ_{θ_p}	ω_{BW}
1/4	0.01	0.501
1/2	0.01	0.540
3/4	0.01	0.577
Original	0.01	0.612
2	0.01	0.726
3	0.01	0.819
4	0.01	0.898

The two pitch stiffness derivative variations that caused the largest difference in flying qualities were the case in which C_{m_α} was multiplied by 1/4 and the case in which it was multiplied by 4. According to the short-term pitch response requirements, these

variations both resulted in a Level 1 aircraft. However, according to the bandwidth requirements, it is clear that these two variations resulted in significant differences from the nominal aircraft open-loop bandwidth.

4.7.2 Pitch Damping Derivative (C_{m_q}) Variation

The pitch stiffness derivative was also varied by several multiples ranging from 1/4 to 2. For each modification of C_{m_q}, the aircraft trim and linearization scripts were executed to yield the linearized aircraft equations of motion. Then, the longitudinal LOES models were approximated. The resulting literal factors are shown in Table 20 and plotted in Figure 65

Table 20. Lower Order Equivalent System Approximation with C_{m_q} Variations

C_{m_q} Variation	K_θ	T_{θ_1}	T_{θ_2}	τ_θ	ω_p	ω_{sp}	ζ_p	ζ_{sp}
1/4	1.86	41.03	2.926	0.01	0.0682	0.3478	0.0100	0.7173
1/2	1.86	69.81	2.893	0.01	0.0595	0.4001	0.0100	0.7626
3/4	1.86	95.67	2.934	0.01	0.0534	0.4443	0.0111	0.8094
Original	1.86	111.03	3.000	0.01	0.0494	0.4822	0.0163	0.8582
5/4	1.86	136.82	3.065	0.01	0.0461	0.5161	0.0131	0.9082
3/2	1.86	163.30	3.136	0.01	0.0436	0.5463	0.0100	0.9587
2	1.87	195.14	3.294	0.01	0.0398	0.5977	0.0100	1.0611

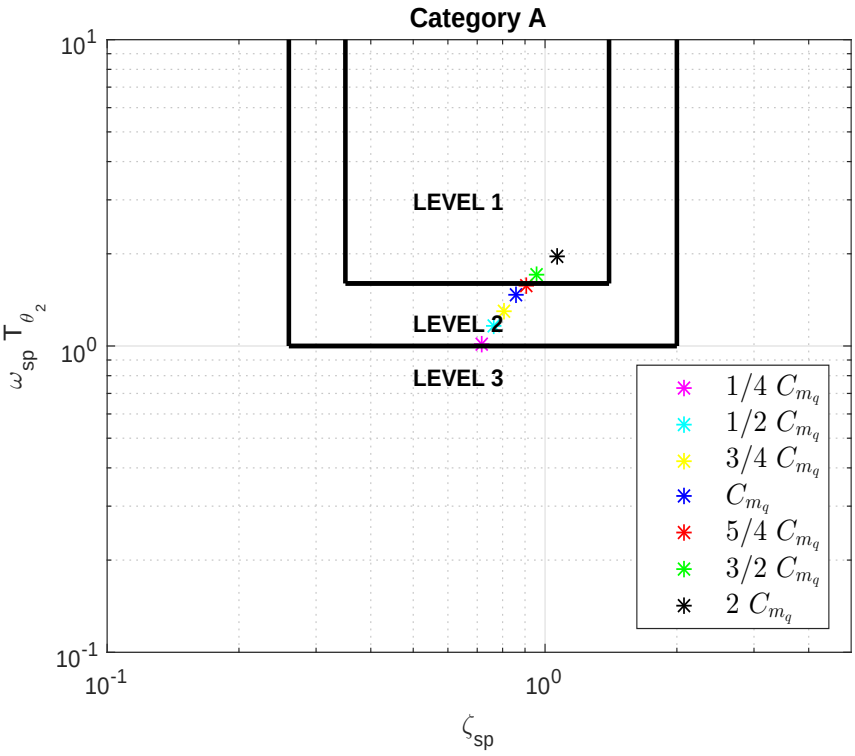

Figure 65. Calculated Flying Qualities Level for C_{m_q} Variations according to MIL-STD-1797A [4] Short-Term Pitch Response Requirements

The calculated changes to the bare airframe bandwidth are listed in Table 21.

Table 21. Bandwidth and Phase Delay for C_{m_q} Variations

C_{m_q} Variation	τ_{θ_p}	ω_{BW}
1/4	0.01	0.325
1/2	0.01	0.422
3/4	0.01	0.516
Original	0.01	0.612
5/4	0.01	0.707
3/2	0.01	0.806
2	0.01	1.012

It is abundantly evident in Figure 65, that varying the pitch damping derivative, C_{m_q}, by multiples on either extreme (i.e. 1/4 and 2) would result in aircraft configurations with the largest difference in level of flying qualities. The case of doubling the pitch damping derivative yields a bare airframe aircraft that exhibits Level 1 flying

qualities. It also results in the highest bandwidth. However, according to the bandwidth criteria for Category A flight, a bandwidth of at least three radians per second is required for Level 1 flying qualities.

Varying the pitch damping derivative by 1/4, results in an aircraft that borderlines flying qualities level 3, and has the lowest bandwidth.

4.8 Workload and Performance Comparisons of Varied Stability Models

The previous analysis served to confirm that varying stability derivatives would result in aircraft with different levels of flying qualities. The cases in which the stability derivatives were varied by the highest and lowest multiples, yielded aircraft with the furthest varied flying qualities.

To determine how these variations in stability derivatives affect aircraft workload and performance, the extreme cases of varied C_{m_α} and C_{m_q} were evaluated against the nominal aircraft configuration, while maneuvering through each mission task.

4.8.1 Pitch-Attitude Tracking

First, a new pitch-attitude tracking task was constructed in the form of Equation 71.

$$\theta_{CMD} = 10^\circ \sin(0.1t + 10^\circ) + 5^\circ \sin(0.4t + 30^\circ) + 2^\circ \sin(0.6t + 50^\circ) \qquad (71)$$

The phase angles are depicted in Equation 71 in units of degrees. This is for ease of understanding. They were actually entered in JSBSim in units of radians.

The first set of simulations were run with the aircraft in its nominal configuration, and then with the pitch stiffness derivative, C_{m_α}, varied by one a factor of 1/4, and then by a factor of 4. The simulated pitch-attitude tracking results are shown relative to the commanded pitch-attitude in Figure 66.

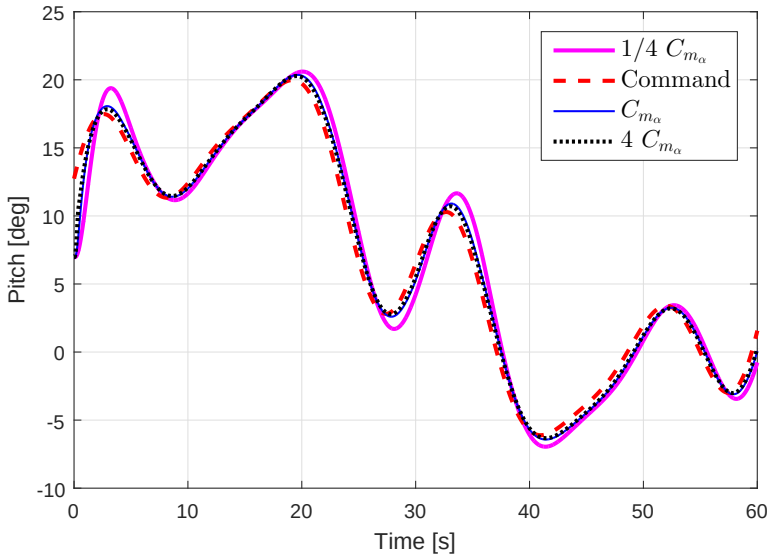

Figure 66. Simulated Pitch-Attitudes Shown Against Command Pitch Input for Nominal and C_{m_α} Varied Cases

Inspecting Figure 66, it can be seen that decreasing the pitch stiffness derivative causes the aircraft to have noticeable overshoot while attempting to track the pitch-attitude input. On the other hand, in the case of increasing the pitch stiffness derivative, the change in tracking is not significantly different from the aircraft in its nominal configuration. Said in other words, the aircraft with $4C_{m_\alpha}$ seemed to perform almost like the nominal, unchanged, aircraft.

The elevator deflection time history is shown in Figure 67.

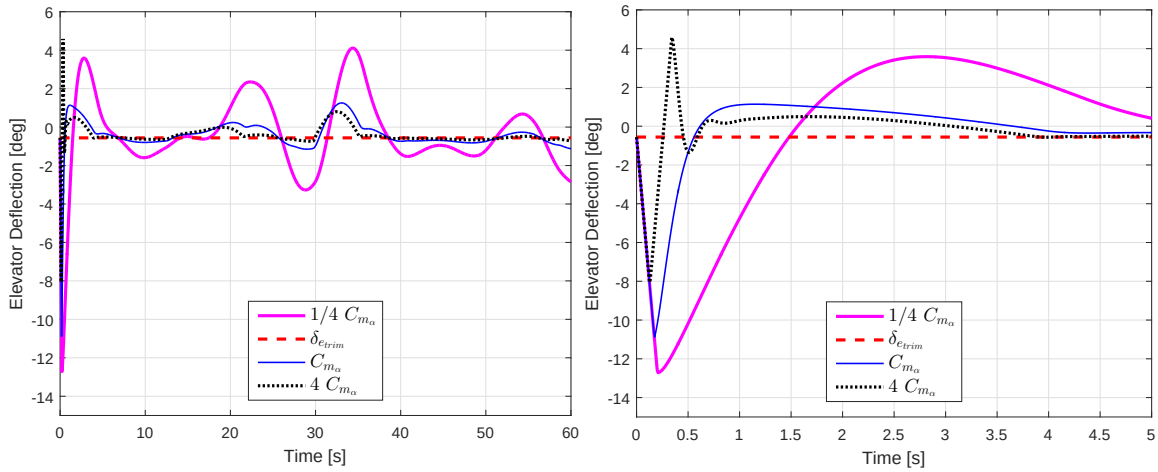

(a) δ_e vs $\delta_{e_{trim}}$ (0 to 60 seconds) **(b) δ_e vs $\delta_{e_{trim}}$ (0 to 5 seconds)**

Figure 67. Pitch-Attitude Tracking Elevator Deflection for Nominally Configured Aircraft and C_{m_α} Varied Cases

There are very small differences that can be seen in pitch-attitude tracking in the previous Figure 66. However, the deflection time histories are markedly different, as illustrated in Figure 67a. Further examining the the first five seconds of the pitch-attitude tracking maneuver, clearly reveals that the elevator actuator experiences rate saturation in all three aircraft stability configurations. The two sharp lines in elevator deflection response, indicate that saturation is worst for the $4C_{m_\alpha}$ case, as seen by the multiple triangular response shapes in the first five seconds of simulation. It can also be deduced from Figure 67a, that the elevator actuator will experience the highest workload in the $1/4C_{m_\alpha}$ stability configuration.

The workload and performance values are quantified and compared in Figure 68.

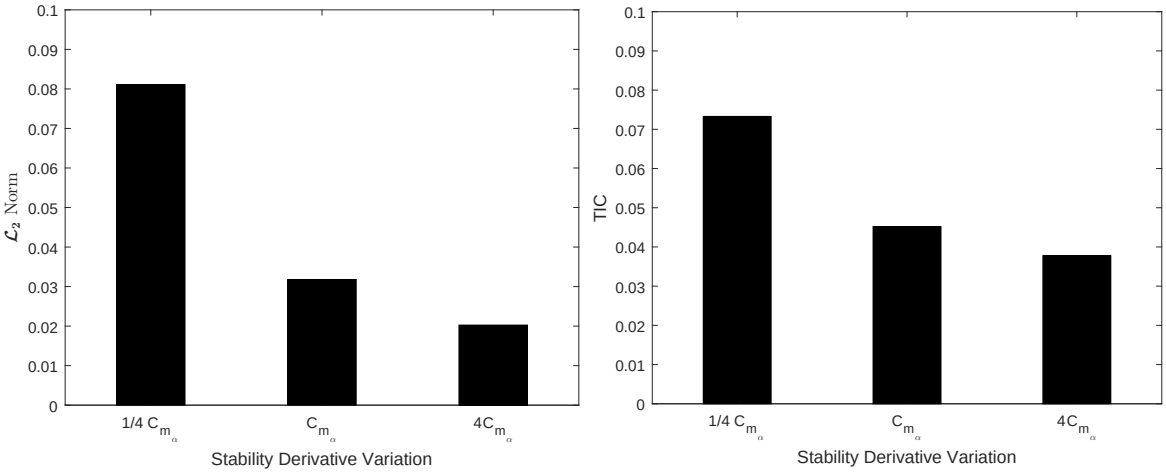

(a) Aircraft Workload **(b) Aircraft Performance**

Figure 68. Pitch-Attitude Tracking Workload and Performance for Nominally Configured Aircraft and C_{m_α} Varied Cases

Just as predicted, decreasing the pitch stiffness stability derivative strongly increases the aircraft's workload, and degrades its performance. Conversely, increasing the pitch stiffness stability derivative decreases aircraft workload, and improves performance, when compared to the nominal aircraft. However, caution must be exercised. While workload favorably decreases, and performance favorably increases, the increased pitch stiffness derivative causes actuator rate saturations during both the positive and negative elevator deflections, as can be clearly seen with the straight lines in Figure 67b.

After the pitch stiffness derivative was varied, the pitch-attitude tracking tasks were repeated. This time, with variations to the pitch damping derivative, C_{m_q}. The resulting simulated pitch-attitudes are shown for the nominal, and varied aircraft, along with the command input time history, in Figure 69.

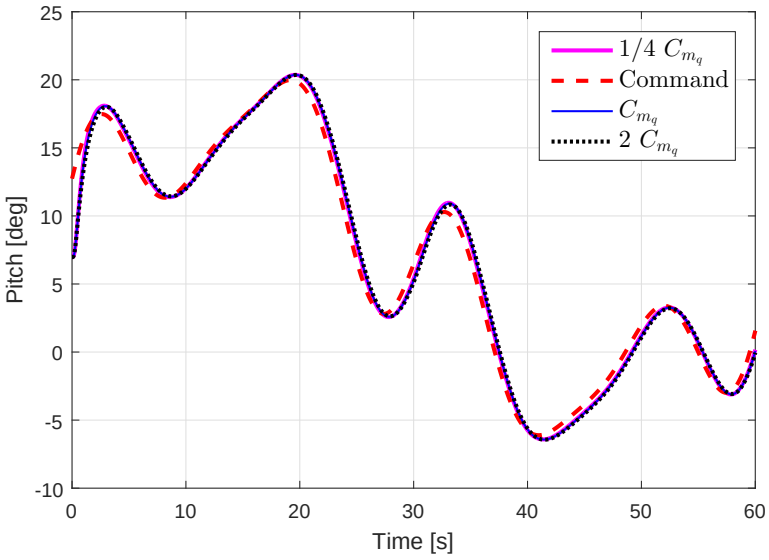

Figure 69. Simulated Pitch-Attitudes Shown Against Command Pitch Input for Nominal and C_{m_q} Varied Cases

At first look, it appears as if the aircraft is able to achieve the same performance regardless of its stability configuration. This is interesting to note, when recalling the initial flying qualities evaluations (Figure 65), which identified the $1/4C_{m_q}$ bare airframe as a Level 3 aircraft, versus the $2C_{m_q}$ bare airframe, which was identified as Level 1.

The elevator deflections required by the aircraft to maintain pitch-attitude tracking, with varied pitch damping derivatives, are presented in Figure 70.

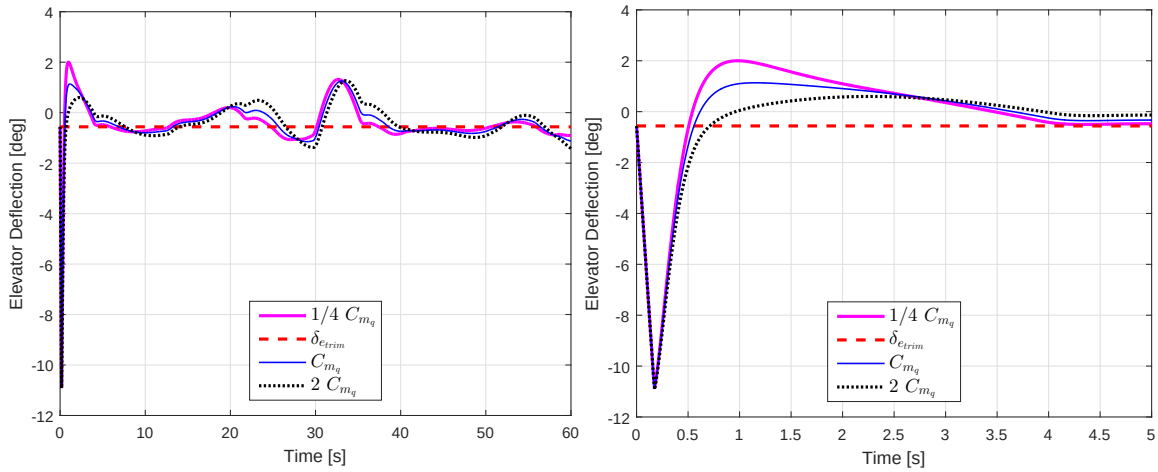

(a) δ_e vs $\delta_{e_{trim}}$ (0 to 60 seconds) **(b) δ_e vs $\delta_{e_{trim}}$ (0 to 5 seconds)**

Figure 70. Pitch-Attitude Tracking Elevator Deflection for Nominally Configured Aircraft and C_{m_q} Varied Cases

The resulting pitch-attitude time histories between each pitch damping stability variation have clear differences. As the pitch stiffness is decreased, overshoots increase, as seen in Figure 70b. This particular pitch-attitude tracking command causes almost the same amount of rate limiting, regardless of the aircraft stability configuration. The case in which the pitch damping derivative is increased, almost seems to show a better response, in that there is a lower overshoot. However, it seems that it takes longer for the elevator to settle on a particular commanded setting.

The workload and performance metrics for the pitch-attitude tracking task, with pitch damping derivative variations, are shown in Figure 71.

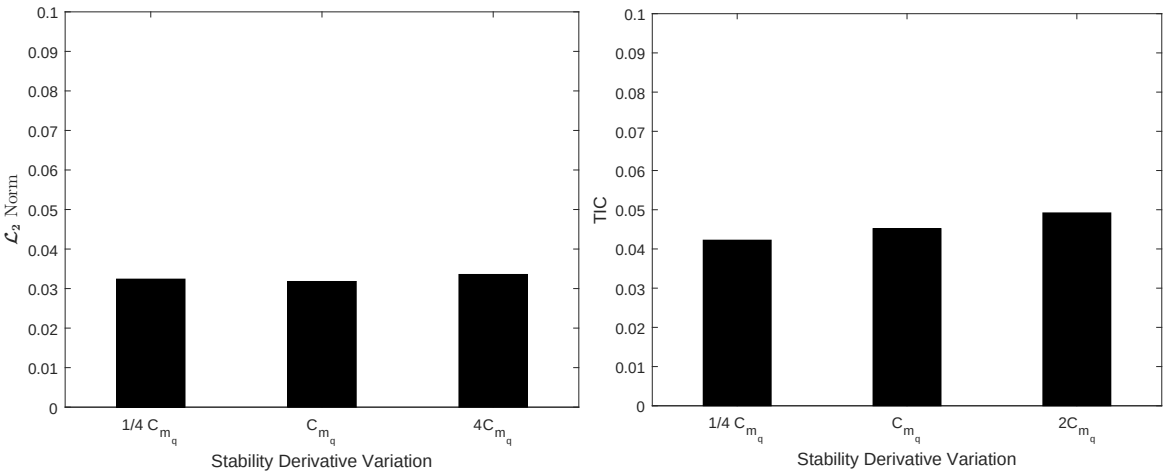

(a) Aircraft Workload **(b) Aircraft Performance**

Figure 71. Pitch-Attitude Tracking Workload and Performance for Nominally Configured Aircraft and C_{m_q} Varied Cases

While the workload of the aircraft does not appear to significantly vary over the three cases, it is clear that performance is most degraded when the pitch damping derivative is increased. This is contrary to the findings of the flying qualities evaluation, summarized in Figure 65. The thumbprint plot clearly identified that when the pitch damping derivative was increased, the bare airframe started to exhibit Level 1 flying qualities. Even according to Table 21, the aircraft design is shown to improve, with greater bandwidth, when the pitch damping stability derivative is increased. Thus it is fascinating to find that, under autopilot control, the increased pitch damping derivative is counterproductive. This case serves to highlight the consequences of not redesigning autopilots after making modifications to UAV geometry.

4.8.2 Altitude Tracking

The altitude tracking command took the form of the multisine input shown in Equation 72. Just as with the multisine input constructed for the pitch-attitude tracking task, the phase angles were specified in JSBSim in units of radians. For

clarity, they are shown here in units of degrees.

$$h_{CMD} = 25 \text{ ft } \sin(0.1t + 10^\circ) + 10 \text{ ft } \sin(0.4t + 30^\circ) + 5 \text{ ft } \sin(0.6t + 50^\circ) \quad (72)$$

The first set of simulation cases were conducted with the aircraft in the nominal stability configuration, and then with varied values for the pitch stiffness derivative, C_{m_α}. The resulting altitudes that the F-16 attained in simulation are shown, against the commanded altitude inputs, in Figure 72.

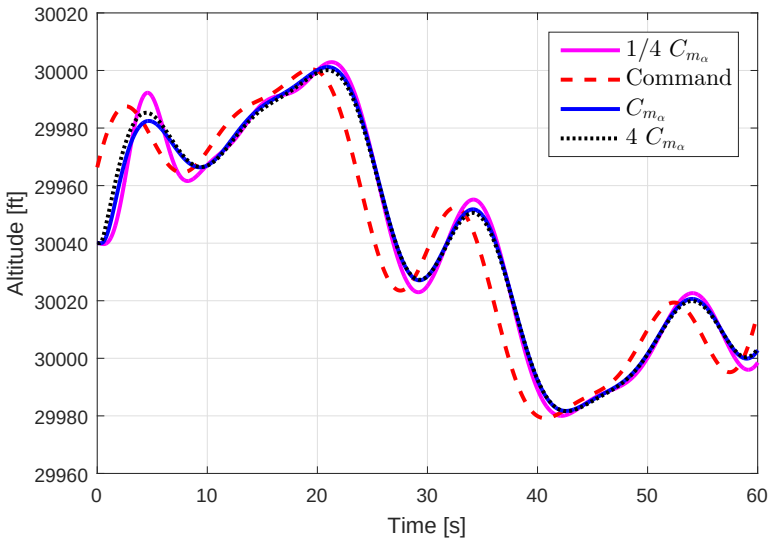

Figure 72. Simulated Altitudes Shown Against Command Altitude Input for Nominal and C_{m_α} Varied Cases

It is immediately seen that the tracking response of the aircraft configured with $4C_{m_\alpha}$, significantly varies from the response of the nominally configured aircraft. To further examine the outcome of the simulations, the time history of the elevator deflection angle is compared against the trimmed elevator deflection position in Figure 73.

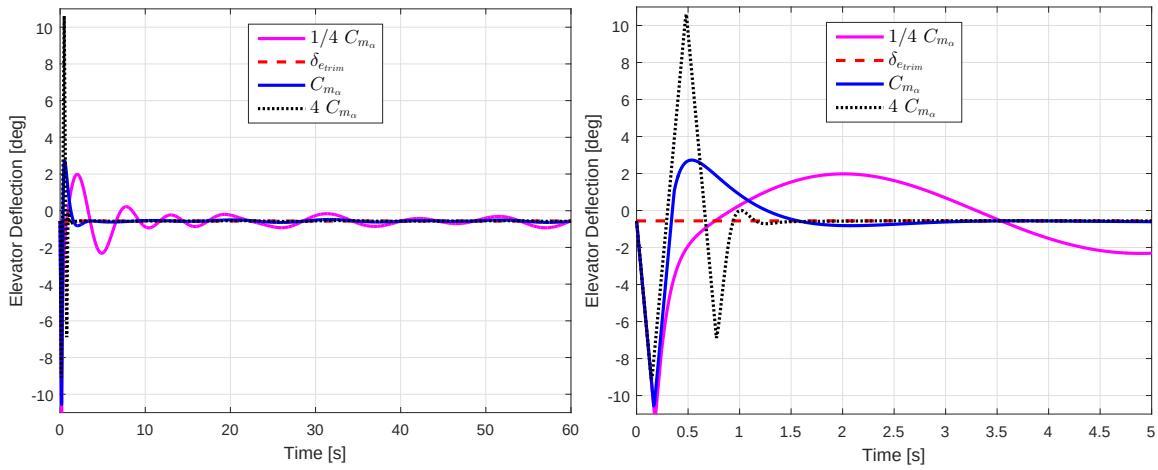

(a) δ_e vs $\delta_{e_{trim}}$ (0 to 60 seconds) **(b) δ_e vs $\delta_{e_{trim}}$ (0 to 5 seconds)**

Figure 73. Altitude Tracking Elevator Deflection for Nominally Configured Aircraft and C_{m_α} Varied Cases

An initial look at Figure 73a, reveals clear signs of elevator actuator rate saturation, especially in the $4C_{m_\alpha}$ case. It also indicates that the workload of the aircraft, modified for $1/4C_{m_\alpha}$, should be higher, as the elevator has to deflect more often to maintain altitude tracking. Inspecting the elevator deflections during the first five seconds of the maneuver, as shown in Figure 73b, confirms these indications of rate saturation. The effects of rate limiting are worse for the $1/4C_{m_\alpha}$ case, when compared to the nominally configured aircraft. The $4C_{m_\alpha}$ case shows the worst effects of rate limiting. By the same token, for both the nominally configured, and $4C_{m_\alpha}$ cases, after the initial rate saturation, the elevator returns to making small corrections for the remainder of the tracking task.

In order to make a more exact judgment as to the workload and performance of the two stability varied aircraft, relative to the nominally configured airplane, the $\mathcal{L}_2$ norm and TIC were calculated. The values are shown in Figure 74.

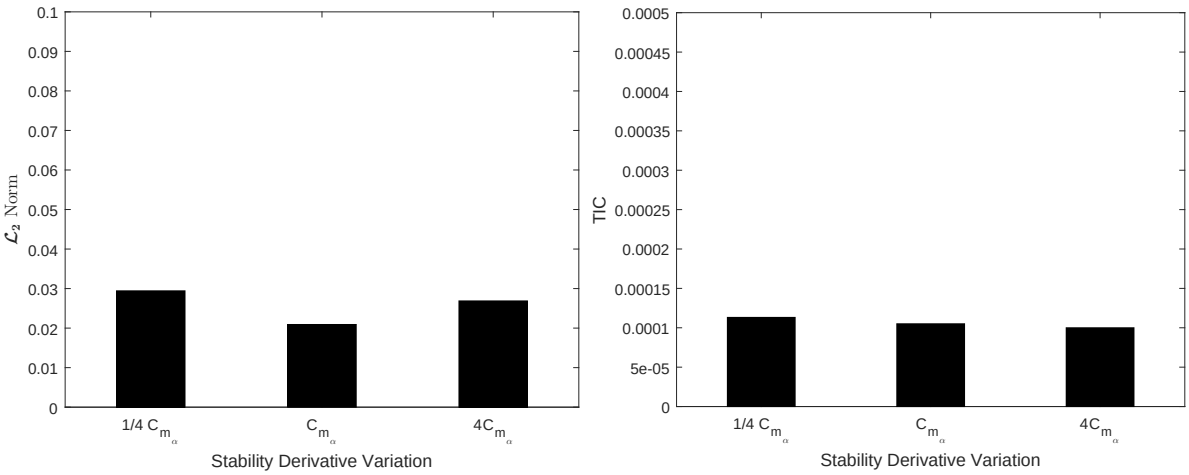

(a) Aircraft Workload **(b) Aircraft Performance**

Figure 74. Altitude Tracking Workload and Performance for Nominally Configured Aircraft and C_{m_α} Varied Cases

Figure 74a serves as solid evidence that the $1/4C_{m_\alpha}$ varied aircraft required a higher workload to maintain tracking, although it is surprising how little the effect was captured by the $\mathcal{L}_2$ metric. The $4C_{m_\alpha}$ aircraft also had a similar workload. This serves to further motivate the importance of control system redesign, and re-evaluation, any time the dimensions or configurations of UAV control surfaces are modified.

Figure 74b shows TIC values that are consistent with the baseline tracking tasks completed with the nominally configured aircraft. Across the board, it seems that the altitude tracking trials were too benign to adequately show any degradation in aircraft performance. However, it can be seen that the performance of the $1/4C_{m_\alpha}$ aircraft is slightly worse than the other two aircraft configurations. In contrast, multiplying C_{m_α} by a factor of 4, resulted in slightly better performance than the nominal case.

The next stability value to be varied was the pitch damping derivative, C_{m_q}. The time histories of the achieved altitudes for the varied aircraft are compared to that of the nominal aircraft, in Figure 75.

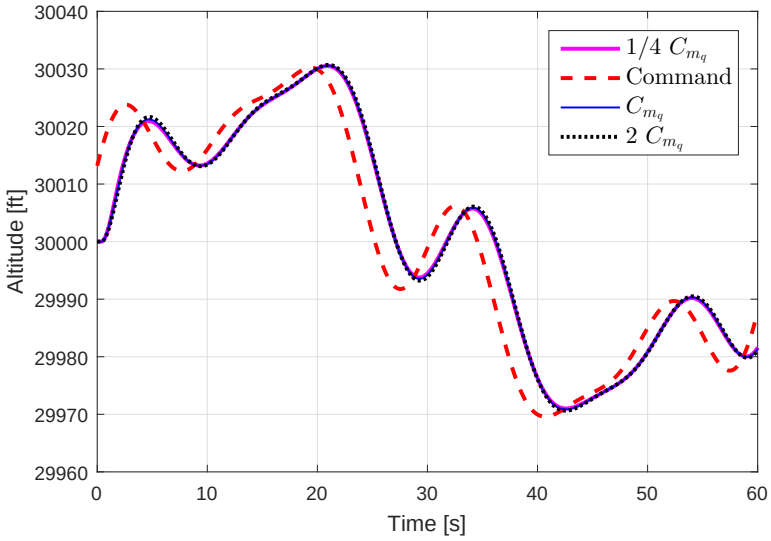

Figure 75. Simulated Altitudes Shown Against Command Altitude Input for Nominal and C_{m_q} Varied Cases

In examining Figure 75, it appears as if the aircraft performance is almost agnostic to variations of the pitch damping derivative, C_{m_q}. The time histories of the flight simulation altitudes, of each of the three aircraft configurations, seem to lie right on top of one another, and vary almost equally from the command altitude input.

The time histories of the elevator deflections throughout the simulations are graphed in Figure 76.

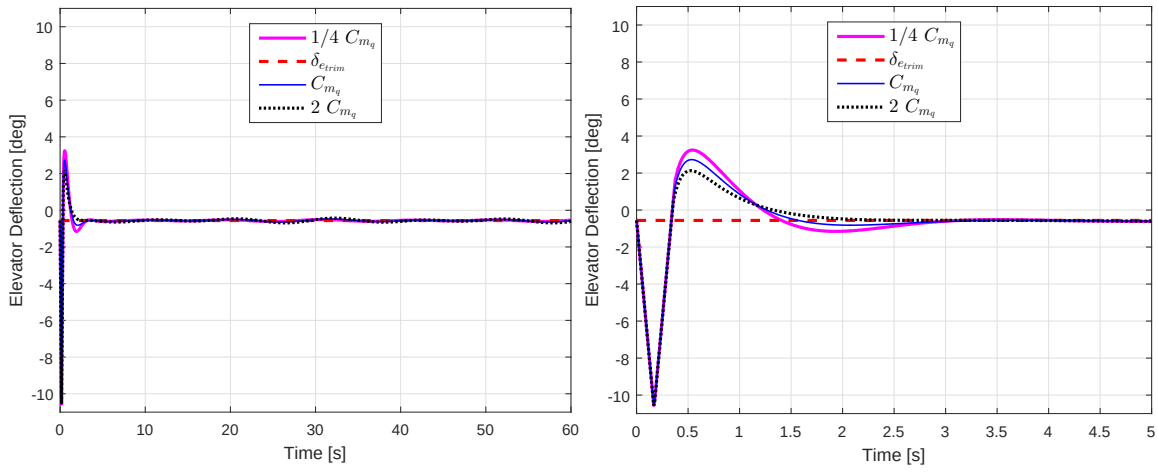

(a) δ_e vs $\delta_{e_{trim}}$ (0 to 60 seconds) **(b) δ_e vs $\delta_{e_{trim}}$ (0 to 5 seconds)**

Figure 76. Altitude Tracking Elevator Deflection for Nominally Configured Aircraft and C_{m_q} Varied Cases

Just as surmised from the graphs of altitude time histories in Figure 75, the elevator deflection time histories are almost the same for the nominal, and C_{m_q} varied aircraft configurations, as shown in Figure 76a. A closer look, examining elevator deflections during the first five seconds of the maneuver, in Figure 76b, reveals that decreasing the pitch damping derivative causes slightly larger initial elevator deflections. On the other hand, doubling the pitch damping derivative, results in slightly smaller elevator deflections. This is consistent with the effect of varying C_{m_q} on the short period damping coefficient, ζ_{sp}. Higher values of this damping coefficient, yield smaller oscillations, or overshoots in system response, at the expense of response speed. Conversely, lowering the short period damping coefficient results in faster rise time at the cost of higher overshoot.

The aircraft workload ($\mathcal{L}_2$ norm) and performance (TIC) are shown graphically, for the nominal aircraft configuration, and each of the two variations, in Figure 77.

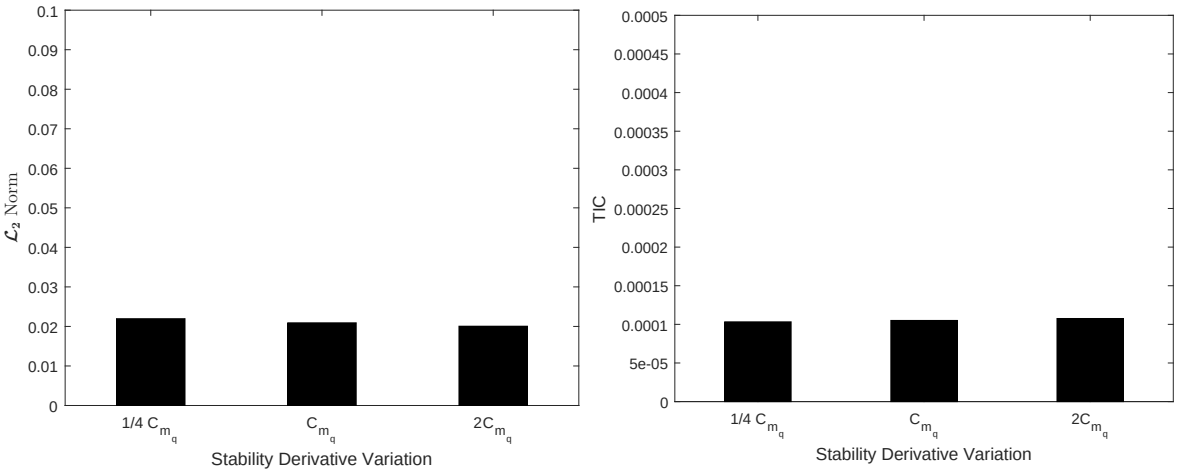

(a) Aircraft Workload **(b) Aircraft Performance**

Figure 77. Altitude Tracking Workload and Performance for Nominally Configured Aircraft and C_{m_q} Varied Cases

The results of the workload evaluation, shown in Figure 77a, are in accordance with what was seen in Figure 76b. As the pitch damping derivative is decreased, the elevator deflects slightly more, thereby increasing the aircraft workload, albeit by an

almost negligible amount. Performance, on the other hand, is not seen to vary at all, as illustrated in Figure 77b.

The computed workload and performance metrics for each stability derivative varied case, corresponding to each of the two tracking tasks is shown in Figure 78.

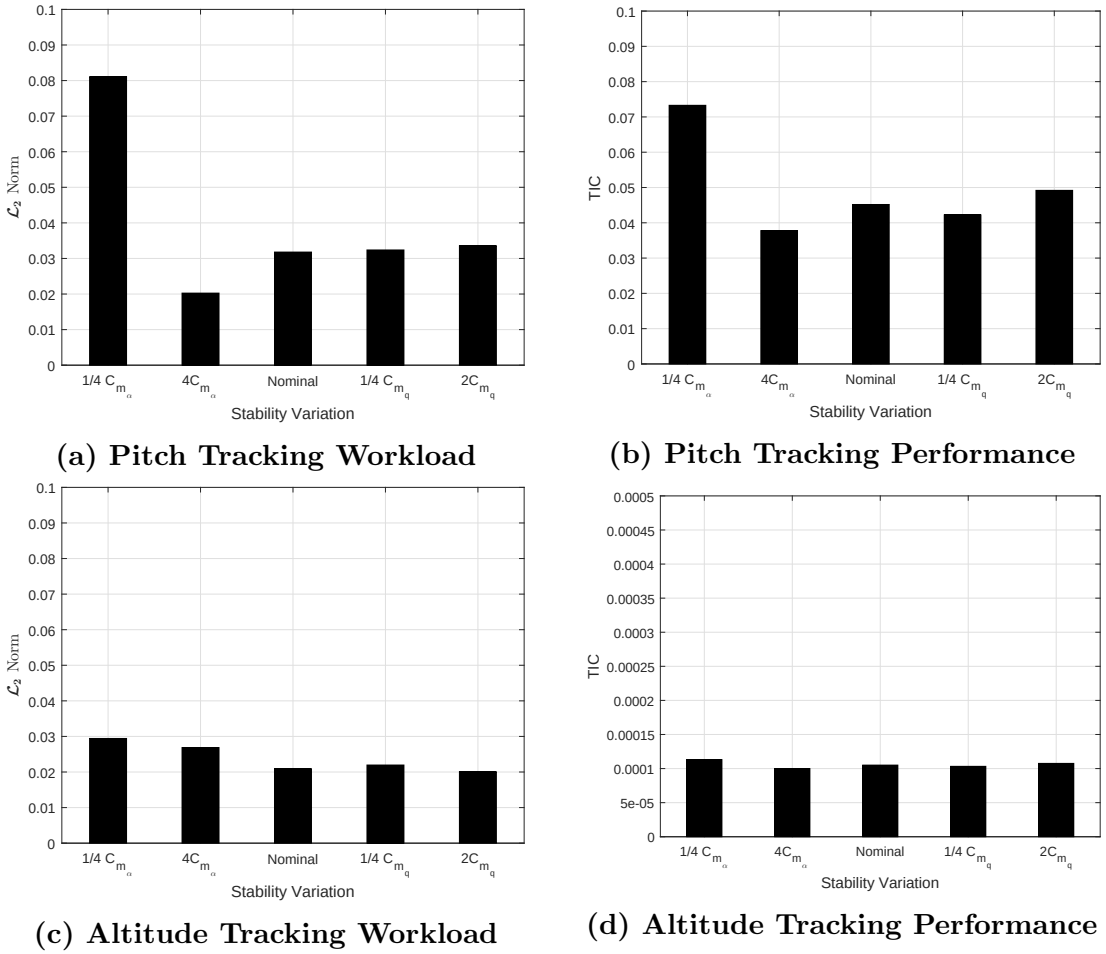

(a) Pitch Tracking Workload

(b) Pitch Tracking Performance

(c) Altitude Tracking Workload

(d) Altitude Tracking Performance

Figure 78. Workload and Performance for Each Stability Derivative Variation for Pitch-Attitude Tracking and Altitude Tracking Tasks

Overall, it is clearly evident that the values for the $\mathcal{L}_2$ norm and TIC are highly dependent on specific aircraft mission tasks. It would not be logical to use these metrics to evaluate UAV flying qualities, or quote specific values as design constraints, without first specifying exactly what maneuver the UAV is to perform. For highly dynamic, and aggressive maneuvers, like pitch-attitude tracking, values for $\mathcal{L}_2$ and

TIC can be expected to be larger. On the contrary, $\mathcal{L}_2$ and TIC values should be expected to be very low for maneuvers that require a greater deal of precision, like lining up with an aerial refueling boom.

Once these metrics are specified in light of a specific mission task, they can be invaluable in assessing UAV flying qualities, as they can quickly call attention to flaws in the inherent stability characteristics of an aircraft, or an autopilot system that lacks the optimal settings.

4.9 Suggested Techniques for Using Workload and Performance Metrics as Flying Qualities Requirements

Flight testing in the past, using variable stability aircraft, enabled the development of flying qualities standards, based on the correlation between inherent aircraft stability characteristics and pilot opinion of how they affected the level of effort required to perform specific sets of maneuvers, like take-off, landing, or target acquisition. Many of the requirements in MIL-STD-1797B [6] are specified by using thumbprint plots, which visually depict the relationship between flying qualities and stability and control values.

It is suggested that plots like these also be used for UAV design requirements. Instead of specifying a specific stability and control literal factor, like bandwidth, or phase delay, the axes of this plot could be composed of the $\mathcal{L}_2$ norm and TIC value. Just like in MIL-STD-1797 [4], these UAV thumbprint plots would have to be specific to certain classes of aircraft and specific categories of mission tasks.

Two examples of how these plots could be manifested are illustrated as follows. They are initially populated with data garnered through the flight simulations conducted in this research effort. The notional pitch-attitude tracking workload and performance requirement thumbprint in Figure 79, shows more relaxed envelopes for

specific levels of flying qualities. This is because it is intended to specify requirements for aggresive maneuvers, in which workload and performance must be more balanced.

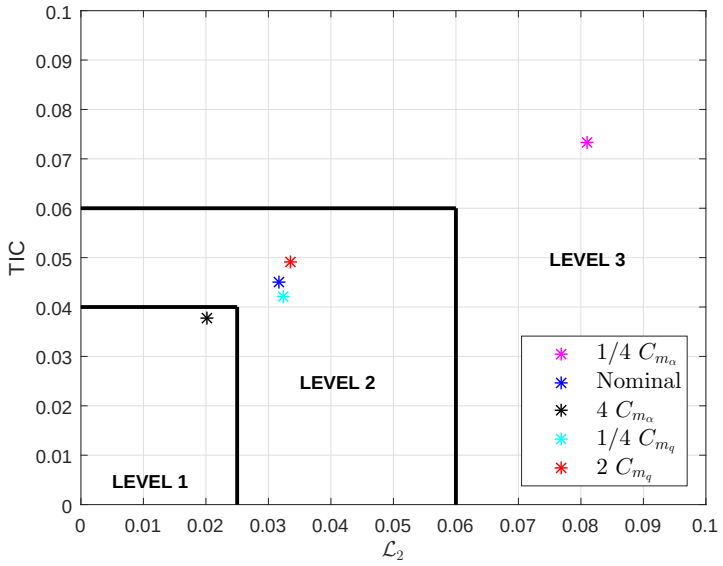

Figure 79. Notional Pitch-Attitude Tracking Workload and Performance Thumbprint Plot

The notional altitude-tracking workload and performance requirement thumbprint, shown in Figure 80, depicts tighter requirements for both performance and workload. This is because it represents design demands for an aircraft that must be capable of very precise tracking in the immediate vicinity of other aircraft, like during aerial refueling.

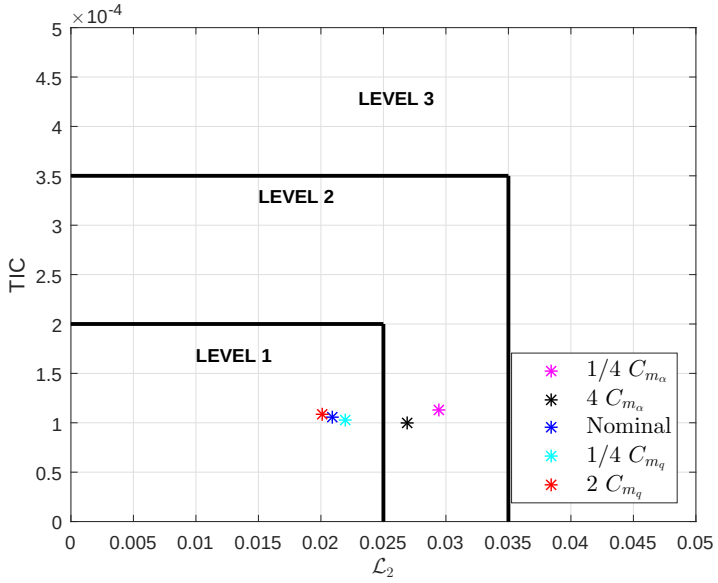

Figure 80. Notional Altitude Tracking Workload and Performance Thumbprint Plot

From these hypothetical diagrams, it can be seen that as performance degrades, the TIC value on the y-axis increases, and as workload increases the $\mathcal{L}_2$ value on the x-axis increases. As the workload of an aircraft moves to the right, and as the performance value of the aircraft moves up, the aircraft flying qualities degrade.

A wide range of data, using many different classes of aircraft, is still needed to accurately define the flying qualities envelopes that would be depicted on these plots. For example, a turbine powered UAV may be able to cycle its actuators thousands of times before ever needing maintenance. Battery powered UAVs, however, do not enjoy the same operational latitude. An $\mathcal{L}_2$ norm specification would be vastly different for each of the two aircraft, and therefore the envelopes of flying qualities specifications would look very different.

4.10 Summary

The preceding chapter served to present and analyze the results of this research effort. Beginning with successfully trimming the F-16 aircraft at a nominal refu-

eling altitude and airspeed, an extensive flying qualities evaluation was conducted, using well-established techniques from MIL-STD-1797 [6]. Once the longitudinal flying qualities of the F-16 were determined, a pitch tracking and an altitude tracking autopilot were designed, using linear systems theory. These autopilots were then configured, and loaded into JSBSim, which was used to simulate the F-16 executing several varying pitch-attitude tracking and altitude tracking maneuvers. The results of these simulations were analyzed using the $\mathcal{L}_2$ norm, which measured elevator actuator workload, and TIC, which measured aircraft performance. A baseline for the sensitivity of these metrics to specific mission task was then determined. Next, nominal pitch-attitude and altitude tracking maneuvers were devised through the use of a multisine command input. The aircraft was simulated to track this input in a nominal configuration, as well as in configurations with select variations of stability derivatives. The $\mathcal{L}_2$ norm and TIC metrics were again used to analyze how aircraft stability characteristics relate to workload and performance. Finally, techniques for the employment of these metrics toward evaluating UAV flying qualities were suggested.

V Conclusions and Recommendations

5.1 Conclusions

Drawing its impetus from the many aerospace engineering challenges sparked by the burgeoning field of unmanned flight, this research undertaking harnessed the power of flight simulation, in carrying out an extensive investigation of aircraft stability and control characteristics, or flying qualities, which would have the most important bearing on the safe and sustained flight of an unmanned aircraft. The ultimate intent of this effort was to contribute toward the establishment of a basis for precise and applicable airworthiness standards for these innovative machines. There were five specific objectives of this work:

1. Model the F-16 aircraft in JSBSim and evaluate its flying qualities using current standards outlined in MIL-STD-1797.

2. Design two autonomous flight controllers that enable the aircraft to perform two types of precision-aggressive longitudinal tracking tasks.

3. Simulate the aircraft executing the designated maneuvers and establish a baseline for metrics that capture aircraft workload and performance.

4. Increase the complexity of maneuvers and evaluate the workload and performance of the aircraft in a nominal flight configuration. Then, vary the aircraft stability and re-evaluate its workload and performance throughout the same set of maneuvers.

5. Compare simulation results and provide a path forward for establishing metrics that can eventually guide the development of design requirements for autonomous aircraft.

There is no substitute for real-world flight testing. As such, this research aspires to serve as a precursor for experiments using a functional aircraft. In order to allow for accurate comparisons of real-world flight test data, with flight simulated data, the F-16 aircraft model was chosen. A permanently modified, experimental version of the F-16, known as the Variable stability In-flight Simulator Test Aircraft (VISTA) is currently in use at the US Air Force Test Pilot School, and would make an excellent candidate as a test bed for furthering this research.

Pertinent information for simulating the flight dynamics of the F-16 was readily found in open source text [64]. The model that was incorporated into JSBSim was actually an approximation of a more complex version, developed at NASA, for flight simulation [55]. While the approximated model did not include the dynamics of the F-16's automatically deploying leading edge slats, and while higher order engine dynamics were not readily integrated into JSBSim, the exclusion of these features did not hinder the research effort.

Previous research [48] advocated for a mission task oriented set of flying qualities requirements. Four categories of mission task elements (MTEs) were designated, including a list of precision-aggressive tasks, which were the subject of this investigation. As such, two mission tasks were selected for evaluation. The first was a pitch-attitude tracking task, and the second was an altitude tracking task. The latter of the two, most closely resembles air-to-air refueling. For this reason, the F-16 aircraft was initialized in JSBSim at a nominal refueling altitude and airspeed. Once initialized in flight, native features of JSBSim, like the trim and linearization functions, served as powerful tools for flying qualities analysis.

After the linearized state space representation of the F-16 aircraft dynamics was obtained from the simulation software, an initial flying qualities evaluation was conducted. For this analysis, longitudinal flying qualities standards, like the short-term

pitch response to pitch control requirement, and the bandwidth and time delay criteria, were applied. The overall results of this initial analysis indicated that the F-16 bare-airframe would be predicted to exhibit Level 2 flying qualities when airborne at the initialized flight configuration.

The linearized state space model of the simulated F-16 was used again, in the design of two autopilots which made it possible for the aircraft to track pitch commands and altitude commands. After these controllers were designed, they were integrated into JSBSim, and a series of fully non-linear flight simulations was conducted. Using data gathered from these tests, the sensitivities of the workload metric, $\mathcal{L}_2$ norm, and performance metric, TIC, were analyzed for their dependence on specific mission tasks. It was found that the values of these metrics are highly correlated to specific mission tasks. The aircraft workload and performance values were significantly lower when comparing even the most stressing altitude tracking case to the least stressing pitch-attitude tracking case. Thus, if the $\mathcal{L}_2$ norm and TIC metrics are to be used to specify design requirements, they must do so in light of specific mission tasks.

Once a baseline for the workload and performance metrics was established, aircraft stability derivatives were varied. Consistent with aeronautical design theory [23], the effect of increasing pitch stiffness, increased the short period natural frequency. Also, increasing the pitch damping derivative was seen to increase the short period damping coefficient.

For each stability derivative variation, a new flying qualities assessment was conducted. The stability derivative variations that resulted in the greatest changes to flying qualities were then incorporated into the F-16 model, and subsequent pitch-attitude and altitude tracking maneuvers were simulated. The workload and performance of the aircraft in the nominal configuration, and in the stability varied configurations was then compared. It was found that while some stability derivative

variations improved the F-16's flying qualities, its actual workload and performance may have degraded.

Generally speaking, the altitude tracking task proved to be benign, and did not significantly burden the elevator actuator. Pitch-attitude tracking tasks, however, did show marked increases in aircraft workload, and decreases in aircraft performance.

Based on these observations, a method for using the workload and performance metrics to specify flying qualities requirements was suggested. These metrics would be highly specific to a particular type of aircraft, and to the mission task to be performed. It is hypothesized that once enough data is collected from various different classes of vehicles, a trend between stability and control characteristics and aircraft workload and performance will begin to identify itself. These uncovered relationships can then be used to establish tried and tested standards for the design and modification of unmanned aircraft.

5.2 Future Research Recommendations

In light of continuing the research effort, there were several areas identified for further exploration. One phenomenon that was seen in the computer simulations, was actuator rate saturation. This was identified by sharp and straight lines depicting elevator deflection over time. JSBSim outputs many values natively, but there are no built-in classes for outputting the actual actuator deflection rates. Perhaps using a PID block with the proportional and integral gains set to zero, and the derivative gain set to unity, would suffice as a valid method for obtaining this information.

While this research effort made use of the multisine input, many UAVs, including the Google Solara 50 [9], crashed after being exposed to turbulence. The innovative materials and non-classical structural configurations of unmanned aircraft may allow them to be more resistant to these airmass disturbances. It is the autopilot control

system that, then becomes the limiting factor. The gust model specified in MIL-STD-1797 [6], is a native feature of the JSBSim software. Subsequent investigations can use this feature to test autopilots optimized for disturbance rejection. Data on the resulting aircraft workload and performance could help identify focus areas for the design of new autopilots that respond more favorably to these highly variable atmospheric effects.

Speaking of autopilot design, this research effort relied primarily on conventional linear control system design techniques. Future research efforts could design autopilots through the use of Linear Quadratic Regulators and Estimators, or pole placement techniques.

In manned aircraft standards [6], levels of flying qualities are specified even during degraded vehicle states, or failure states. Perhaps JSBSim can be used to analyze the effects of losing a control surface actuator. For example, JSBSim could be used to simulate the flight of an F-16 with only the port side of the elevator operable, with the starboard side locked in a failure position.

Finally, the powerful capabilities of JSBSim, in running batch scripts, could be harnessed to produce large sets of flight simulation data. Simulations in greater volume, could serve to reveal which stability and control characteristics have the most important bearing on unmanned flight.

5.3 Summary

The current standards for flying qualities of piloted aircraft simply do not directly translate to the design of UAVs. The open loop requirements specified in MIL-STD-1797B [6], offer a good starting place for the design of unmanned aircraft. Ultimately however, augmenting the design of UAVs to exhibit classical aircraft dynamics, may be restrictive. The flying qualities of a UAV are more heavily dependent on its underlying

control system. Measuring the actual workload of an aircraft, in deflecting its control surfaces, and relating those metrics to the aircraft's performance of specific mission task elements, can ultimately reveal just what stability criteria must be optimized. This information will enable the safe modification of existing unmanned systems, and the development of robust future designs.

Bibliography

1. *Military Specification - Flying Qualities of Piloted Airplanes*. Technical Report MIL-F-8785, Department of Defense, 1954.

2. *Aviation: An Historical Survey from its Origins to the End of World War II*. Her Majesty's Stationary Office, London, 1970.

3. *RPV Flying Qualities Design Criteria*. Technical Report AFFDL-TR-76-125, Rockwell International Corporation, December 1976.

4. *Flying Qualities of Piloted Aircraft*. Interface Standard MIL-STD-1797A, Department of Defense, 1995.

5. *Aeronautical Design Standard, Performance Specification, Handling Qualities Requirements for Military Rotorcraft*. Interface Standard ADS-33E-PRF, U.S. Army Aviation and Missile Command, March 2000.

6. *Flying Qualities of Piloted Aircraft*. Interface Standard MIL-STD-1797B, Department of Defense, 2006.

7. *Airworthiness Certification Criteria*. Interface Standard MIL-HDBK-516C, United States Air Force, 2014.

8. "RQ-4 Global Hawk", 2014. URL `http://www.af.mil/AboutUs/FactSheets/Display/tabid/224/Article/104516/rq-4-global-hawk.aspx`.

9. *Aviation Accident Final Report: Solara 50*. Technical Report DCA15CA117, National Transportation Safety Board, November 2015.

10. *Aviation Accident Final Report: Aquila*. Technical Report DCA16CA197, National Transportation Safety Board, December 2016.

11. *Perdix Fact Sheet*. Technical report, Department of Defense Strategic Capabilities Office, 2016.

12. *United States Standards Related Document for Air to Air Refueling*. Interface Standard ATP-3.3.4.2.(C), Department of Defense, 2016.

13. Abdulrahim, M., A. Mohamed, and S. Watkins. "Control Strategies for Flight in Extreme Turbulence". *AIAA Guidance, Navigation, and Control Conference*, AIAA 2017-1909. Grapevine, TX, January 2017.

14. Abzug, M and E. Larrabee. *Airplane Stability and Control*. Cambridge University Press, Cambridge, MA, 2002.

15. Amazon.com. "Amazon Prime Air". URL `https://www.amazon.com/b?node=8037720011`.

16. Anderson, J, W Boyne, F Culick, F Hooven, H Jex, H Lippincot, and H Wolko. *The Wright Flyer: An Engineering Perspective*. Washington, D.C., 1987.

17. Anderson, John. "The Wright Brothers". *The Wright Flyer: An Engineering Perspective*. Smithsonian Institution Press, Washington, D.C., 1987.

18. Anderson, John D. *Introduction to Flight: Its Engineering and History*. McGraw-Hill Education, New York, NY, 2015.

19. Armitage, M. *Unmanned Aircraft*. Brassey's Defence Publishers, London, UK, 1988.

20. Berndt, J and A de Marco. "Progress on and Usage of the Open Source Flight Dynamics Model Software Library, JSBSim ". *AIAA Modeling and Simulation Conference*, AIAA 2009-5699. Chicago, IL, August 2009.

21. Berndt, Jon S. *JSBSim, An Open Source, Platform-Independent, Flight Dynamics Model in C++*. JSBSim, Providence, RH, 2011.

22. Bihrle, William. *A Handling Qualities Theory for Precise Flight-Path Control*. Technical Report AFFDL-TR-65-198, USAF, 1966.

23. Blakelock, John H. *Automatic Control of Aircraft and Missiles*. John Wiley & Sons, Inc., New York, NY, 1965.

24. Burk, S. M. and C.F. Wilson. *Radio-Controlled Model Design and Testing Techniques for Stall/Spin Evaluation of General-Aviation Aircraft*. Technical Report NASA-TM-80510, 1975.

25. Chalk, C. R. "In-Study for a Fighter Total In-Flight Simulator". Calspan Flight Research Memorandum 566. July 1982.

26. Chatfield, Charles H. and Charles F. Taylor. *The Airplane and Its Engine*. McGraw-Hill book Company, Berkeley, CA, 1936.

27. Chow, Emily, Alberto Cuadra, and Craig Whitlock. "Fallen from the skies: drone crashes database", 2016. URL `https://www.washingtonpost.com/graphics/national/drone-crashes/database/`.

28. Cooper, G. E. and R. P. Harper Jr. *The Use of Pilot Rating in the Evaluation of Aircraft Handling Qualities*. Technical Report 567, Advisory Group for Aerospace Research and Development, April 1969.

29. Cotting, M. *Evolution of Flying Qualities Analysis: Problems for a New Generation of Aircraft*. Dissertation, Virginia Polytechnic Institute and State University, Blacksburg, Virginia, March 2010.

30. Deptula, D. "Air Force Unmanned Aerial System (UAS) Flight Plan 2009-2047", 2009.

31. Dorobantu, A, P Seiler, and G Balas. "Validating Uncertain Aircraft Simulation Models Using Flight Test Data". *AIAA Atmospheric Flight Mechanics Conference*, AIAA 2013-4984. Boston, MA, August 2013.

32. Finnegan, Phil, David Rockwell, and Steve Zaloga. "Teal Group's World Military Unmanned Aerial Systems Market Profile & Forecast 2016", 2016.

33. Foster, T. M. and W.J. Bowman. "Dynamic Stability and Handling-Qualities of Small Unmanned-Aerial-Vehicles". *43rd AIAA Aerospace Sciences Meeting and Exhibit*, AIAA 2005-1023. January 2005.

34. Gearhart, G. "Resume of Aerial Torpedo Development". April 1926.

35. Gibbs-Smith, Charles H. *Aviation: an historical survey from its origins to the end of World War II.* Her Majesty's Stationary Office, London, 1970.

36. Gillipse, Charles. *The Montgolfier brothers and the invention of aviation, 1783-1784.* Princeton, NJ, 1983. ISBN 0691083215.

37. Gilruth, R. R. *Requirements for Satisfactory Flying Qualities of Airplanes.* Technical Report NACA Rept. 755, National Advisory Committee for Aeronautics, Langley Field, VA, 1941.

38. Goppert, James M., Agnostino De Marco, and Inseok Hwang. "On Some Trim Strategies for Nonlinear Aircraft Flight Dynamics Models with Open Source Software JSBSim". *3rd CEAS Air and Space Conference*, volume 1 of *Lecture Notes in Computer Science*. Council of European Aerospace Studies (CEAS), Venice, Italy, October 2011.

39. Greene, K., D. Kunz, and M. Cotting. "Toward a Flying Qualities Standard for Unmanned Aircraft". *AIAA Atmospheric Flight Mechanics Conference*, AIAA 2014-2194. Atlanta, GA, June 2014.

40. Harper, R. P. "In-Flight Simulation of the Lateral-Directional Handling Qualities of Entry Vehicles". *AIAA Atmospheric Flight Mechanics Conference*, WADC-TR-61-147. February 1961.

41. Heppenheimer, T. A. *First flight : the Wright brothers and the invention of the airplane*. Wiley, Hoboken, NJ, 2003.

42. Jategaonkar, R., D. Fischenberg, and von Grauenhageni. "Aerodynamic Modeling and System Identification from Flight Data - Recent Applications at DLR". *Journal of Aircraft*, Vol. 21 No. 4. 2004.

43. Kim, J. *Evaluation of Unmanned Aircraft Flying Qualities Using JSBSim*. Ms thesis, Air Force Institute of Technology, Wright-Patterson AFB, OH, March 2016.

44. Lockheed Martin Corporation. *Supplemental Flight Manual F-16C/D*, 2003.

45. Magee, John G. "High Flight", 1941.

46. McFarland, M. W. *The Papers of Wilbur and Orville Wright*. McGraw-Hill, New York, NY, 1953.

47. Miller, T. "F-16 VISTA", 2015. URL `http://aviationphotodigest.com/history-is-made-at-edwards-afb/`. [Online; accessed July, 2015].

48. Mitchell, David G., Rogerr Hoh, Bimal L. Aponso, and David H. Klyde. *Proposed Incorporation of Mission-Oriented Flying Qualities into MIL-STD-1797A*. Technical Report WL-TR-94-3162, 1994.

49. Naftel, J. Chris. *NASA Global Hawk: A Unique Capability for the Pursuit of Earth Science*. Technical Report TM-2007-214613, NASA Dryden Flight Research Center, 2007.

50. NASA. "NASA Armstrong Fact Sheet : Global Hawk High- altitude , long-endurance", 2014. URL `http://www.nasa.gov/centers/armstrong/news/FactSheets/FS-098-DFRC.html`.

51. NASA. "NASA Flies Dragon Eye Unmanned Aircraft Into Volcanic Plume", 2016. URL `https://www.nasa.gov/topics/earth/earthmonth/volcanic-plume-uavs.html`.

52. Neal, T. P. and R.E. Smith. "A Flying Qualities Criterion for Design of Fighter Flight-Control Systems". 8(10):803–809, October 1971.

53. Nelson, Robert C. *Automatic Control of Aircraft and Missiles*. McGraw-Hill Companies, Inc., Notre Dame, IN, 1998.

54. Newcome, L. *Unmanned Aviation: A Brief History of Unmanned Aerial Vehicles*. Reston, VA, 2004.

55. Nguyen, L, M Ogburn, W Gilbert, K Kibler, P Brown, and P Deal. *Simulator Study of Stall/Post-Stall Characteristics of a Fighter Airplane With Relaxed Longitudinal Stability*. Technical Report NASA-TP-1538, 1979.

56. Niccoli, Ricardo. *Book of Flight: From the Flying Machine of Leonardo Da Vinci to the Conquest of Space*. Friedman, 2002.

57. Pennington, S. "DoD UAS Operations in the National Airspace System", 2015.

58. Phillips, W. "Mr. Sperry's Mighty Midget". *Air Classics*, volume 15. May 1979.

59. Phillips, William H. "NACA Report 927: Appreciation and Prediction of Flying Qualities". 1949.

60. Robertson, J. C. "Sir George Cayley's Governable Parachutes". *Mechanics' Magazine*, September 1852.

61. Rosenberg, Z. "US Navy probes demonstrator crash". *Flight International*, 2012.

62. Saxena, A, I Roychoudhury, and C. Neukom. "Evaluating the Impact of Deploying Unrestricted Unmanned Aircraft Systems in the National Airspace". *Infotech at Aerospace*, AIAA 2012-2436. Garden Grove, CA, June 2012.

63. Scott, J and C Scott. "Drone Delivery Models for Healthcare". *50th Hawaii International Conference on System Sciences*. 2017.

64. Stevens, B, F Lewis, and E Johnson. *Aircraft Control and Simulation*. Wiley and Sons, Hoboken, NJ, 2016.

65. Stillwell, Ruth E. "Unmanned Aircraft and Balloons in Class E Airspace above FL600, Challenges and Opportunities". *Space Traffic Management Conference*, 2016.

66. Taylor, John W. R. *Jane's All the World's Aircraft 1976-77*. McGraw-Hill Book Company, London, UK, 1976.

67. Thirtle, M.R., R. V. Johnson, and J. L. Birkler. "The Predator ACTD". RAND, Santa Monica, CA, 1997.

68. Tise, Larry E. *Conquering the Sky: The Secret Flights of the Wright Brothers at Kitty Hawk*. Palgrave Macmillan, New York, NY, 2009.

69. UAVGlobal. "Unmanned Systems and Manufacturers". URL `http://www.uavglobal.com/list-of-manufacturers/`.

70. US Army Signal Corps. "Advertisement and Specification for a Heavier-Than-Air Flying Machine. Signal Corps Specification 486", 1907.

71. USAF. "MQ-1B Predator", 2015. URL `http://www.af.mil/AboutUs/FactSheets/Display/tabid/224/Article/104469/mq-1b-predator.aspx`.

72. USAF. "MQ-9 Reaper", 2015. URL `http://www.af.mil/AboutUs/FactSheets/Display/tabid/224/Article/104470/mq-9-reaper.aspx`.

73. Weingarten, Norman C. "History of In-Flight Simulation & Flying Qualities Research at Calspan". *AIAA Atmospheric Flight Mechanics Conference*, AIAA 2003-5464. Austin, TX, August 2003.

74. White, Lynn. *Eilmer of Malmesbury, an Eleventh Century Aviator: A Case Study of Technological Innovation, Its Context and Tradition.* Johns Hopkins University Press, 2nd edition, 1961.

75. Winnefeld, J and F. Kendall. "Unmanned Systems Integrated Roadmap FY 2013-2038". Office of the Secretary of Defense, US, 2013.

76. Woschnagg, E. *Evaluating Forecast Accuracy.* Technical report, University of Vienna, 2004.

Vita

Captain Ali M. Hamidani completed undergraduate studies at Embry-Riddle Aeronautical University, where he was commissioned through the Air Force Reserve Officer Training Corps, with a degree in Aerospace Engineering. His first assignment was at Kirtland AFB, NM, where he served as a spacecraft flight test director on the Autonomous Navigation & Guidance Experiment for Local Space (ANGELS) mission, through the AFRL Space Vehicles Directorate. During the assignment, Captain Hamidani led a team of 40 personnel, across multiple organizations, in planning and executing over one hundred space flight test sorties, and directly supported space experiments worth $300 million.

After gaining invaluable experience with space vehicles research, Captain Hamidani was selected to pursue a graduate degree in Astronautical Engineering at the Air Force Institute of Technology. Throughout the program, he studied space attitude dynamics, and completed a course sequence in rocket propulsion. An avid glider and single-engine private pilot, with a keen interest in flight test engineering, Capt Hamidani also took a specialty sequence in aircraft stability and control, through which he studied automated control systems and aircraft flying qualities. His thesis research is a culmination of those studies.

Upon completion of graduate school, Captain Hamidani was assigned to serve as a flight dynamics engineer at the National Air and Space Intelligence Center, Wright-Patterson AFB, OH. He is charged with analyzing technical intelligence which keeps the nation one step ahead of foreign threats to air and space operations, and informs operational, policy, and acquisition decisions of key leadership personnel, including The Office of the President, Congress, and military commanders across the joint services.

REPORT DOCUMENTATION PAGE

Form Approved
OMB No. 0704–0188

1. REPORT DATE *(DD–MM–YYYY)*	2. REPORT TYPE	3. DATES COVERED *(From — To)*
23–03–2017	Master's Thesis	Sept 2015 — Mar 2017

4. TITLE AND SUBTITLE

Evaluating the Autonomous Flying Qualities of a Simulated Variable Stability Aircraft

5a. CONTRACT NUMBER

5b. GRANT NUMBER

5c. PROGRAM ELEMENT NUMBER

6. AUTHOR(S)

Hamidani, Ali M., Capt, USAF

5d. PROJECT NUMBER

16Y279,17Y279

5e. TASK NUMBER

5f. WORK UNIT NUMBER

7. PERFORMING ORGANIZATION NAME(S) AND ADDRESS(ES)

Air Force Institute of Technology
Graduate School of Engineering and Management (AFIT/EN)
2950 Hobson Way
WPAFB OH 45433-7765

8. PERFORMING ORGANIZATION REPORT NUMBER

AFIT-ENY-MS-17-M-261

9. SPONSORING / MONITORING AGENCY NAME(S) AND ADDRESS(ES)

Department of Aeronautics and Astronautics
2950 Hobson Way
WPAFB OH 45433-7765
DSN 271-0690, COMM 937-255-3636
Email: ali.hamidani.1@us.af.mil

10. SPONSOR/MONITOR'S ACRONYM(S)

AFRL/RQQ

11. SPONSOR/MONITOR'S REPORT NUMBER(S)

12. DISTRIBUTION / AVAILABILITY STATEMENT

DISTRIBUTION STATEMENT A:
APPROVED FOR PUBLIC RELEASE; DISTRIBUTION UNLIMITED.

13. SUPPLEMENTARY NOTES

14. ABSTRACT

Delivering communications from high altitudes, at airspeeds of just 30 knots, gathering data from active volcanoes and forming hurricanes, and collecting ISR over hostile territories, UAVs are at the ready to perform those missions that are too 'dull, dirty, or dangerous' for manned aircraft. However, the proliferation of this new technology has its fair share of challenges. Over 460 DoD UAV mishaps have occurred since 2001, with almost half resulting in damages of $2M or more. One incident almost ended in fatalities, when a UAV, suffering from loss of control, collided with a C-130. That loss of control is what this undertaking aims to address—toward establishing design criteria for UAV stability and control characteristics, or flying qualities. The JSBSim flight simulation software was used to investigate the correlation between the flying qualities of an F-16, and its workload and performance, while executing a set of precision-aggressive tasks under autopilot command. The results suggest techniques and metrics that can be used to specify design requirements for UAVs. This research effort is intended to serve as a precursor for real-world flight testing using the NF-16D VISTA.

15. SUBJECT TERMS

Variable Stability, Control, Flying Qualities, Handling Qualities, MIL-STD-1797, Unmanned, Autonomous, NF16-D VISTA, Flight Simulation, Workload, Performance, Flight Test

16. SECURITY CLASSIFICATION OF:			17. LIMITATION OF ABSTRACT	18. NUMBER OF PAGES	19a. NAME OF RESPONSIBLE PERSON
a. REPORT	b. ABSTRACT	c. THIS PAGE			Dr. D. Kunz, AFIT/ENY
U	U	U	UU	185	19b. TELEPHONE NUMBER *(include area code)* (937) 255-3636, x4547; donald.kunz@afit.edu